ΕΘΝΙΚΟ ΜΕΤΣΟΒΙΟ ΠΟΛΥΤΕΧΝΕΙΟ
Σχολή Ηλεκτρολόγων Μηχανικών και Μηχανικών
Ηλεκτρονικών Υπολογιστών

Organisation Européenne pour la Recherche Nucléaire

Διπλωματική Εργασία

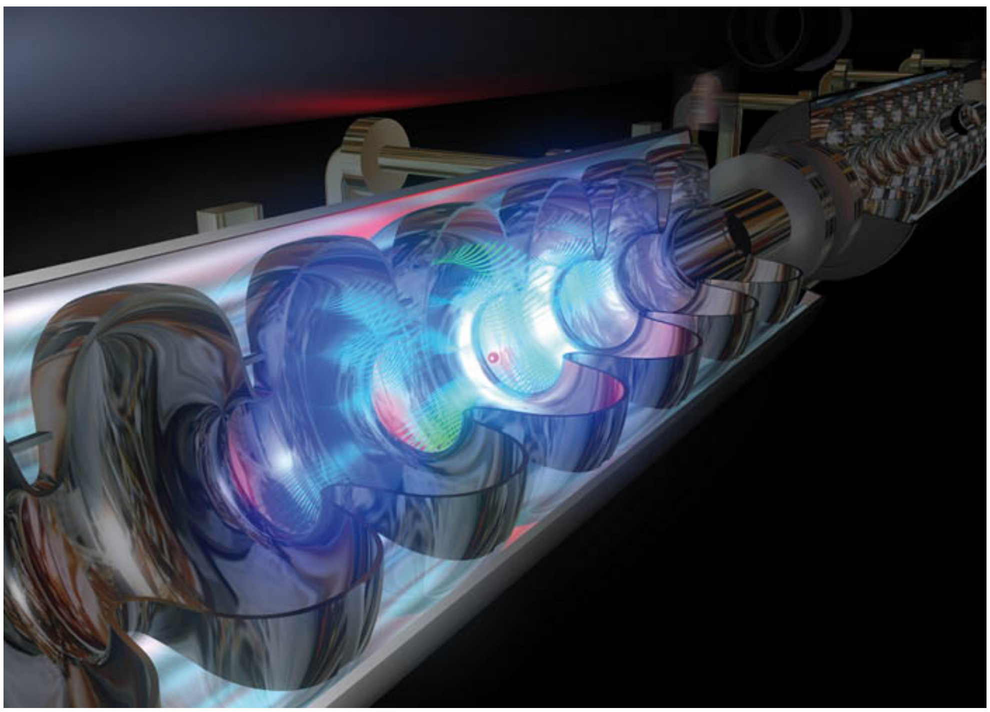

Ανάπτυξη λογισμικού Φυσικής Σωματιδιακών Δεσμών στους γραμμικούς επιταχυντές του CERN

του Εμμανουήλ Ι. Τραχανά

Επιβλέπων: Ευάγγελος Γαζης
Καθηγητής Ε.Μ.Π

Γενεύη, Ελβετία 2016

Εθνικό Μετσόβιο Πολυτεχνείο

Σχολή Ηλεκτρολόγων Μηχανικών και Μηχανικών Ηλεκτρονικών Υπολογιστών

Ανάπτυξη λογισμικού Φυσικής Σωματιδιακών Δεσμών στους γραμμικούς επιταχυντές του CERN

Διπλωματική Εργασία

Εμμανουήλ Ι. Τραχανας

Επιβλέπων: Ευάγγελος Γαζής.

Εγκριθηκε από την τριμελή εξεταστική επιτροπή την Τετάρτη 21 Ιουνίου 2017

(Υπογραφή)	(Υπογραφή)	(Υπογραφή)
....	....	....
Ευάγγελος Γαζής	Κυριάκος Χιτζανίδης	Ηλίας Γλύτσης
Καθηγητής Ε.Μ.Π	Καθηγητής Ε.Μ.Π	Καθηγητής Ε.Μ.Π

....

Εμμανουήλ Ι. Τραχανάς,
Διπλωματούχος Ηλεκτρολόγος Μηχανικός και
Μηχανικός Ηλεκτρονικών Υπολογιστών.

Περίληψη

Οι γραμμικοί επιταχυντές στην διεθνή βιβλιογραφία αναφέρονται ώς Linacs (συντόμευση του όρου linear accelerators) Στις μέρες μας υπάρχουν πάνω από 20.000 γραμμικοί επιταχυντές παγκοσμίως που βρίσκουν εφαρμόγή στην έρευνα, την ιατρική και την βιομηχανία. Η συγκεκριμένη διπλωματική εργασία που υποβλήθηκε στην Σχολή Ηλεκτρολόγων Μηχανικών και Μηχανικών Ηλεκτρονικών Υπολογιστών του Εθνικού Μετσόβιου Πολυτεχνείου εκπονήθηκε με βάση την εργασία ως Technical Student του συγγραφέα στο Κέντρο Πυρηνικών Ερευνών της Γενεύης (CERN) το διάστημα Οκτώβριος 2015-Δεκέμβριος 2016. Σε αυτο το διάστημα ο συγγραφέας συμμετείχε σε πρωτοπόρα ερευνητικά project όπως το πρώτο παγκοσμίως *Radio Frequency Quadrupole* (*RFQ*) υψηλών συχνοτήτων στα 750 *MHz* και το *commissioning* του νέου γραμμικού επιταχυντή *Linac4*. Το *CERN*, αποτελεί το μεγαλύτερο ερευνητικό κέντρο του κόσμου και αποτελεί το ιδανικότερο περιβάλλον για μελέτες και έρευνα πάνω στους γραμμικούς επιταχυντές. Η εργασία μπορεί να χωρίστει σε δύο μέρη. Στο πρώτο μέρος παρουσιάζονται οι βασικές αρχές σχεδιασμού των γραμμικών επιταχυντών, ενώ στο δεύτερο μέρος περιλαμβάνεται το λογισμικό που αναπτύχθηκε ή συντηρήθηκε για τις προσομοιώσεις, την διεξαγωγή και ανάλυση μετρήσεων.

Όσον αφορά τις σχεδιαστικές αρχές και την αρχιτεκτονική ενός γραμμικού επιταχυντή μπορούμε να στρέψουμε τις προσοχή μας σε δύο ερωτήματα. α) Πώς η παραγόμενη ισχύς και τα ηλεκτρομαγνητικά πεδία διαχεόνται μέσα στα στοιχεία του επιταχυντη, στις ηλεκτρομαγνητικές κοιλότητες· και β) Πώς μία δέσμη σωματιδίων μπορεί να μεταφερθεί από το ένα άκρο του επιταχυντή στο άλλο χώρις να χαθεί ο συγχρονισμός μεταξύ των σωματιδίων και των χρονομεταβλητών πεδίων μέσα στις κοιλότητες· Αυτά τα ερωτήματα καλούμαστε απαντήσουμε στην παρούσα εργασία. Το **πρώτο κεφάλαιο** είναι μια εισαγωγή στις εγκαταστάσεις και τα πειραμάτα του *CERN*. Στο **δεύτερο κεφάλαιο** παρουσιάζονται οι λύσεις των εξισώσεων των Η/Μ κυμάτων στο εσωτερικό των επιταχυντικών κοιλοτήτων και οι διάκριση τους σε TE, TM και στάσιμου ή συνεχούς κύματος μαζί με τις εφαρμογές τους. Ξεκινώντας από τις κυματικές εξισώσεις του *Maxwell* αναζητούμε αρμονικές χωροχρονικές λύσεις για την μορφή των πεδίων. Η παράγραφος 2.3.1 παρουσιάζει την μορφή των εξισώσεων για την πιο απλή μορφή επιταχυντικής κοιλότητας, την *pillbox cavity* ενώ η παράγραφος 2.4 παρουσιάζει αναλυτικά τα μεγέθη που χρησιμοποιούνται για την ποσοτικοποίηση των σχεδιαστικών απαιτήσεων ενός νέου επιταχυντή.

Η τελευταία παράγραφος παρουσιάζει τα κυριότερα είδη κοιλότητων με τις παραλλαγές τους και το πεδίο χρήσης τους. Οι διαφορετικές απαιτήσεις και εφαρμογές για την επιτάχυνση των σωματιδιων και την μορφή των πεδίων οδηγούν σε διαφορετικές μηχανικές υλοποιήσεις. Παρουσιάζονται αναλυτικά οι σημαντικότεροι τύποι ($DriftTubes, IH - Structure$ και συζευγμένες κοιλότητες) και δίνεται ιδιαίτερη αναφορά στο σχεδιασμό, τις ικανότητες και τις μαθηματικές εξισώσεις που διέπουν την λειτουργία των $Radio - Frequency\ Quadrupoles$ (RFQ) ενώ γίνεται μια σύντομη εισαγωγή στις φυσικές και μηχανικές ιδιότητες των υπεραγώγιμων επιταχυντών.
Το **τρίτο κεφάλαιο** προσπαθεί να απαντήσει στο δεύτερο ερώτημα που τέθηκε παραπάνω, περιγράφοντας λεπτομερώς τις βασικές εξισώσεις που διέπουν την κίνηση των σωματιδίων στα εγκάρσια κα διαμήκη επίπεδα της κίνησης. Το κεφάλαιο ξεκινά από την απλή σχέση της δύναμης που δέχονται τα σωματίδια από το πεδίο και καταλήγει να συζήτα περίπλοκα φαινόμενα που παρουσιάζονται στις διευθύνσεις κίνησής τους.

Ο μητρικός φορμαλισμός για την περιγραφή της φυσικής των σωματιδιακών δεσμών διαδραματίζει κεντρικό ρόλο στην ανάλυση των φαινομένων στην υπολογιστική μοντελοποίηση και στην ανάπτυξη λογισμικού προσομοιώσεων. Στό χώρο των φάσεων η δέσμη απεικόνιζεται με την μορφή μιας έλλειψης και ένα χαρακτηριστικό ποιότικο της μέγεθος είναι η $emittance$ που εκφράζει την διασπορά της δέσμης γύρω από το βαρύκεντρο της και αποτελεί μέτρο της επιφάνειας που καταλαμβάνει η έλλειψη στον χώρο των φάσεων. Αφου μελετήσαμε αναλυτικά την κίνηση των σωματιδίων στο εγκαρσιο επίπεδο της κίνησης καταλήγουμε στο συμπέρασμα ότι η κίνηση των σωματίδιων είναι μια ταλάντωση που ονομάζεται βητατρονική ταλάντωση.

Στην συνέχεια μπορούμε να αναλυσουμε τα φαινόμενα που περιγράφουν την κίνηση στο διαμήκες επίπεδο της κίνησης, το οποίο αποτελεί σημαντικό σημείο μελέτης καθώς είναι το επίπεδο που πραγματοποιείται η επιτάχυνση των σωματιδίων. Συνηθίζεται στους γραμμικούς επιταχυντές ο άξονας της δέσμης (ο άξονας κατα μήκους του οποίου παρουσιάζεται επιταχυνση της δέσμης) να ταυτίζεται με τον άξονα z. Παρουσιάζεται αναλυτικά ό τροπος με τον οποίο δημιουργείται και διατηρείται ο συγχρόνισμός ανάμεσα στο πεδίο και τα σωματίδια, ο μηχανισμός της επιτάχυνσης και η ανάλυση ευστάθειας της κίνησης.

Το **κεφάλαιο 4** προσπαθεί να καταδείξει τον τρόπο που οι παραπάνω σχεδιαστικές αρχές και εξισώσεις εφαρμόζονται στην πράξη στο $CERN$ με λεπτομερή περιγραφή των γραμμικών επιταχυντών του ερευνητικού κέντρου με ιδιαίτερη έμφαση στον νέο $Linac4$. Παρουσιάζονται ο αναλυτικά τα συστατικά μέρη των εν υπηρεσία επιταχυντών του $CERN$, $Linac2$, $Linac3$ και $Linac4$ ενώ για λόγους πληρότητας παρουσιάζεται ο πρώτος γραμμικός επιταχυντής $Linac1$. Στόχος είναι να παρουσιαστουν ρεαλιστικές περιπτώσεις επιταχυντών η διαδικασία και τα $trade - offs$ ανάμεσα στα σχέδια, τους στόχους και την οικονομοτεχνική μελέτη για έναν νέο επιταχυντη.

Τα **τελευταία κεφάλαια** αποτελούν την εργασία του γράφοντος ως μέλος του $BE - ABP - HSL$ *section* του $CERN$. Η πολυπλοκότητα των φαινομένων που παρουσιάζεται κατά την διάδοση μιας δέσμης μέσα από επιταχυντικά στοιχεία προτάσσει την ανάγκη για ανάπτυξη και χρήση λογισμικού που μας παρέχουν τα κατάλληλα εργαλεία και αριθμητικές μεθόδους για την προσσεγγιστική λύση των εξισώσεων της κίνησης. Στο πεδίο της φυσικής σωματιδιακών δεσμών, οι προσομοιώσεις με αυτούς τους κώδικες παίζουν καθοριστικό ρόλο στην κατανόηση και εφαρμόγη των φυσικών νόμων που διέπουν την λειτουργία τους. Όταν μιλάμε για έναν επιταχυντή οι προσομοιώσεις υπεσέρχονται σε όλες τα στάδια, από τον σχεδιασμό και το *commissioning* μέχρι την λειτουργία και την συλλογή και επεξεργασία δεδομένων. Το λογισμίκο που θα αναλυθεί και θα χρησιμοποιηθεί σε αυτήν την εργασία είναι το "$Travel$" , το πρόγραμμα διεπαφής με το χρήστη "$PathManager$" καθώς το λογισμικό στατιστικής ανάλυσης σφαλμάτων "$Delta$" Τα *beam dynamics* λογισμικά $Travel$ και $Path\ Manager$ είναι αξιόπιστα υπολογιστικά εργαλεία που χρησιμοποιούνται από όλα τα μέλη του *section* για τις απαραίτητες προσομοιώσεις που απαιτούνται για την έρευνα στους γραμμικούς επιταχυντές. Κύριο καθήκον ήταν ή συντήρηση, η ανάπτυξη και η επιτάχυνση του κώδικα καθώς και επίβλεψη της νέας έκδοσης που διαμοιράστηκε στο *section* το Μάρτιο του 2016. Το "$Travel$" είναι ένα λογισμικό ανίχνευσης σωματιδίων γραμμένο σε γλώσσα $Fortran90$ αποτελούμενο από πληθώρα υπολογιστικών ρουτίνων σε δυναμική διασύνδεση μεταξύ τους. Επιπρόσθετα το '$Path\ Manager$ ' γραμμένο σε $Visual\ Basic$ παρουσιάζει και επιτρέπει την διεξαγωγή προσομοιώσεων απο το "$Travel$" σε ένα πιο φιλικό περιβάλλον για το χρήστη.

Ιδιαίτερη ανάλυση και μελέτη έγινε στις ρουτίνες του κώδικα που δέχονται σαν είσοδο έναν χάρτη ηλεκτρομαγνητικού πεδίου και προσομοιώνουν την κίνηση των σωματιδίων μέσα απο αυτό. Παρουσιάζεται και αναλύεται διεξοδικά ο τρόπος με τον οποίο το πρόγραμμα διακριτοποιεί το πεδίο και λύνει τις εξισώσεις κίνησης με αριθμητικές μεθόδους. Το κεφάλαιο αυτό έμεινε σαν *documentation* στα μέλη του *section* για να διευκολύνει την κατανόηση των εργαζομένων στο μέλλον.

Στα πλαίσια του έργου για την συντήρηση και βελτίωση του κώδικα πραγματοποιήθηκαν εκτεταμένες αναλύσεις της συμπεριφοράς του και συγκρίσεις με το *Matlab* για πεδία με διαφορετική ευκρίνεια και διαφορετικό αριθμό σωματιδίων. Τα συμπεράσματα που προέκυψαν έδειχναν την ανάγκη για κάποιες αλλαγές και βελτιώσεις στον κώδικα όπως διορθώσεις στις εξισώσεις της τροχιάς των σωματιδίων της δέσμης και στην επεξεργασία των υπολογιστικών σημείων. Επιπρόσθετα, αλλαγές πραγματοποιήθηκαν σε διάφορες κάρτες και ρουτίνες του λογισμικού άλλοτε για λογούς διόρθωσης και άλλοτε για λόγους βελτίωσης των αποτελεσματων. Στο πεδίο της ανάπτυξης του κώδικα το λογισμικό μπορεί πλέον να προσομοιώνει *pepperpots* και *RFQs* χρησιμοποιώντας το χάρτη του ηλεκτρομαγνητικου τους πεδίου. Το *pepperpot* είναι μια συσκευή που χρησιμοποιείται ευρέως για την μέτρηση και την εκτίμηση της *emittance* σε ένα σημείο της επιταχυντικής διάταξης. Η πιο σημαντική προσθήκη στο λογισμικό είναι είναι η νέα ρουτίνα που επιτρέπει την προσομοίωση $Radio - Frequency\ Quadrupoles$ διαμέσου του πεδιακού τους χάρτη. Αφορμή για την προσθήκη αυτή έπαιξε ο σχεδιασμός και η κατασκευή του πρώτου *RFQ* υψηλών συχνοτήτων στα 750 MHz για ιατρικές εφαρμογές στην αδρονικη θεραπεία. Τα *RFQs* χρησιμοποιούνται στις χαμηλές ενέργειες στην έρευνα και σπάνια στην ιατρική και την βιομηχανία. Ωστόσο η χρήση εξαιρετικά υψηλών συχνοτήτων για *RFQ* οδήγησε στην δημιουργία ενός με μικρές διαστάσεις που ζυγίζει μόνο 220 κιλά και το κάνει κατάλληλο για χρήση σε τέτοιες εφαρμογές. Το επαστατικό αυτό *RFQ* φτάνει σε ενέργεια 5 MeV σε δύο μόλις μέτρα παρουσιάζοντας *transmission* 30 %. Εκτός από την αδρονική καρκινική θεραπεία μπορεί να εγκατασταθεί στα νοσοκομεία για την παραγωγή ισοτόπων για *PET scanning* καθώς και για την παραγωγή Τεχνιτιου και νετρονίων για άλλες εφαρμογές.

Ένα από τα πιο ενδιαφεροντα καθήκοντα ήταν η ανάλυση του κώδικα για πιθανά *bottlenecks* και καθυστερήσεις που αύξάνουν τον χρόνο εκτέλεσης και να αναζητήσουμέ τρόπους για την αντιμετώπισή τους.

Οι τεχνικές που εφαρμόστηκαν μείωσαν τον χρόνο των προσομποιώσεων και οδήγησαν στην νέα έκδοση του $Travel -$"$Travel$ 4.0.8" και "$Path\ Manager$ 2.8.5" που διαμοιράστηκε σε ολόκληρο *section* τον Μάρτιο του 2016. Δημιουργήθηκε και διανεμήθη το πακέτο εγκατάστασης της νέας έκδοσης που περιλαμβάνει εκτός από τα δύο προγράμματα το λογισμικό ανάλυσης σφαλμάτων *Delta* το πρόγραμμα ανάλυσης *Beam Iteration v*.1.0 το απαραίτητο *documentation* όπως επίσης και κατάλληλα παραδείγματα. Η τελευταία παράγραφος του πέμπτου κεφαλαίου παρουσιάζει τον τρόπο με τον οποίο χρησιμοποιήθηκε το *Path Manager* και το *Travel* στο *commissioning* του *Linac*4. Για την εξέταση ρεαλιστικών σεναρίων επιλέχτηκαν να παρουσιαστούν προσομοιώσεις που αφορουν το *commissionig stage* στα 100 *MeV* σχετικά με την εκκίνηση των *DTL tanks*.

Το **τελευταίο** κεφάλαιο περιλαμβάνει την σχεδίαση ενός πλήρως αυτοματοματοποιημένης εφαρμογής που λαμβάνει μετρήσεις και ανακατασκευάζει την χαρακτηριστικη έλλειψη της δέσμης (*emittance reconstruction*) στον *Linac*3. Οι πρώτες παράγραφοι του κεφαλαίου αναλύουν την μέθοδο ανακατασκευής της δέσμης που θα χρησιμοποιηθεί, το σημείο του επιταχυντή που θα πραγματοποιείται η ανακατασκευή τους οι σχεδιαστικούς και μηχανικούς περιορισμούς που έπρεπε να ληφθούν υπ΄ όψην για την εφαρμογή αυτού του *project* στον *Linac*3. Στην συνέχεια του κεφαλαίου παρουσιάζονται το όργανα μέτρησης και αναλύονται διεξοδικά το πολυεπίπεδο δίκτυο μετάδοσης πληροφοριών και δεδομένων από τα $low - level$ ηλεκτρονικα του επιταχυντή μέχρι τις εφαρμογές στο κέντρο ελέγχου. Η εφαρμογή γραμμένη σε γλώσσα *Java* και υλοποιημένη πάνω στο *framework* του *Inspector* αποτελεί το αντικείμενο του νέας δημοσίευσης απο τους , Εμμανουήλ Τραχανά, Γεώργιο Βουλγαράκη, *Veliko Atanasov Dimov Alessandra Lombardi* , *Giulia Bellodi* και Ευάγγελο Γαζή που βρίσκεται σε διαδικασία έκδοσης την στιγμή που γράφονται αυτές οι γραμμές.

Λέξεις Κλειδιά: Γραμμικός Επιταχυντής, Ανάπτυξη Λογισμικού, Φυσική Σωματιδιακών δεσμών ,ηλεκτρομαγνητικές κοιλότητες και σχεδιαστικες αρχες, CERN, Υπολογιστικά Εργαλεία, Λογισμικό Travel, PathManager, ERIS,

National Technical University of Athens
School of Electrical and Computer Engineering

Organisation Européenne pour la Recherche Nucléaire

Diploma Thesis

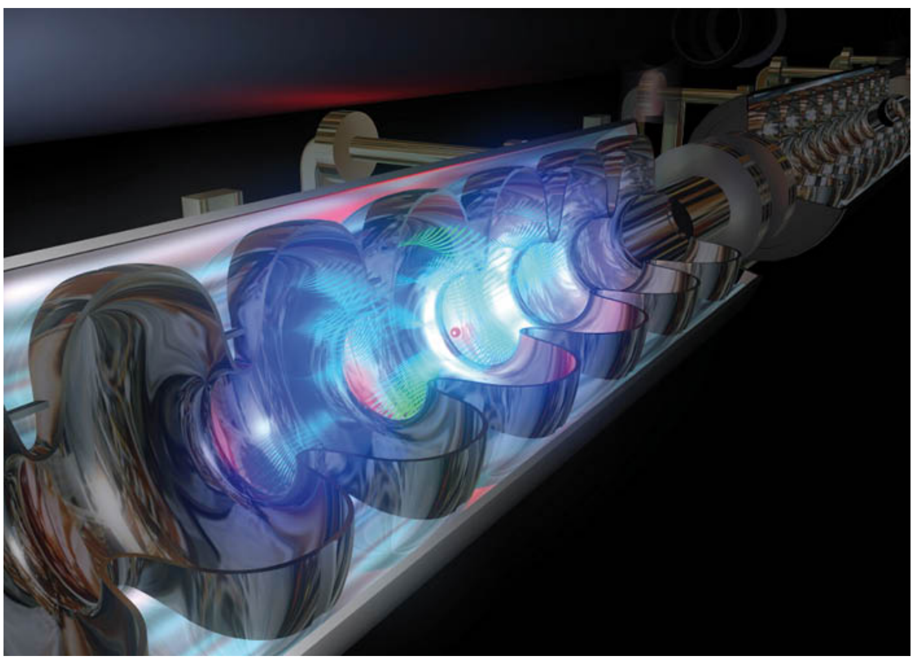

Beam Dynamics Software Studies at CERN Linacs

Author:
Emmanouil Trachanas

Supervisors:
Evangelos Gazis
Alessandra Lombardi
Veliko Atanasov Dimov

Geneva 2016

Life has no meaning a priori. It is up to you to give it a meaning, and value is nothing but the meaning that you chooose.

Jean-Paul Sartre

Acknowledgements

I would like to thank my professor, mentor and thesis supervisor **Evangelos Gazis** for his inspirational teaching and guidance through this effort. I am deeply grateful for the encouraging words and the ambitious plans and work we made together, the advice and the belief in me.

I would like to express my gratitude and appreciation to my CERN supervisor, the HSL- section leader **Alessandra Lombardi** for the life-opportunity she gave me to be a member of this section, her suggestions and the strong belief that i can participate and excel in challenging projects during my internship in a outstanding working environment.

The efforts to complete my thesis would be fruitless without **Veliko Atanasov Dimov** my dearest colleague, supervisor and friend who always stood by me in this trip. Veliko thank you, for your advice, tolerance, support and time spend to help me in the beginning of my career. You where always there, no matter the circumstances, to answer my questions, guide me and help to confront the problems that appeared.

The development of ERIS whould not be possible without the work and assistance of my colleague and friend **Georgios Voulgarakis**. Giorgos, thank you for your enormous contribution on our application, patience and the great amount of time you spend teaching and helping me. It was an invaluable experience working with you in this demanding project.

Last but not least, i whould like to thank all the members of our team, **Jean-Baptiste Lallement**, **Giulia Bellodi**, **James Matthew Garland**, **Ville Toivanen** , **Marc Maintrot**, **Stefano Mattei**,**Alberto Degiovanni** for our collaboration, the knowledge and advice, i gained from our meetings and conversations. The most important of all, for the warm environment and the feeling that i was member of a family.

I would like also express my appreciation to the professors **Kyriakos Hitzanidis**, and **Ilias Glitsis** for being members of the committee for the examination of this thesis.

This thesis is dedicated to my family which made the sacrifices and provided all the means for this great life- experience

Abstract

The word Linac is an abbreviation for Linear Accelerator. Nowadays 20.000 Linacs are in use, finding applications in Medicine , Industry and Research. This thesis which is submitted to School of Electrical and Computer Engineering of National Technical University of Athens for the acquisition of the diploma of Electrical and computer engineer was written during the Technical Student internship at CERN where the author was involved at eminent and innovative projects such as the first ever 750MHz RFQ (Radio Frequency Quadrupole) and the commissioning of the new Linac , Linac4. CERN is the biggest research center in the world, providing state-of-the-art accelerator infrastructure thus leading the progress at the domains of physics and technology. Because of that fact, constitutes the ideal environment for studies on linear accelerators. **The first two chapters of this thesis** are trying to shed light to the design principles of a Linac. For clarity we can divide the design of such a complex structure to two questions: a) How the power and the field are dissipated with minimum losses inside the cavity ? and b) How a particle beam can be transferred inside the cavity without losing the synchronicity between the particles and the field? **The first chapter** is an overview of CERN facilities and experiments. **The second chapter** debates how an accelerator is designed from the electromagnetic waves point of view. First of all, presents a cursory overview of different type of Linacs and their historical origins. The rest of the chapter is dedicated on how the electromagnetic waves are produced and propagate inside the cavity which will guide the particle beam. In more detail, the solution of the electromagnetic wave equations inside the cavities used for acceleration and the distinction of their operating modes to Transverse Electric (TE) and Transverse Magnetic (TM), standing and traveling wave modes with their field of use. Sub-section 3.2.1 presents an example, the form of solution of the electromagnetic field components inside a simple cylindrical pillbox cavity. Section 2.4 is dedicated to the fundamental design parameters of accelerating structures. The last section of this chapter presents the most commonly used particle accelerating and focusing structures, as far as their design and field of application.

Chapter 3 answers the second above question, concerning the beam dynamics design of the cavity describing in detail the transverse and longitudinal parti-

cle's motion. The chapter starts from the Lorentz force, the energy gain in a cavity, goes through the particle coordination system and the formalism of their equation of motion and ends up discussing phenomena such us space charge and radio-frequency defocusing.

Chapter 4 debates in a more detailed way the Linacs at CERN and their elements, giving more weight to new Linear accelerator Linac4. Aim of this chapter is to show how the design principles described in the previous part of this thesis find application to a real machine meeting CERN needs.

Chapters 5 and 6 present the work done by the author as a member of BE-ABP-HSL group during the Technical Student contract. PATH Manager and Travel are the simulation tools used by the BE-ABP-HSL group members for their work on linacs. **Chapter 5** presents the maintenance and development of this software until the release of the new version of the code at March 2016. During this period the source code and the physics in the software routines where screened for the detection of possible bugs and mistakes and various changes and corrections where applied. In the development domain, Travel can now simulate Radiofrequency quadrupoles via their fieldmap as well as pepperpots. In addition efforts were made for the reduction of the simulation time. Travel and PathManager now provide the vital tools to simulate RFQs supporting the work of the section stuff at the design, construction and commissioning of the first ever 750MHz RFQ designed by section leader Alessandra Lombardi. The last part of chapter 5 shows the use of the new PATH Manager version to the 100 MeV commissioning stage of Linac4 for the phase scans of the DTL tanks.

A different project is presented at chapter 6 :the development of a new control-room application at Linac3 for prompt emittance reconstruction using the quadrupoles variation method. The application changes the strength of quadrupoles of a triplet at Linac3 LEBT and reconstructs the beam emmitance before the triplet.this application is the subject of the new publication from Emmanouil Trachanas, Georgios Voulgarakis, Veliko Atanasov Dimov, Giulia Bellodi, Alessandra Lombardi and Evangelos Gazis that is under the publish procedure while these lines are written [64].

Keywords: CERN, Linear Accelerators, Medical and Industrial Applications, E/M waves and Cavities, Design Principles, Transverse and Longitudinal beam dynamics, Linac4, Simulation Tools, Software Development and Maintenance, Travel, PathManager, ERIS.

Contents

List of Figures

List of Tables

Chapter 1

Introduction

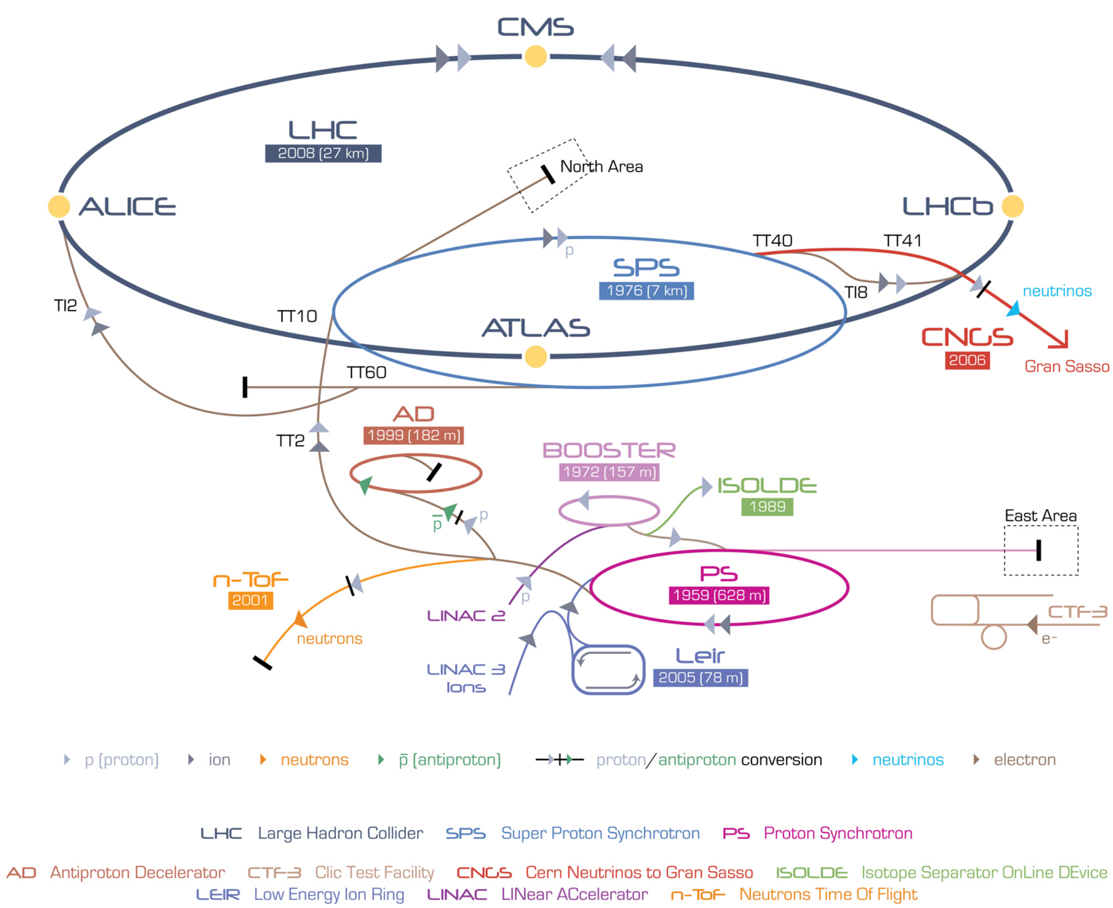

Figure 1.1: Cern Accelerator Complex [5].

The acronym **CERN** stands for *"Organisation Européenne pour la Recherche Nucléaire"* - European Organization for Nuclear Research. Established in 1954, CERN is the largest particle physics Laboratory in the world located at the city of Geneva near Franco-Swiss borders. CERN provides the particle accelerators,detectors and the technology needed for the high-energy physics research with the aim to cast light to the fundamental structure of the universe. Numerous experiments are being held at CERN with accelerators and detectors focused on different fields of physics created by international Collaborations. Accelerators are used to accelerate the beams to high-energies before their collision with another beam or a stationary target. Detectors are used to observe and record the results of the collisions permitting to improve our knowledge and our theories on the ways that particles interact according to the fundamental laws of physics. CERN consists of 22 members states, and has 2,513 permanent stuff members and 12,313 fellows,associates and students representing hundreds of universities and research facilities worldwide.

In order to reach so high energies the charge particle beams must go through accelerator stages in order to end up at the Large Hadron Collider (LHC) Ring. The proton beam source comes from a simple bottle of hydrogen gas and once produced at the ion source they get injected to the next accelerator [2].

The CERN Accelerator chain consists of [1], [2], [3] :

- **Linac2** which accelerates protons to 50 MeV for injection to Proton Sychrotron Booster (PSB)
- **Linac3** which accelerates heavy ions for injection to Low Energy Ion Ring (LEIR)
- **Low Energy Ion Ring** accelerates the ions injected from Linac3 and transports them to the Proton Synchrotron. This accelerator is the successor of the Low Energy Antiproton Ring.
- **Booster** accelerates the particles to 1.4 GeV
- **Proton Synchrotron (PS)** which accelerates the particles to 28 GeV and injects them to Super Proton Sychrotron

- **Super Proton Sychrotron** which has diameter of 2 km and initially delivered protons at 300 GeV and then updated to 450 GeV. It has been used as proton-antiproton collider and as accelerator providing electrons and positrons for LEP and after of LEP decommissiong used for feeding protons and heavy ions the Large Hadron Collider.

- **LHC**: Large Hadron Collider is the final stage of the acceleration chain at CERN and the largest particle accelerator in the world. It has 27 km circumference and it is constructed 100m beneath the ground. LHC accelerates proton beams up to 7 TeV for each beam before colliding them to the sites of the detectors. LHC has also the ability to accelerate Lead ions (Lead Ion Runs one month every year.). Experiments on the LHC (CMS, ATLAS, LHCb ,MoEDAL, TOTEM, LHC-forward) consist of different technologies and study the particle collisions from different aspects. It is easily assumable that the enormous amount of data created by the collisions are being processed with the help of a worldwide computational grid. LHC is a state of the art machine, which accelerates 2 particle beams at different parallel pipes at opposite direction. The pipes are at ultrahigh vacuum and the beams are guided from strong magnetic fields produced by superconducting magnets [3].

  Other accelerators and experiments which complete the accelerator chain are Antiproton Decelerator (AD) used for the research of antimatter, ISOLDE which is used for the study of unstable and novel nuclei and CLIC test facility which studies the possibility of construction of an electron-electron linear collider at CERN sight.

Chapter 2

Linac Architecture

This chapter presents the basic types of linacs as well as their elements, design parameters and solution for the electromagnetic fields.

2.1. Historical Milestones

Linacs can generally be divided in two categories:

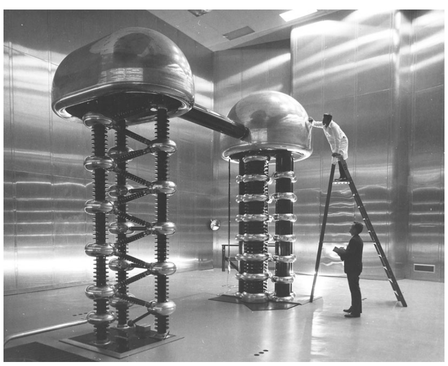

Figure 2.1: The Cockroft-Walton accelerator [6].

Static linacs: which are operating with static electric fields. However their capabilities are limited due to electric field breakdown at a low energy point. The most renown example is the Cockroft-Walton accelerator. In 1928-1932 John Cockroft and Ernest Walton accelerated protons to 400 kV , enough to split the lithium atom. Nowadays they are still used at the initial points of acceleration as pre-injectors [7], [9].

Time Vaying Linacs:

- **Induction linacs:** When a beam with a certain current travels through a beam pipe induces a current on the walls that it is opposite to the direction of motion. This effect known as "beam loading " can cause problems to the structure and beam stability. That effect leads to the fact that common accelerator structures cannot handle high intensity beams. In these applications which require high currents an induction linac can be used to surpass the beam loading effect. In induction Linacs an applied time varying magnetic field inducts an electric field which accelerates the particles [8], [9].

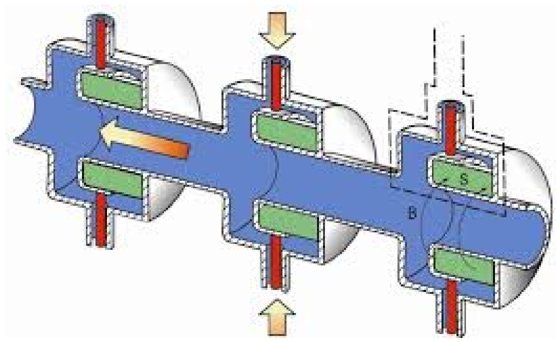

Figure 2.2: A modern induction Linac that exploits the Maxwell's laws for creating an electric from a magnetic field [9].

- **RF Linacs:** Where the particles are Accelerated by time varying radio-frequency electromagnetic fields. First Gustav Ising proposed in his paper the first accelerator that used time-varying voltage in 1924. It was until 1928 when Rolf Wideroe build the first drift tube accelerator (Figure: 2.3) using a 25 KV oscillator at 1 MHz to achieve final energy of 50 KeV with potassium atoms. The problems of the Wideroe accelerator where the long gap distances at low frequencies and high power losses at high frequencies [10], [29].

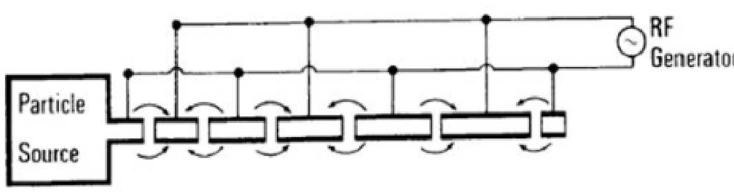

Figure 2.3: The Wideroe Linac [9].

In 1931-1934 E.O Lawrence and D.Sloan at Berkeley managed to accelerate Hg atoms to 1.26 MeV via a Wideroe type linac with an RF oscillator of 7 MHz. At the same time General Electric Company and L. Snoddy at University of Virginia accelerated electrons from 28 keV to 2.5 MeV. The breakthrough in the design of Linacs came with the Alvarez design at 1945; a design that is the most popular amongst research centers around the world. As the acceleration energy increases the drift length becomes longer. Exempt from that at high frequencies a Wideroe Linac radiates a large amount of power and presents a capacitance behavior resulting in great losses. The innovation at Alvarez design was that the tubes are placed inside a single resonant cavity introducing an inductive load at the system and fed by a single RF Source [10].

2.2. Linac Supporting System

Figure 2.4: Thales TH1801,Multi-Beam Klystron (MBK), 1.3 GHz,117 kV [11].

The general layout of Linac consists of the particle source, the accelerating cavities and the supporting system. Various elements can be added depending on the Linac application.

The support systems of a Linac contain the vacuum system, the water colling system that ensures the operation at proper temperatures and the RF system. The RF system is responsible for delivering the necessary microwave power for the particle acceleration.

It is comprised by the RF source (example: magneton or klystron -see Figure:2.4), waveguides for the transmission of the power,circulators. that control the RF power flow and protects the device from the reflected power, a modulator for providing the current and voltage pulses to the RF source, and a high power load to absorb the reflected power. Finally a Automatic Frequency Control (AFC) is used as control system to adjust the frequency of the RF source to the one of the cavity [25].

2.3. Electromagnetic Waves and Cavities

It is well known from the Electromagnetic field theory that we can categorize the waveguides to Transverse Electric (TE) and transverse Magnetic(TM) modes. We remind that in TE modes the electric field is perpendicular to the direction of motion and at TM modes the magnetic field is perpendicular to the direction of motion. The accelerating cavities are just waveguides with the following categorization:

- TE mode:
  - RFQ
  - IH (Interdigital-H Structure)
- TM mode:
  - DTL (Drift Tube Linac)
  - Cavity Coupled Linac (CCDTL)
  - PI Mode Structure: PIMS
  - Superconducting Cavities

Furthermore RF accelerators are often operate in standing wave or in traveling wave mode. Each mode has its own characteristics and is chosen depending the application energy and the accelerated particles. Standing waves are often used in synchrotrons and storage rings in order to compensate for the synchrotron radiation loss. Furthermore standing wave mode can accelerate oppositely charged beams traveling in opposite directions. The Traveling wave accelerators are categorized through their characteristics to constant-shunt impedance and constant-gradient structures and used for light particles such as electrons.

Ther are many types of standing wave Linacs, for example are constructed by several coupled cavities fed by an RF source (klystron) in the middle of the device. The fields propagating inside the cavities and they are reflected at the conducting walls of the Linac. The waves are propagate an reflected several times, creating standing-wave pattern. In the traveling wave Linacs the RF excitation is placed at the beginning of the structure, and the waves created propagate until the end of the structure, where they absorbed with no acceleration or exit and get absorbed by an external resistive load.

Starting from the wave equations for the fields:

$$\nabla^2 \overrightarrow{E} - \mu\epsilon \frac{\partial^2 \overrightarrow{E}}{\partial t^2} = 0 \tag{2.1}$$

$$\nabla^2 \overrightarrow{H} - \mu\epsilon \frac{\partial^2 \overrightarrow{H}}{\partial t^2} = 0 \tag{2.2}$$

where μ, ϵ are the magnetic permeability and electric permitivity respectively. The solution of fields inside a cavity has the following form:

$$\overrightarrow{E}(\overrightarrow{r}, t) = \overrightarrow{E}(\overrightarrow{r})e^{-j\omega t} \tag{2.3}$$

$$\overrightarrow{H}(\overrightarrow{r}, t) = \overrightarrow{H}(\overrightarrow{r})e^{-j\omega t} \tag{2.4}$$

Where the vector $\overrightarrow{r}$ represents the spatial vector. The spatial and time components of the fields are not conjugated and are subject to the boundary conditions:

$$\overrightarrow{E}_{||} = 0 \tag{2.5}$$

$$\overrightarrow{B}_{\perp} = 0 \tag{2.6}$$

It is proven that assuming homogeneous and isotropic material with harmonic functions, the spatial components of the fields obey the Helmholtz equation:

$$\nabla^2 \Psi + k_0^2 \epsilon_r \mu_r \Psi = 0 \tag{2.7}$$

where the wavenumber k_0 is defined as:

$$k_0 = \frac{2\pi}{\lambda}\ , \ \ k_0^2 = \omega^2 \epsilon_0 \mu_0 \tag{2.8}$$

The general solutions of the equations may get simplified exploiting the geometry of the accelerating cavity. The solution for the first TE_{npq}, TM_{npq} modes in cylindrical cavities are shown in Figure: 2.5:

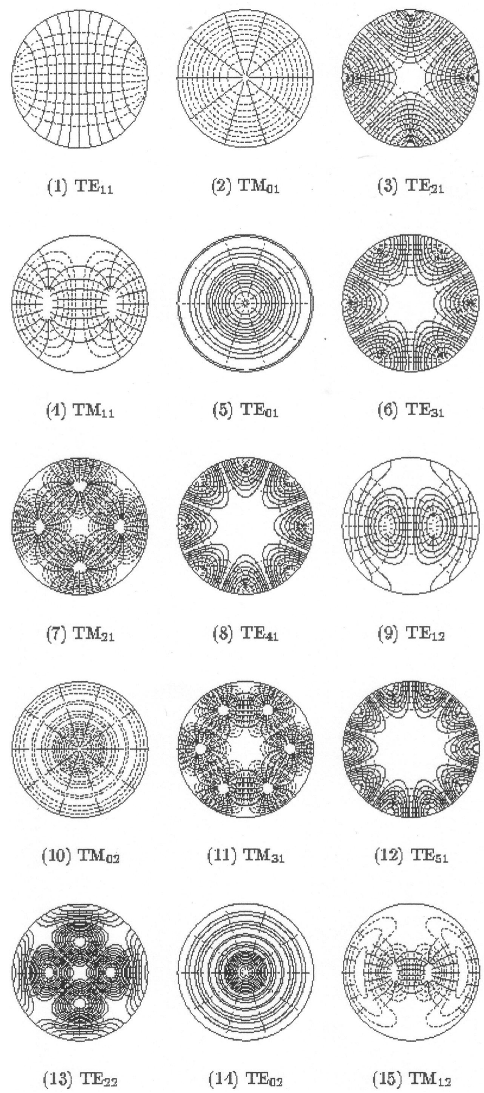

Figure 2.5: Created by Dr. Ray Kwok at San Jose State University shows the contour plots for the first Transverse Electric (TE) and Transverse Magnetic (TM) modes of a cylindrical cavity. [50]

References for this chapter: [10], [12], [13], [14], [15], [16], [17], [19], [20], [21], [22]

2.3.1 Field in a Cylindrical Pillbox cavity

To enlight more the procedure of the field equations extraction from Helmholtz equation the example of a simple cavity is presented in this section. The comp-nents for the fields in TM_{npq} modes in a simple pillbox cavity may get simplified to:

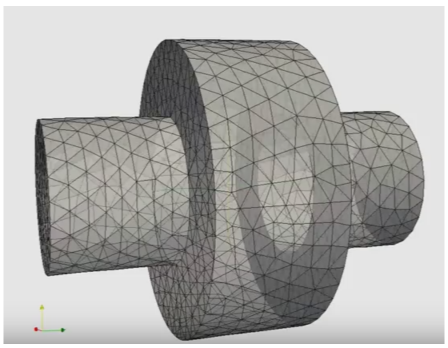

Figure 2.6: A 3D model of a pill box cavity [49].

$$E_z = k_2^2 cos k_1 z J_n(k_2 r) cos n\theta \tag{2.9}$$

$$E_r = -k_1 k_2 sin k_1 z J_n(k_2 r) cos n\theta \tag{2.10}$$

$$E_\theta = \frac{nk_1}{r} sin k_1 z J_n(k_2 r) sin n\theta \tag{2.11}$$

$$H_z = 0 \tag{2.12}$$

$$H_r = -\frac{j}{Z_0}\frac{nk}{r} J_n(k_2 r) sin n\theta \tag{2.13}$$

$$H_\theta = -\frac{j}{Z_0} k k_2 J_n'(k_2 r) cos n\theta \tag{2.14}$$

It is known that:

$$Z_0 = \sqrt{\frac{\mu_0}{\epsilon_0}} \tag{2.15}$$

where J_n is the Bessel function of order n and the fields satisfy the boundary conditions at the boundaries along z direction of the device 0,l and α the boundary along radial direction :

$$E_r = E_\theta = 0 \; for \; z = 0 \;\; and \; z = l \tag{2.16}$$

$$Ez = E_\theta = 0 \; for \; r = \alpha \tag{2.17}$$

In the TE, TM definition the index n indicates the order of Bessel function, p the number of zeros of the Bessel function and q the number of maxima of the field in z axis.

A Electromagnetic field in a drift tube behaves like the T_{010} mode where the field has only two components:

$$E_z = J_0(kr), H_\theta = -\frac{j}{Z_0} J_1(kr) \tag{2.18}$$

The stored energy in a cavity is defined:

$$W_s = \frac{\mu}{2}\int_V \mid H \mid^2 dV = \frac{\epsilon}{2}\int_V \mid E \mid^2 dV \tag{2.19}$$

then the losses are defined by :

$$P_d = \frac{1}{2}\int_S R_w H^2 dS \tag{2.20}$$

where R_w is the surface resistance for a layer of unit area and skin depth δ:

$$R_w = \frac{1}{\sigma\delta} \ , \ \ \delta = \frac{1}{\sqrt{\pi\mu\sigma f}} \tag{2.21}$$

where σ is the material conductivity and f the RF frequency.

Two important magnitudes which play a major role in case of particle acceleration with traveling waves are the phase and group velocity.

$$v_{group} = \frac{d\omega}{d\beta} \tag{2.22}$$

$$v_{phase} = \frac{\omega}{k} \tag{2.23}$$

The group velocity is equal to the energy flow of in the waveguide and the u_{phase} indicates the rate at which the phase of the wave propagates in space.

In order to have a propagating wave in the cavity it must:

$$v_{phase} > c \tag{2.24}$$

In order to achieve a proper acceleration then we have to reduce the phase velocity of the cavity to the velocity of the particles ($u < c$). To achieve this, discs or irises (Figure:2.7) should be mounted at the structure. It is obvious that, at this point the solutions to the Maxwell equations should change to obey to the new periodical boundary condition. Other methods to reduce the u_{phase} of the electromagnetic fields in the cavities are the helix, split ring, and Quarter wave designs.

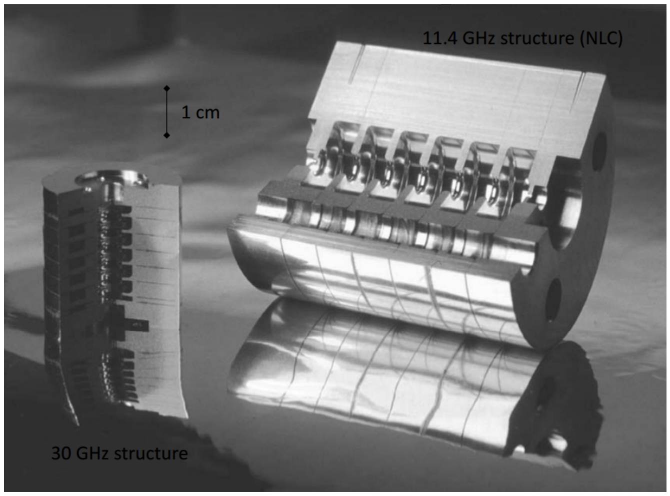

Figure 2.7: Iris loaded Cavity. [20]

Reference for this section: [10], [29]

2.4. Design Parameters of Accelerating Structures

The figures of merit that play a major role in the design of the Linac are presented to these section:

2.4.1 Average axial electric field:

$$E_0 = \frac{1}{L}\int_0^L E(0,0,z)dz \tag{2.25}$$

Average axial electric field, (units: V/m) describes how much field is available for acceleration and depends on cavity geometry , resonant mode and frequency [9], [10].

2.4.2 Shunt Impedance:

The shunt impedance (unit: Ω) inside the RF cavity is defined as:

$$Z = \frac{V_0^2}{P_d} \tag{2.26}$$

Where V_0 is the effective acceleration voltage and P_d the dissipated power. Shunt Impedance is an important magnitude in Linac design and the goal is to achieve high shunt impedance with low surface field [9]. A convenient formalism in accelerating structures with multiple cells is the shunt impedance per unit length (units: Ω/m):

$$Z_l = \frac{V_0^2}{LP_d} = E_0^2 \frac{L}{P} \quad \left(\frac{\Omega}{m}\right) \tag{2.27}$$

or ,

$$Z_l = E_0^2 \frac{dL}{dP_d} \tag{2.28}$$

where L is the cavity length and E_0 is the average field.

Shunt impedance defines the ratio of the average electric field squared to the power per unit of length dissipated on the walls surface. Shunt impedance depends only on cavity mode and geometry and gives an estimation on how well we concentrate the RF power in the useful region [9], [10].

A more useful tool is the effective shunt impedance:

$$ZT^2 = (E_0 T)^2 \frac{L}{P} \tag{2.29}$$

Where the T is the transient time factor defined in equation (2.35).

The effective shunt impedance measures if the structure is optimized and adapted to the velocity of the particle being accelerated. If we neglect the reflected EM waves at the beam line and the power loss through the transmission, then the power from the RF source is consumed in the acceleration and on cavity walls [9], [10].

2.4.3 Quality factor (QF):

QF defines the ration of stored energy to the power loss in the wall in one RF period. Q is function of the frequency, geometry and of the surface resistance of the cavity material [9], [10].

$$Q = \frac{2\pi f W_s}{P_d} \tag{2.30}$$

Where W_s is the stored energy in the cavity,

2.4.4 Filling Time:

$$t_F = \int_0^L \frac{dz}{v_g(z)} \tag{2.31}$$

where u_g is the group velocity of the EM field.

For traveling wave (Equation:2.31) It expresses the time needed for the electromagnetic field to fill a cavity of length L. For Standing wave (Equation:2.32) expresses the time it takes to the field to decrease by a factor of 1/e after the cavity was beam filled [9], [10].

$$t_F = \frac{2Q}{\omega} \tag{2.32}$$

2.4.5 Transit Time Factor

Transit Time Factor defines the ratio of the energy gained in the time varying RF field to that in a DC field of the same strength. Thus, it is a measure of the reduction in energy gain caused by the sinusoidal time variation of the field in the gap and depends only in the particle velocity and gap length [9], [10].

$$T = \frac{\int\limits_{-L/2}^{L/2} E(0,z) cos\omega t(z)\ dz}{\int\limits_{-L/2}^{L/2} E(0,z)\ dz} - tan\phi \frac{\int\limits_{-L/2}^{L/2} E(0,z) sin\omega t(z)\ dz}{\int\limits_{-L/2}^{L/2} E(0,z)\ dz} \tag{2.33}$$

Beacause E(z) is usually an even function, we have,

$$0 = \int\limits_{-L/2}^{L/2} E(0,z)\ dz \tag{2.34}$$

The Transient time factor equation simplifies to:

$$T = \frac{\int\limits_{-L/2}^{L/2} E(0,z) cos\omega t(z)\ dz}{\int\limits_{-L/2}^{L/2} E(0,z)\ dz} \tag{2.35}$$

2.4.6 Duty cycle

A linac will take the continuous particle beam coming out of an ion source, bunch it a given RF frequency and then accelerate it up to the required final energy. In general, Linacs are **pulsed** accelerators: the beam is generated by the source and then delivered to the users in pulses of a given length (between few microseconds and few milliseconds) at a given repetition frequency f (usually between 1 Hz and 100 Hz). The product of pulse length and repetition frequency is the duty cycle (or beam duty cycle, to distinguish it from the RF duty cycle which is always higher). A linac can as well operate continuously, producing a constant stream of particles: in this case the duty cycle is 100%, and we call it a **continuous wave (CW)** Linac [27].

2.4.7 Kilpatrick Effect

When the electric field in the cavity reaches an certain critical value an electric arch can be caused. The field breakdown is described by an empirical equation by W.D Kilpatrick in 1957 [9]:

$$24.67 \quad \sqrt{f} = E_c \exp^{\frac{-4.25}{E_c}} \tag{2.36}$$

where E_c is the critical value for the electric field and f tha RF frequency. Nowadays, due to advanced processing methods materials and vacuum supporting systems we can reach a value of up to several Kilpatricks [9].

2.5. Accelerating and Focusing Structures

The next step on a Linac design is the choice of accelerating elements, a complicated procedure that requires extensive comparisons of the parameters of the cavities to fit in the designed parameters, the design goals and the available budget. Usually the parameters taken into account into this stage of design are: Particle type (mass and charge), the ratio of the speed of particles compared to the speed of light (β), the beam current, the duty factor(pulsed, CW),the frequency, the energy and the operational constraints. More details on the operation mode and beam dynamics are given to next chapter.

2.5.1 Drift Tube

Using RF fields at long cavities poses the problem of particles' deceleration because of the alternation of the field. The problem is solved with the drift tubes. Drift tubes are metallic cylindrical chambers that shield the particle from the outer field.

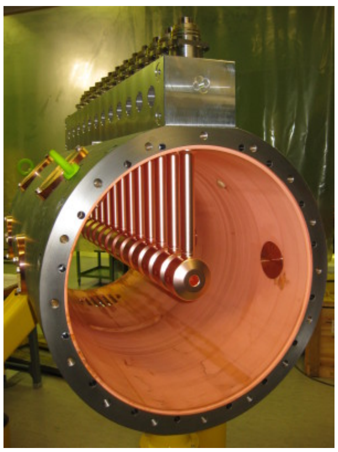

Figure 2.8: Linac 4 drift tube prototype [28].

There are different geometry design for the drift tube cavities which exploit the same principle. One of the most popular designs is the one made by L.Alvarez in 1945 [10] who put the drift tubes inside one single resonant cavity in way that the field in the gaps between them has a zero phase difference.When two or more cavity gaps are adjacent to each other the resulting current is zero at the common walls between them, thus the common wall becomes useless. The length of the drift tubes is increasing as the particles are accelerated in the case of protons and ions. The principles of operation is simple: The particle are injected to the structure in a way that when the field is decelerating the particles are inside the drift tubes which act as Faraday cages and feel no force. On the other hand when the field is accelerating the particles are in the gaps between the drift tubes and gain energy [9], [10].

2.5.2 IH-Structure

The Interdigital-H structure is ideal for low energy ion acceleration (small shunt impedance for low β and frequency range). The Interdigital-H structure is a TE-mode cavity that resembles Alvarez drift tube from a geometrical point of view. Although, their significant difference is the alternate disposition of the stems.

Figure 2.9: An IH drift tube at CERN [30].

The IH structures are distinguished by the small transverse dimensions and their high performance on low energies. Due to their magnetic field pattern the lowest operational mode for a cavity with N accelerating gaps is the $\pi - \pi/N$ mode. The acceleration is performed by the well concentrated electric field created by the intense currents flowing at stems.As shown in Figure: 2.9 Far from the stems and drifts the magnetic field is parallel to the cavity walls. Near the stems and the walls the magnetic field is dominant and decays until the center of the beam pipe, where the region is dominated by the electric field [31], [32].

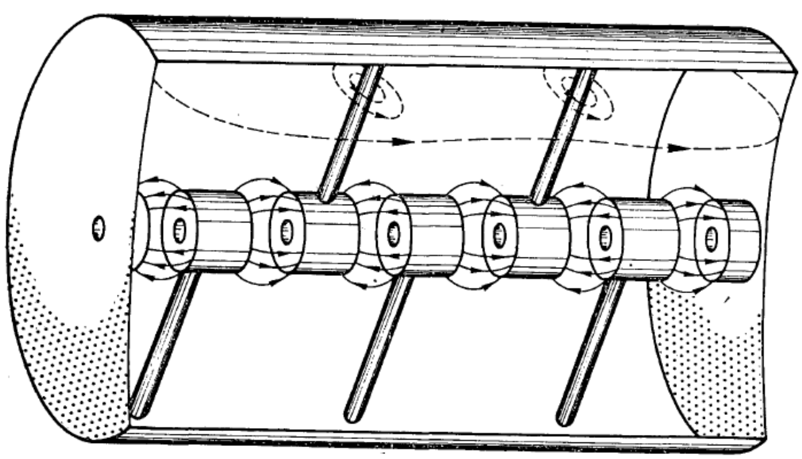

Figure 2.10: An IH structure showing the field distribution [31].

2.5.3 Coupled Structures

Even we optimize the design parameters in our structure (high Q with a excellent material and a high Shunt Impedance) we are limited by the acceleration we can deliver to the cavity. Even we use the best vacuum conditions the acceleration is limited by the breakdown of the electric field at the certain voltage (Killpatrick effect). Moreover we have to synchronize the RF excitation of the cavity to the bunch of particles. A better approach is to feed successive accelerating cavities that are coupled together with a RF source. We can imagine the coupled cavities with their mechanical analogous; two pendulums connected with a spring of strength k. From now on k will be called coupling factor between the cavities. As it is known from the oscillation theory the coupling of N accelerating cavities has N different modes of oscillation with their individual frequency. The frequency of the cavity is chosen by adjusting the RF generated power to a frequency of one of N modes of oscillation. The use of multiple successive cells to accelerate to bigger energies the frequencies of the modes are getting closer and closer then at this particular point the $\pi/2$ mode is the one that has the greatest bandwidth from the oscillation modes. The unique characteristics of this excitation mode has led to its adoption to various designs. It is important to mention that when the cavity is excited in the $\pi/2$ mode every second cavity has no electric field and does not contribute to the acceleration. Although they play a major role in the dispersion of the RF power along the cavities. A proper solution is to make these secondary cavities smaller. These accelerators are called on axis bi- periodic linac. Linac can be even shorter if we move the coupling cavities and put the on the side away from beam channel. This is the principal configuration on the Side-Coupled-Linacs (SCL) [9], [25].

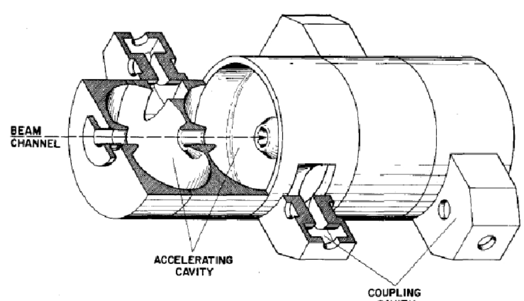

Figure 2.11: An incision design of an Side-Coupled-Linac with the major and coupling cavities. One can notice the nosecones at the beam axis apertures for strengthening the electric field [9].

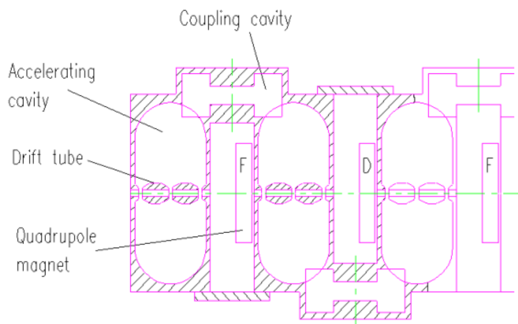

Figure 2.12: A Coupled-Cavity-DTL with the distinguished focusing quadrupoles inside the intertanks of drift tubes [9].

The are two kinds of coupling:

- Electring Coupling : The successive cavities are coupled by the electric field through the coupling apertures at common axis.
- Magnetic Coupling: In order to achieve magnetic coupling, holes are opened to the common wall between two adjacent cavities , where the magnetic field is dominant [25].

2.5.4 Radio-Frequency Quadrupole

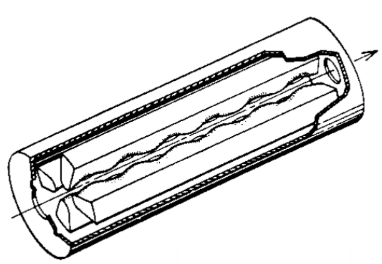

RFQ is an Linac component that brought revolution to the operation of hadron and ion Linear accelerators. RFQ is extremely useful at the first stages of acceleration of ions at low velocities because it **accelerates** ,**focuses**, and **bunches** the beam. The RFQ was invented by Kapchinskiy and Tepliakov and outcasted the need to use DC beam injectors at the Linac. The RFQ permits the propagation of the beam with RF fields and it consists of four vanes or rods (depending on geometry) were alternating voltage is applied and changes sign from one vane to another. The alternating voltage creates transverse RF electric fields which focus the beam. The RFQ vane are modulated in order to create the longitudinal field needed for acceleration. More specifically the

potential on the axis is influenced more from the electrodes that are closer to the axis than the others that are further, thus if a sinusoidal modulation is presented along the axis this will create an alternating accelerating electric field.
The general solution of the potential function along this structure contains infinite terms, although with a specific choice on the vane geometry a solution with only two terms is a good approximation [33], [34], [35] :

$$U(r,\theta,z,t) = \frac{V_0}{2}\left[X\left[\frac{r}{a}\right]^2 cos2\theta + AI_0(kr)cos(kz)\right]sin(\omega t+\phi) \tag{2.37}$$

the dimensionless constants A,X are defined:

$$X = \frac{I_0(ka)+I_0(kma)}{m^2 I_0(ka)+I_0(kma)} \quad , \quad A = \frac{m^2-1}{m^2 I_0(ka)+I_0(kma)} \tag{2.38}$$

The focusing factor B is:

$$B = \left(\frac{q}{m_0}\right)\left(\frac{V}{\alpha}\right)\left(\frac{1}{f^2}\right)\left(\frac{1}{\alpha}\right)\left(\frac{I_0(k\alpha)+I_0(mk\alpha)}{m^2 I_0(k\alpha)+I_0(mk\alpha)}\right) \tag{2.39}$$

and the acceleration efficiency is :

$$E_0 T = \frac{m^2-1}{m^2 I_0(k\alpha)+I_0(mk\alpha)} V \frac{\pi}{2\beta\lambda} \tag{2.40}$$

and their relation:

$$\frac{I_0(k\alpha)+I_0(mk\alpha)}{m^2 I_0(k\alpha)+I_0(mk\alpha)} + \frac{m^2-1}{m^2 I_0(k\alpha)+I_0(mk\alpha)} I_0(k\alpha) = 1 \tag{2.41}$$

Where the first term is the focusing efficiency and the second term the accelerating efficiency.

The quantities presented are defined as : α is the bore radius (aperture), β,γ are the relativistic parameters, f the RF frequency, I_0 the modified Bessel function, k the wave number, λ the wavelength, m the electrode modulation factor, and the factor $\frac{q}{m_0}$ the quantities of the injected particle.

The equations used from now on and the beam dynamics theory are explained in the next chapter, although their adjustment to the RFQ is presented at this point

for a complete description of this accelerating structure.
The fields and the geometry of the RFQ are chosen in order to provide acceleration and the equations of motion at the longitudinal plane are:

$$\frac{d(W-W_s)}{dz} = qE_0T(I_0(kr)cos\phi - cos\phi_s) \tag{2.42}$$

$$\frac{d(\phi-\phi_s)}{dz} = -\frac{2\pi(W-W_s)}{mc^2\beta_s^3\lambda} \tag{2.43}$$

when $-\pi < \phi_s < 0$ we have simple harmonic motion with the wavenumber:

$$k_l^2 = \frac{\pi^2 qAV_0 I_0(kr) sin(-\phi_s)}{mc^2\beta_s^4\lambda^2} \tag{2.44}$$

the quantities with index s are referred to the reference particle. As for the transverse beam dynamics the equation of motion is :

$$\ddot{x} + \left[\frac{qXV_0}{ma^2} + \frac{qk^2AV_0}{4m}cos(kz)\right]xsin(\omega t+\phi) = 0 \tag{2.45}$$

if one uses the well known trigonometric identity $cos(\omega t+\phi)sin(\omega t+\phi) = [sin\phi + sin(2\omega t+\phi)]/2$ we obtain the Mathieu equation which a solution with good approximation is:

$$x = cos\Omega t[1+\epsilon sin(\omega t+\phi)] \tag{2.46}$$

where the amplitude ϵ is approximately :

$$\epsilon \cong \frac{1}{4\pi^2}\frac{qXV_0\lambda^2}{mc^2\alpha^2} \tag{2.47}$$

and :

$$\Omega^2 \cong \frac{1}{2}\left[\frac{qXV_0}{m\omega\alpha^2}\right]^2 + \frac{qk^2V_0Asin\phi}{8m} \tag{2.48}$$

where the first term represents the quadrupole focusing and the second term represent the RF defocusing.

The third merit of the RFQ is that provides beam bunching.The conventional way to bunch a beam is to use RF buncher cavities before the injection to the

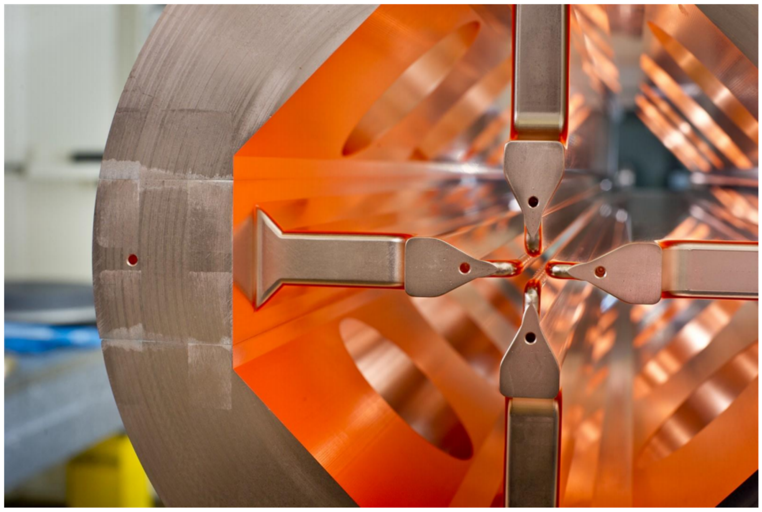

Figure 2.13: A four vane structure RFQ at Cern. Other major layouts for RFQs are the rods, split, coaxial, double-H

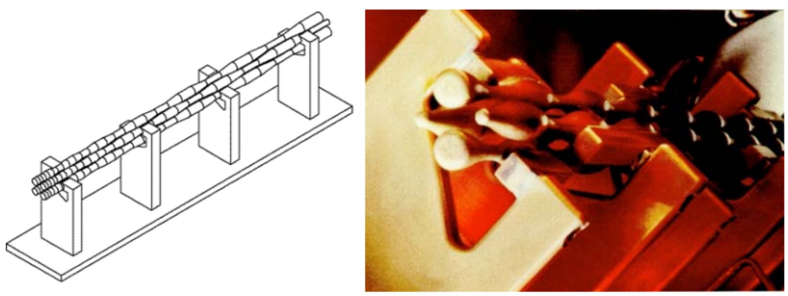

Figure 2.14: The four-rod RFQ and the DESY RFQ2 [35].

Linac. Although RFQ provides adiabatic bunching which has the advantage to collect a large fraction of the beam, split it into well-shaped bunches resulting in good beam quality. The basic principle for the bunching at the RFQ is the following, we inject the beam at low energy and we adjust the synchronous phase around $\pi/2$, where we have the biggest separatrix to collect the beam and the particles together. As we move inside the RFQ we increase gradually the synchronous phase to achieve acceleration and reduce the bunching.

2.5.5 Quadrupole Magnets

In 1945 E.M. McMillan and V.I Veksler discovered the phase focusing. In 1949 Nicholas Christofillos conceived the idea of strong focusing; the effect of beam converging when passing from alternating gradients fields. These ideas led to the development of various magnet structures (dipoles , quadrupoles, sextupoles, octupoles) for manipulating the beam [37]. In 1952 J. Blewett discovered electromagnetic quadrupoles which will be described more in detail (see Figure: 2.15):

In order to solve the RF defoccossing problems caused by the beam propagation one can either use the RF fields, exploiting some characteristics of the incompatibility theorem , solution that is not too practical. The most common way to cope with RF defoccusing is to use periodic structures of quadrupole lenses.The quadrupoles are placed inside the Drift tubes at DTL's and at the intertanks in CCDTL's. In an ideal quadrupole we have a constant quadrupole gradient:

$$G = \frac{\partial B_x}{\partial y} = \frac{\partial B_y}{\partial x} \tag{2.49}$$

If a particle moves along the beam line z the Lorenz force is :

$$F_x = -qvGx \ , \ F_y = qvGy \tag{2.50}$$

if the F_x is negative and the F_y is positive the quadrupole focuses in x and defoccusses in y plane. The gradient is defined :

$$G = \frac{B_0}{a_0} \tag{2.51}$$

where the B_0 is the pole tip field and the a_0 the pole tip radius.The gradient has units T/m and is equivalent:

$$G = \frac{2\mu_0 nI}{\alpha_0^2} \tag{2.52}$$

Where μ_0 is the magnetic rigidity , n the number of windings in coils, I the current through the windings and α_0 is the pole tip radius.

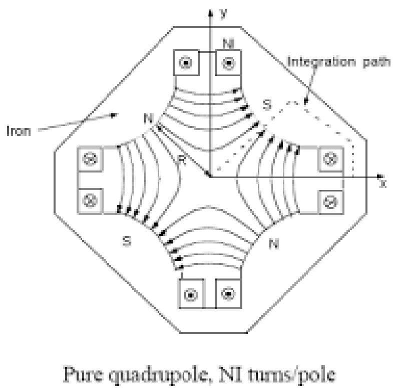

(a) Quadrupole magnet field lines

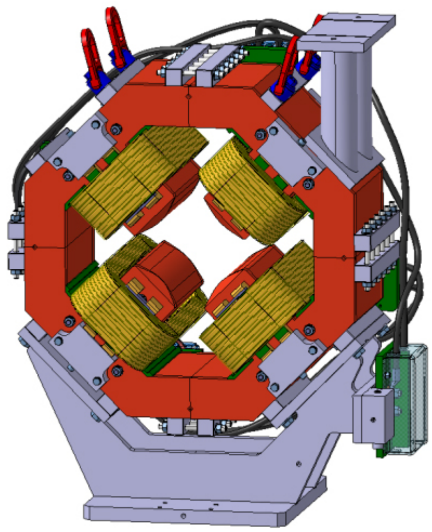

(b) A Quadrupole Magnet

Figure 2.15: Quadrupole Magnets

A magnitude that also plays a major role is the quadrupole strength k :

$$k = \frac{e}{p} G \tag{2.53}$$

given in m^{-2} , where p is the momentum of the particle. Because the quadrupoles provide focusing only in one plane , a lot of quadrupoles are combined in the accelerators in order to achieve transverse focusing to both planes. The combination of the quadrupoles is either periodic or quasi periodic. The most common combinations are FODO , FOFODODO and FDO doublet [57], [36], [37], [9].

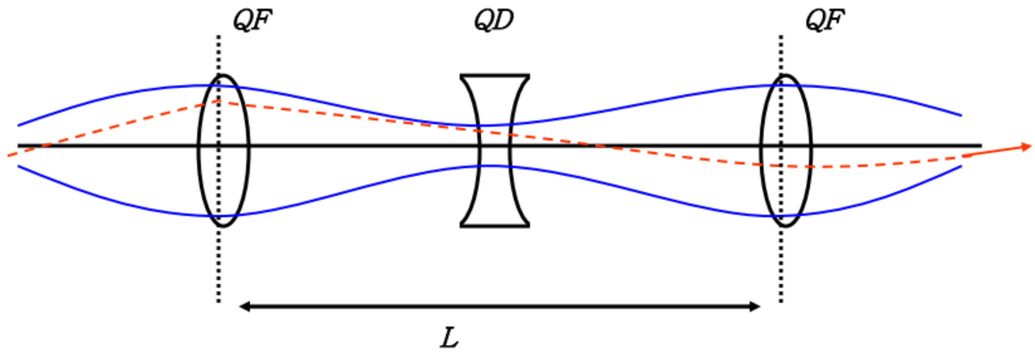

Figure 2.16: The FODO lattice for beam manipulation with two focussing quadrupoles at edges and one defocussing in the middle [38].

2.5.6 Superconducting Cavities

The need to minimize the power loses and maximize the power transferred to the beam to achieve higher energies led to the application of superconducting phenomena to accelerating cavities. The superconducting systems for accelerators started to appear at early 70's and gained ground rapidly in the realm of particle research. The drawbacks are the need for cryogenic system and the meticulous control and maintenance of the structure. Superconducting cavities have been proved to operate at higher gradient, lower AC power demand and more favorable beam dynamics conditions than comparable normal conducting resonators. The are several materials, where Niobium is the most distinguished operated in temperatures of few K (1.8 or 2.4 Kelvin) that are in use in numerous research facilities around the world with the prospect of the industrialization of the superconducting linacs. The main advantage of superconducting accelerating structures is that they enable high gradients under CW operation (10 times greater) and offer freedom in the design of the cavity. Although there are some major drawbacks:

- 'Quenching' : Thermal instabilities often produce heat and finally drive the superconductor to lose its superconducting behaviour.
- Field Emission : Field emitted electrons are accelerated by the electric field , impact at the cavity walls producing heat with γ-radiation, leading to lower Quality factor of the structure.

- Multipacting : Multipacting stands for multiple impact electron amplification , a phenomenon of resonant multiplication of electrons under the influence of RF fields. Electrons created by the hitting of particles in the cavity, resulting in secondary accelerating electrons creating a chain reaction and under the ideal circumstances a particle avalanche [39], [40], [41], [42].

The superconductors are categorized to Type I , which includes pure elements (lead indium , etc.) and Type II which includes the niobium and all its alloys. In superconductors theory the surface currents are carried by the Cooper pairs, thus one can define the surface resistance R_{BCS} which is proportional:

$$R_{BCS} \propto \lambda_L^3 \omega^2 e^{\frac{-1.76T_c}{T}} \tag{2.54}$$

Where λ_L is London penetration depth,ω the frequency of the field , the path of single electron, and T_c the critical temperature of Superconductor. A magnitude called residual surface resistance is caused by material impurities , froze-in magnetic flux and lattice distortions. The power needed for a superconducting system is drastically reduced, including the cryogenic system , compared to normal conducting cavities leading to quality factors of 10^{10} order. The total cryogenic power is given by:

$$P = P_{static} + P_{BCS} + P_{residual} \tag{2.55}$$

where the P_{static} are the static losses , P_{BCS} the losses due to surface resistance and $P_{residual}$ are the losses due to residual surface resistance. Furthermore, the used RF magnetic field should stay below the critical value H_c due to Meissner effect in Type I superconductors:

$$H_c(T) = H_c(0)\left(1 - \left(\frac{T}{T_c}^2\right)\right) \tag{2.56}$$

The behaviour of type II superconductors is different, because the magnetic flux is going in and out producing heat, in a field value spectrum called Shubnikov Phase:

$$H_c = \sqrt{H_{c1}H_{c2}} \tag{2.57}$$

the core of semiconductor is starting to get penetrated above the value of H_{c1} with magnetic flux tubes of field strength of H_{c2}. The remaining material stays at the superconducting phase [42].

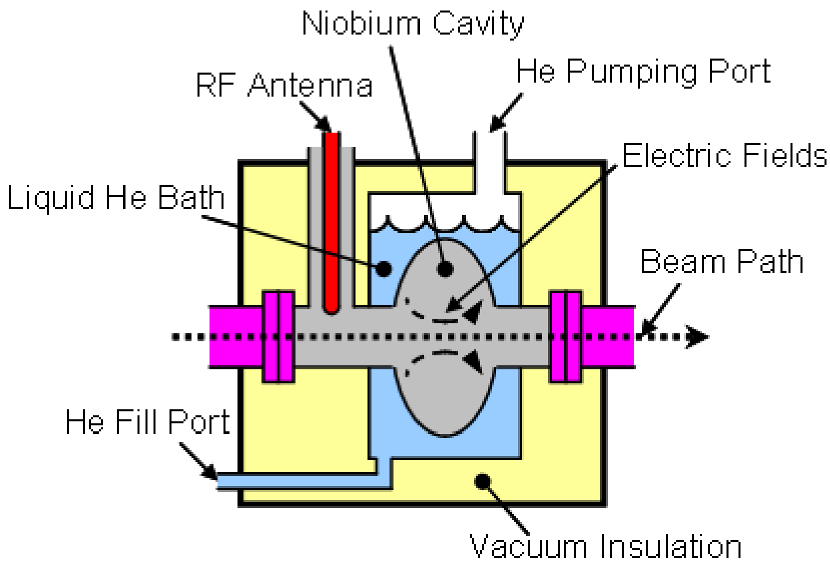

Figure 2.17: A simplified diagram of an SRF cavity in a helium bath with RF coupling and a passing particle beam [39].

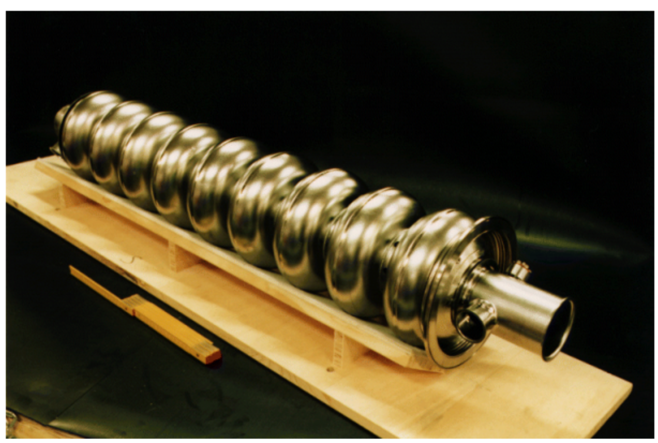

Figure 2.18: A photograph of the nine-cell niobium resonator for the TESLA Test Facility. At the right beam port the opening for the input coupler can be seen [42].

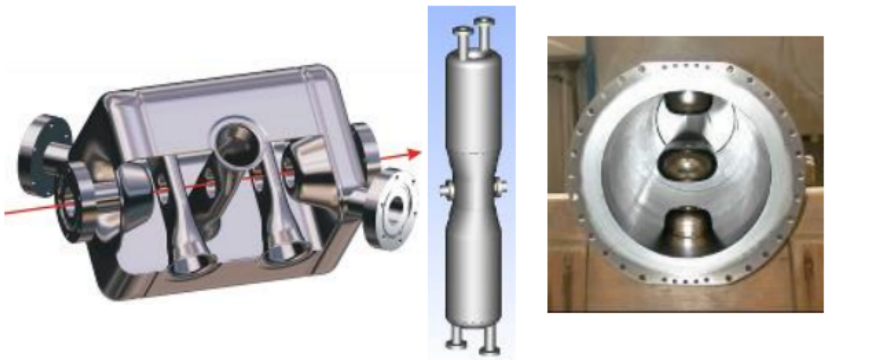

Figure 2.19: Other Superconducting cavities (spoke, HWR, QWR). These structures require a beta range greater that 0.1 and are ideal for continuous wave proton acceleration [9].

Chapter 3

Beam Dynamics Theory

This chapter provides the essential theoretical background behind the operation of the linear accelerator Machines. It will concern only Linear accelerators and not circular machines as their operation and theory are outside the aim of this thesis.The following chapters will shed light on the goals of the beam dynamics studies.

3.1. Relativistic Equations

The well know Lorenz relativistic factors β, γ are defined:

$$\beta = \frac{u}{c} \qquad \gamma = \frac{1}{\sqrt{1-\beta^2}} \tag{3.1}$$

where u is the speed of the particle and c the speed of light.
The Kinetic energy of the particle in special relativity is defined as the difference between the total and the rest energy:

$$E_{Kinetic} = (\gamma - 1)m_0c^2 \tag{3.2}$$

Finally, the momentum in relativistic terms is written:

$$p = \gamma m_0 \beta c = \frac{\beta}{c}E \tag{3.3}$$

where E is the total energy [57], [36] [10].

3.2. Lorenz Force

One of the basic equations in this study is the Lorenz force, the force that a charged particle receives when moving through Electric and magnetic fields [57], [36].

$$\overrightarrow{F} = q(\overrightarrow{E} + \overrightarrow{u} \times \overrightarrow{B}) \tag{3.4}$$

It is known that:

$$\overrightarrow{F} = m\frac{d(\gamma \overrightarrow{u})}{dt} \tag{3.5}$$

If we combine equations 3.4 , 3.5 we find the basic equation that describes the movement of the particles inside the field:

$$m\frac{d(\gamma \overrightarrow{u})}{dt} = q(\overrightarrow{E} + \overrightarrow{u} \times \overleftarrow{B}) \tag{3.6}$$

3.3. Energy Gain on an RF Gap

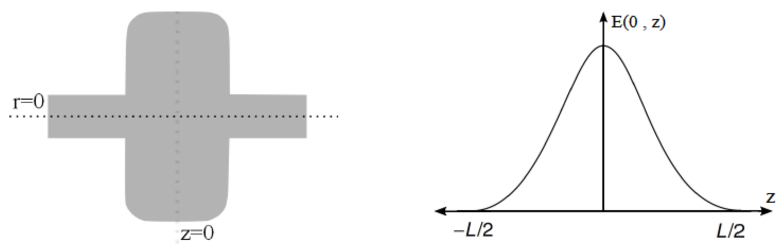

Figure 3.1: RF Pillbox cavity and its Axial electric field [57].

The energy gain of a particle in an RF gap is :

$$\Delta W = q \int_{-L/2}^{L/2} E(0,z)cos(\omega t(z) + \phi)dz \tag{3.7}$$

which becomes after a simple trigonometric transformation:

$$\Delta W = qV_0 T cos\phi \tag{3.8}$$

Where q is the charge, V_0 the effective axial voltage and T the transient time factor [10].

3.4. Particle Coordinate System

The coordinates of the particles in beam are relative to the coordinates of the reference particle. Reference particle is an ideal particle in synchronism with the RF fields that moves in the center of the beam pipe.
Every Particle in the beam dynamics is fully described by a one- column matrix which contains the positions and divergences at both transverse planes (x-x',y-y') the position along the beam axis z and the factor $\frac{\Delta p}{p_0}$ which describes the deviation from the reference particle momentum:

$$M = \begin{bmatrix} x & x' & y & y' & z & \frac{\Delta p}{p_0} \end{bmatrix}^T \tag{3.9}$$

Instead of the z coordinate we can use the $\Delta\phi$ and instead of momentum ΔW which are the phase and energy from difference the reference particle respectively. The definition of the divergences is :

$$x' = \frac{p_x}{dz}, y' = \frac{p_y}{dz} \tag{3.10}$$

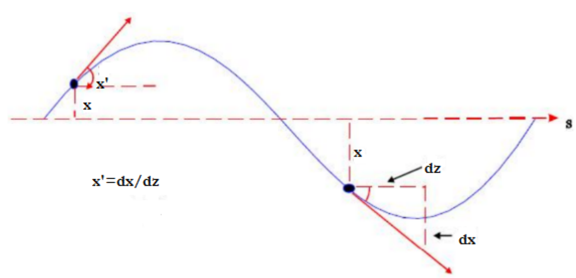

Figure 3.2: Definition of the particles coordinates

The following two equations express the relationship between the z coordinate and phase, and phase-energy:

$$z = -\frac{\beta\lambda}{360}\Delta\phi \tag{3.11}$$

$$\frac{\Delta p}{p_0} = (\frac{\gamma}{\gamma+1})\frac{\Delta W}{W_0} \tag{3.12}$$

Where β, γ are the relativistic factors [57].

3.5. The matrix Formalism

Starting from the equation of Lorenz force assuming linear beam dynamics (forces are linear proportional to the position. The equation of motion of the particles can get simplified to with some approximations to the Hill's equation and describes a pseudo-harmonic oscillations called betatron oscillations:

$$u'' + K_u u = 0 \tag{3.13}$$

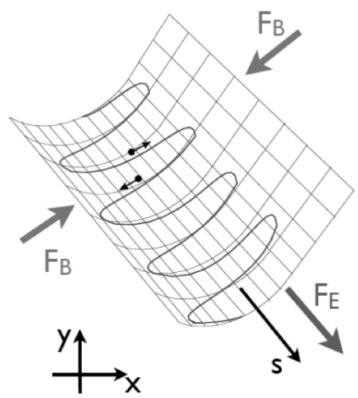

The equation of motion in transverse planes resembles the differential equation of the harmonic oscillator, where u can be both x,y . Coupling has not been taken into regard leading to the fact that the equations of motion are uncorrelated in both planes. Not every element obeys this principle (for example solenoids present correlation). This principle plays a major role in the equations of this section. For every element in a linear accelerator that follows this principle we have the following solutions of the equations of motion:

$$\begin{pmatrix} u(z) \\ u'(z) \end{pmatrix} = \begin{pmatrix} C_u(z) & S_u(z) \\ C'_u(z) & S'_u(z) \end{pmatrix} \begin{pmatrix} u_0(z) \\ u'_0(z) \end{pmatrix} \tag{3.14}$$

where u,u' can be x,y and x',y' respectively. The general solution of this equation ,for example for x transverse plane , has the form :

$$x(s) = \sqrt{\epsilon\beta(s)} cos(\phi(s)) \tag{3.15}$$

the phase is given by :

$$\phi(s) = \int_0^s \frac{d\sigma}{\beta(s)} \tag{3.16}$$

We can define also :

$$\alpha(s) = -\frac{\beta(s)}{2} \tag{3.17}$$

$$\gamma(s) = -\frac{1+\alpha^2}{\beta(s)} \tag{3.18}$$

α, β, γ are called Twiss parameters, whereas ϵ is called emittance (see next section)
This kind of elements can be represented by this 2×2 matrix.Generally we can combine these matrices on a 4×4 matrix that can include coupling effects. Furthermore these matrices can be extended to include more information for the particles' movement such is energy,longitudinal position, spin vector etc. :

$$\begin{pmatrix} x(z) \\ x'(z) \\ y(z) \\ y'(z) \end{pmatrix} = \begin{pmatrix} C_x(z) & S_x(z) & 0 & 0 \\ C'_x(z) & S'_x(z) & 0 & 0 \\ 0 & 0 & C_y(z) & S_y(z) \\ 0 & 0 & C'_y(z) & S'_y(z) \end{pmatrix} \begin{pmatrix} x_0(z) \\ x'_0(z) \\ y_0(z) \\ y'_0(z) \end{pmatrix} \tag{3.19}$$

As it is easily understood, the element acts like a system with a transfer matrix which transforms the initial positions and divergencies (with 0 indexes) at the entrance of the element to the ones at the exit of the element.
for Various beam manipulating elements we the folowing matrices:

- Drift Space: Any Drift Space with length l can be easily described by the following matrix formulation:

$$\begin{pmatrix} u(z) \\ u'(z) \end{pmatrix} = \begin{pmatrix} 1 & l \\ 0 & 1 \end{pmatrix} \begin{pmatrix} u_0(z) \\ u'_0(z) \end{pmatrix} \tag{3.20}$$

- Quadrupole Magnet: The matrix formalization for a quadrupole in the focusing plane is:

$$\begin{pmatrix} u(z) \\ u'(z) \end{pmatrix} = \begin{pmatrix} cos\phi & \frac{1}{\sqrt{k}} sin\phi \\ -\sqrt{k} sin\phi & cos\phi \end{pmatrix} \begin{pmatrix} u_0(z) \\ u'_0(z) \end{pmatrix} \tag{3.21}$$

  where k is the quadrupole strength, $\phi = \sqrt{k}l$ where l is the length of the quadrupole.

These matrices are called transfer matrices, and if we have a beam line with multiple elements with their transformation matrices $\mathfrak{R}_j$ where $j = 1, 2, 3...$ the number of elements .Then, the full transformation matrix is [57], [36], [10], [24] :

$$\mathfrak{R} = \mathfrak{R}_j \mathfrak{R}_{j-1} ... \mathfrak{R}_1 \tag{3.22}$$

3.6. Beam Dynamics Parameters

In order to observe the behavior of the beam we use the transverse (x-x' (horizontal), y-y' (vertical)) and $\Delta\phi - \Delta W$ plots which are called phase-spaces. From phase-spaces we can evaluate emmitance which is given by the following equation:

$$\epsilon_{rms} = \sqrt{\langle x^2\rangle\langle x'^2\rangle - \langle xx'\rangle^2} \tag{3.23}$$

where,

$$\langle x^2\rangle = \frac{1}{N}\sum_{i=1}^{N}(x_i - \langle x\rangle)^2 \tag{3.24}$$

$$\langle x'^2\rangle = \frac{1}{N}\sum_{i=1}^{N}(x'_i - \langle x'\rangle)^2 \tag{3.25}$$

$$\langle xx'\rangle = \frac{1}{N}\sum_{i=1}^{N}(x_i - \langle x\rangle)(x'_i - \langle x'\rangle) \tag{3.26}$$

Emittance indicates the quality of the beam and it is the region occupied by the beam in the phase-space plots. In that way, it is easily understandable that we define three independent emittances. Emittancce depends on the source characteristics and on other effects during the beam transfer. The rms emmitance is a statistical magnitude that expresses the spread of the beam particles around their varycenter. [57], [10], [24]

The function of the rms envelope is an ellipse:

$$\gamma(s)x^2 + 2\alpha(s)xx' + \beta(s)x'^2 = \epsilon \tag{3.27}$$

The parameters α, β, γ are the Twiss parameters and from them we can construct the beam matrix.

$$\sigma = \epsilon \begin{bmatrix} \beta & -\alpha \\ -\alpha & \gamma \end{bmatrix} = \begin{bmatrix} \langle x^2\rangle & \langle xx'\rangle \\ \langle x'x\rangle & \langle x'^2\rangle \end{bmatrix} \tag{3.28}$$

From the matrix formalism of the 3.31 we can easily derive that:

$$\epsilon = det(\sigma) \tag{3.29}$$

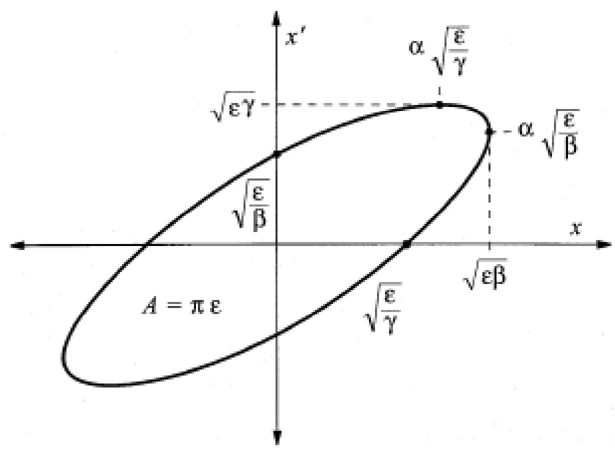

Figure 3.3: Phase Space Ellipse anf its parameters

Furthermore the area covered by the beam is $A = \pi\epsilon$
The transfer and the beam matrix (which describes the rms values of the distribution) are connected under the following equation:

$$\sigma_1 = \Re\sigma_0\Re^T \tag{3.30}$$

Emittance has dimension of length or length times angle (mrad). Liouville's theorem states that, under the influence of conservative forces, the particle density in phase space is invariant [24]. It follows that ϵ_{rms} of the distribution in a phase space is constant. Emittance is preserved only in linear systems, (systems where the external forces acting on the beam are linear), but when particles are accelerated the values used so far to describe the transverse emittance (x,x',y,y'), don't preserve the numerical emittance value if the velocity is changing. Indeed, the acceleration process modies only the longitudinal component of the velocity so that the angular divergence decreases as the velocity increases, which means that the emittance decreases during acceleration. In this case the unnormalized emittance is considered Therefore it is more convenient to define the so-called normalized emittance which is not affected by acceleration, since it uses the transverse momentum variable instead of the divergence. The normalized emittance is related to the unnormalized one by the following expression:

$$\epsilon^* = \beta\gamma\epsilon \tag{3.31}$$

where β, γ are the relativistic factors, and ϵ is the unnormalised emittance. [57], [36], [10], [24], [26]. The maximum emittance that an beam transport element is able to transmit is called acceptance.

3.7. RF Transverse Defocusing

A principle named the incompatibility theorem suggests that when we have longitudinal acceleration and stability this results in defocussing forces on transverse planes. When a particle propagates through an RF gap it feels also an radial kick from electric and magnetic fields. The field variation in time, the increase of the velocity of the particles across the gap and the radial particle distribution across the gap are the causes of this phenomenon called RF defocussing.
For example we can write the transverse momentum impulse to a particle delivered by the RF fields of a synchronous traveling wave:

$$\frac{dp_r}{dt} = q(E_r - \beta c B_\theta) = -q\gamma_s(1 - \beta\beta_s)I_1(Kr)E_0 T sin\phi \tag{3.32}$$

where E_0 is the axial electric field , T the transit time factor and I_1 the 1^{st} order modified Bessel function. Finally with the index s we separate the relativistic factors of the particle from the synchronous ones. K is defined:

$$K = \frac{2\pi}{\gamma_s \beta_s \lambda} \tag{3.33}$$

The RF defoccussing is greater at low velocities and is getting lower as we reach the relativistic limit as the electric force is cancelled by the magnetic force . The Laplace equation in the cavity gives:

$$\frac{\partial^2 V}{\partial^2 x} + \frac{\partial^2 V}{\partial^2 x} + \frac{\partial^2 V}{\partial^2 x} = 0 \tag{3.34}$$

The Earnshaw's theorem states that the potential cannot reach a maximum or minimum at the empty space. As a consequence in our case if the longitudinal forces provide focusing at a given point, the two transverse-force components cannot both be focusing at the same point. Moreover in a 1956 paper Panofsky and Wenzel considered the transverse momentum imparted to a fast particle moving parallel to the axis of the cavity a relation called Panofsky-Wenzel theorem :

$$p_\perp = \left(\frac{q}{\omega}\right) \int_0^l (-i)\nabla_\perp E_z dz \tag{3.35}$$

Where l is the cavity length. The Panofsky-Wenzel (PW) Theorem was originally used to describe the relationship between the longitudinal and transverse wake fields produced by a beam as it travelled through a device. A particle, as it travels through a device and encounters an aperture (or some other perturbation), generates a wave excitation that can produce an integrated longitudinal and transverse momentum kick [10], [24], [9].

3.8. Longitudinal Beam Dynamics

As equation 3.5 indicates the responsible field for the acceleration is the electric field. In order to achieve proper acceleration the particles must remain synchronous to the field. The synchronicity condition depends strongly on the operational mode of the accelerating structure. We call operational mode the phase difference between two consecutive cells in an accelerating structure. For example in a Alvarez Drift Tube Linac two consecutive gaps have zero phase difference between them. Thus, Drift Tube Linac is an 0 (or 2π) mode, with a synchronicity condition:

$$L = \frac{u}{f_{RF}} = \beta c \frac{\lambda}{c} = \beta\lambda \tag{3.36}$$

where u is the particle speed, f_{RF} the RF frequency and λ the wavelength.

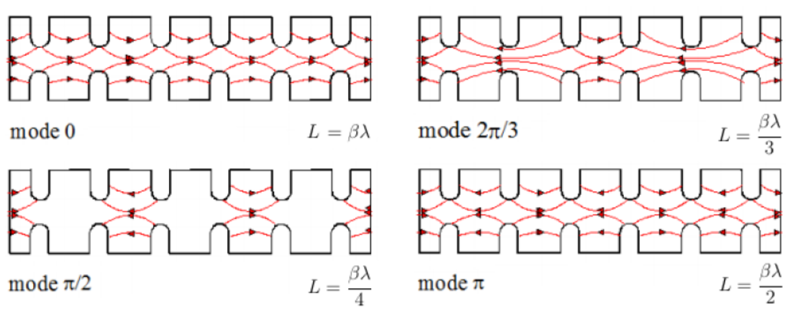

Figure 3.4: Operational Modes and their synchronicity Conditions [36]

As the figure 3.6 indicates the reference particle is exactly synchronous with the

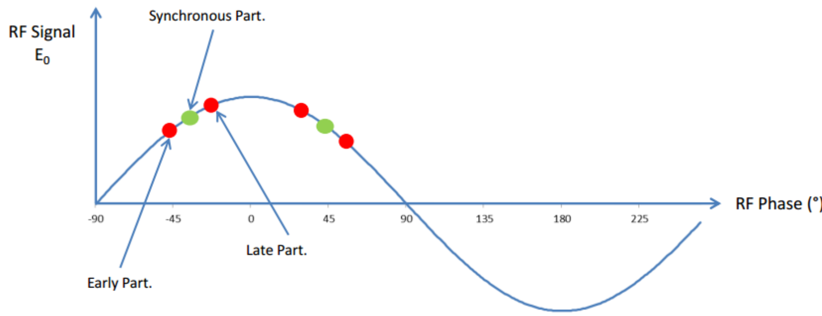

Figure 3.5: Synchronicity and bunching of the particles in an RF E/M field [9].

RF field. That means that a particle of the beam that comes after the reference particle feels a force that tends to compensate this phase difference from the reference particle, and absorbs more energy from the field. Similarly an early particle absorbs an slight lower amount of energy in order to come closer to the reference particle. With this simple principle we achieve acceleration and longitudinal focusing of the beam as it propagates through the RF cavities. Likewise, The alternation of the electric field causes different effects on the beam in a 2π RF period [10]:

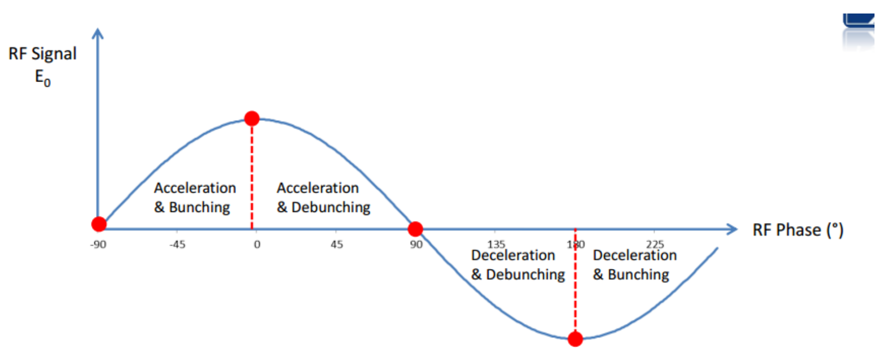

Figure 3.6: The manipulation of beam shape inside an alternating accelerating field [9].

At this point two important figures of merit can be presented:
Longitudinal Phase advance per unit of length:

$$k_{0l} = \sqrt{\frac{2\pi q E_0 T sin(-\phi_s)}{mc^2 \beta_s^2 \gamma^3 \lambda}} \tag{3.37}$$

and the Longitudinal Phase advance per period $[N\beta\lambda]$:

$$\sigma_{0l} = \sqrt{\frac{2\pi q E_0 T N^2 \lambda sin(-\phi_s)}{mc^2 \beta_s \gamma^3}} \tag{3.38}$$

Where the index s refers to the reference particle quantities.E_0 is the average axial electric field, T the transient time factor,λ the wavelength and $\beta, \gamma therelativisticfactors$

3.9. The separatrix

When designing an accelerator one must make sure that the particles in a bunch stay in stable trajectories. The movement of a particle inside an alternating RF field produces oscillations on phase and energy, an energy which is easily evaluated in linacs and depended on the structure geometry. As mentioned above , in order to achieve the proper focusing and bunching of the beam we take advantage of this synchronicity between the oscillations of the RF field and the reference particle. In that way the early particles compared to the reference feel a smaller field and the later ones feel a greater field. This fact lead in stable bunches of particles near the reference particle [57], [36], [10], [24], [26]. The difference equations for the energy change of a particle compared to reference particle are:

$$\Delta(W_i - W_s) = qE_0TL(cos\phi_i - cos\phi_s) \tag{3.39}$$

$$\Delta(\phi_i - \phi_s) = -2\pi N \frac{(W_i - W_s)}{mc^2 \gamma_{i,s}^3 \beta_{i,s}^2} \tag{3.40}$$

if we make the variables continuous , by assuming that we have a continuous field we obtain the differential equations of motion:

$$\frac{d(W_i - W_r)}{ds} = qE_0TL(cos\phi_i - cos\phi_r) \tag{3.41}$$

$$\gamma_s^3\beta_s^3\frac{d(\phi_i-\phi_s)}{ds}=-2\pi\frac{(W_i-W_s)}{mc^2\lambda} \tag{3.42}$$

If we differentiate 3.42 and replace it at 3.41 we obtain the second order deifferential equation for motion:

$$\gamma_s^3\beta_s^3\frac{d^2(\phi-\phi_s)}{ds^2}+3\gamma_s^2\beta_s^2\left[\frac{d}{ds}(\gamma_s\beta_s)\right]\left[\frac{d(\phi-\phi_s)}{ds}\right]+2\pi\frac{qE_0T}{mc^2\lambda}(cos\phi-cos\phi_s)=0 \tag{3.43}$$

Solving the equation we obtain the Hamiltonian of the system (typically the energy) which contains the terms of kinetic energy and the potential.

$$\frac{2\pi}{2\beta_s^3\gamma_s^3\lambda}\left[\frac{W-W_s}{mc^2}\right]^2+\frac{qE_0T}{mc^2}(sin\phi-\phi cos(\phi_s))=H \tag{3.44}$$

We introduce the $\phi, \Delta W$ plot below showning some phase space trajectories.The boundary trajectory which distinghish the stable from unstable movement it is called the separatrix ,and satisfies the following equation:

$$\frac{2\pi}{2\beta_s^3\gamma_s^3\lambda}\left[\frac{W-W_s}{mc^2}\right]^2+\frac{qE_0T}{mc^2}(sin\phi-\phi cos(\phi_s))=-\frac{qE_0T}{mc^2}(sin\phi_s-\phi_s cos\phi_s) \tag{3.45}$$

The stable area inside the separatrix is called the bucket [57], [36], [10], [24], [26]. It is clear that the max energy corresponds for $\phi=\phi_s$:

$$w_{max}=\sqrt{\frac{2qE_0T\beta_s^3\gamma_s^3\lambda}{\pi mc^2}(\phi_s cos\phi_s-sin\phi_s)} \tag{3.46}$$

3.10. Space Charge

One more phenomenon which must be taken into consideration in our studies is the repulsive forces between the particles of the beam due to their charge state. Space-charge depends on beam distribution and intensity and affects the beam dynamics (cause of emmitance growth). In more detail, if we want to estimate the magnitude of this force we can follow this simple procedure: Assuming to have a beam with volume (η) and linear (λ) density propagating in a cylindrical beam pipe. Then this moving beam has a current density J.

All the three densities are connected to each other under the following equations:

$$\lambda=\pi\alpha^2\eta \qquad J=u\eta=\beta c\eta \tag{3.47}$$

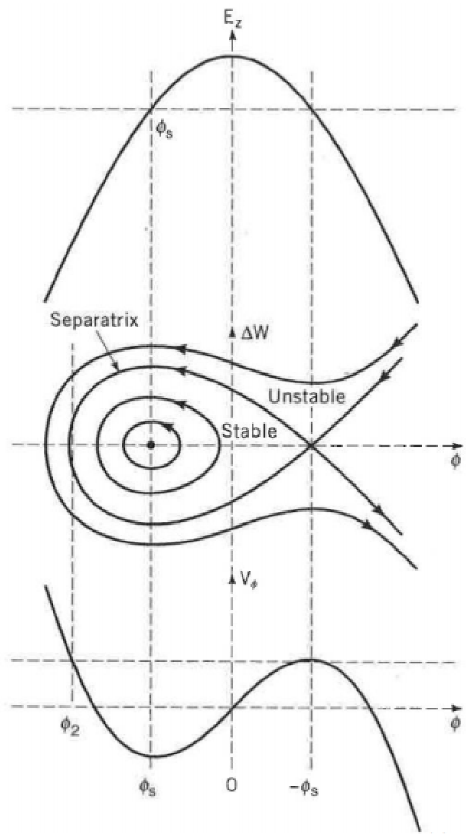

Figure 3.7: The axial electric field, the potential function and the separatrix .

By applying Gauss and Ampere laws to surface S and volume V:

$$\oint_L \overrightarrow{B} \cdot \overrightarrow{dl} = \mu_0 \int_S \overrightarrow{J} \cdot \overrightarrow{dS} \qquad\qquad \int_S \overrightarrow{E} \cdot \overrightarrow{dS} = \frac{1}{\epsilon_0} \int \rho dV \tag{3.48}$$

$$E_r 2\pi r = \frac{\eta}{\epsilon} \pi r^2 \Rightarrow E_r = \frac{\lambda r}{2\pi\epsilon_0\alpha^2} \tag{3.49}$$

$$2\pi r B_{phi} = \mu_0 J \pi r^2 \Rightarrow B_\phi = \frac{\lambda\beta r}{2\pi\epsilon c\alpha^2} = \frac{\beta}{c} E_r \tag{3.50}$$

From the Lorenz force equation we estimate the force exerted from the space charge to a particle:

$$F_r = e(E_r - \beta c B_\phi) = \frac{e}{\gamma^2} \frac{\lambda}{2\pi\epsilon_0} \frac{r}{\alpha^2} \tag{3.51}$$

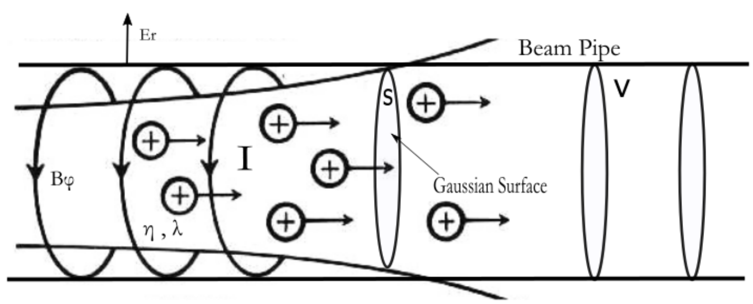

Figure 3.8: Space Charge fields.

As we can see from this equation the repulsive force is inversely proportional to γ^2, so it decreases as the velocity increases.

Chapter 4

Linacs At CERN

This Thesis is focused at Linacs and their Basic elements, thus Linacs at CERN will be discussed in detail at this chapter. Linear accelerators are the first accelerator stages at the large CERN accelerator chain and often are called : *"injectors"*. There are two operating hadron Linacs at CERN (Linac2, Linac3) , and Linac4 is at the commissioning stage. Furthermore, there are designs and Test facilities for a Compact Linear Collider (CLIC) and various designs of accelerators for medical applications.

The CERN hadron Linacs are described below:

4.1. Linac1

Linac1 was the first linear accelerator of CERN, it was fully commissioned in 1959 when delivered 50 MeV protons to PS. Linac1 accelerated also light ions (deuterions, alpha particles, oxygen , sulfur ions for fixed target experiments at SPS. Linac 1 was replaced at 1978 by Linac2. [45]

4.2. Linac2

Linac2 is the current accelerator for the injection of protons along the entire CERN accelerator chain. The proton source is a bottle of hydrogen at the beginning of the accelerator. Hydrogen atoms pass through an electric field to separate the atom from its electrons, permitting only at the protons to enter at the accelerator. Linac2 will end its service and will retire at 2020 when it will be replaced by Linac4. Linac2 gives at the entrance of the Booster pulsed beams of up at 175 mA at 50 MeV. The ion source is a Duoplasmaton giving a beam current of up to 300 mA connected to the hydrogen bottle. The preinjector for the Linac2 is 4-vane RFQ (93 kV injection energy , output energy 750 keV) which replaced the initial 750kV Cockroft-Walton preinjector directly connected to the DTL tanks. The complete Layout of Linac 2 is shown in the Figure 4.1.

When Linac2 replaced Linac1 offered an increase at current and pulse length by a factor of 2 when simultaneously increased the reliability and reduced maintenance. Until now, Linac2 counts more than 30 years in service, although the need for its replacement is now present to achieve higher values of Linac energy and due to various problems that affect its operation. [44], [46]

Figure 4.1: The Linac2 layout at CERN. One can recognize the RFQ at the beginning of the acceleration line, and then the drift tubes until the end of the room (orange cavities) with all their supporting systems for vacuum, cooling and RF excitation. At the center of the picture Richard Scrivens and Christian Mastrostefano of BE-ABP-HSL group with the Duoplasmatron ion source for Linac 2. [44]

Thus, in June 2007 Cern approved the construction of the 160 MeV Linac4 which is placed in a new building parallel to the present Linac2 location.

4.3. Linac3

Linac3 injected its first beam to PS booster at on June 1994 and is built inside the linac 1 hall. The goal from its design was to meet the expectations of light and heavy ions experiments on CERN Linac3 was constructed to accelerate lead ions to the energy of 4.2 MeV/u; The ion beam is produced by an Electron Cyclotron Resonance Ion Source (ECRIS) by a microwave heated plasma. After the extraction of the beam with the energy of 2.5 keV/u there is the LEBT were the mixture of lead charge states (also there is an oxygen beam created by the oxygen supported plasma which is used for the ionization of the pure lead) are separated in a spectrometer. After the spectrometer the beam is ready for the injection into the RFQ (2.66m long, 101.28 Mhz) with a pair of solenoids and a triplet of quadruples. The output of the RFQ is ions of energy of 250 keV/u which are injected to the next stage the MEBT. The Medium Energy Beam Transport contains four magnetic quadrupoles and a four gap RF cavity. The magnetic quadrupoles match the beam to the tanks and the RF cavity matches the longitudinal parameters. The last part of Linac3 is an IH-Structure 8.13 m long which accelerates the beam to 4.2 MeV/u. The IH is constructed by 3 cavities one with the frequency of the RFQ and the rest two at the operational frequency of 202.56 MHz. To achieve the focusing of the beam there are four triplets of quadrupoles two at the first cavity and one between each gap of the IH cavities. In addition to the Linac3 elements there are diagnostics performing the vital measurements at Linac3. [47]. The Linac3 inside its hall is shown in Figure: 4.2

Figure 4.2: The Linac3 Layout. At the right part of the picture is the source in the cage and the spectrometer. At the foreground, the LEBT, the RFQ, the MEBT and the IH tanks of the structures can be recognized. [47]

4.4. Linac4

Linac 4 is located in a new building in an underground tunnel connected to the PSB. The building contains the RF equipment the power supplies and the electronics for the new accelerator. The new Linac is expected to increase the brightness of the Proton Sychrotron Booster by a factor of 2 making feasible the increase of the LHC luminosity in the future. The main Linac4 parameters are based on the requirements for PSB injection. The beam dynamics are adjusted to the needs of the LHC while the number of ions per pulse are defined by ISOLDE experiment. The operating frequency of Linac4 is dictated by the RF equipment available from LEP and the RFQ. The Linac architecture (total Linac length 86 meters) is similar to the modern Linacs with the source (45 keV) the RFQ (3 MeV), the chopper lines and the accelerating structures (DTL (50 MeV , 7 CCDTL modules up to 102 MeV and the PIMS (Pi-mode cavity) cavity which deliver the beam to final energy. After the PIMS there is the injection line to PSB. It is essential to mention that, the Linac4 is operating with low duty cycle (0.1%), although the elements are designed for high duty cycle (10%) to support the future CERN projects for the Superconducting Proton Linac (SPL) that it is designed. In more detail, most of the hardware components (accelerating structures, magnets, RF high-power components, etc.) will be built for high duty cycle operation, while electronics (power supplies, etc.) and infrastructure (cooling, electricity) will be dimensioned for the low duty cycle in order to adjust Linac 4 to the futute plans. [52]

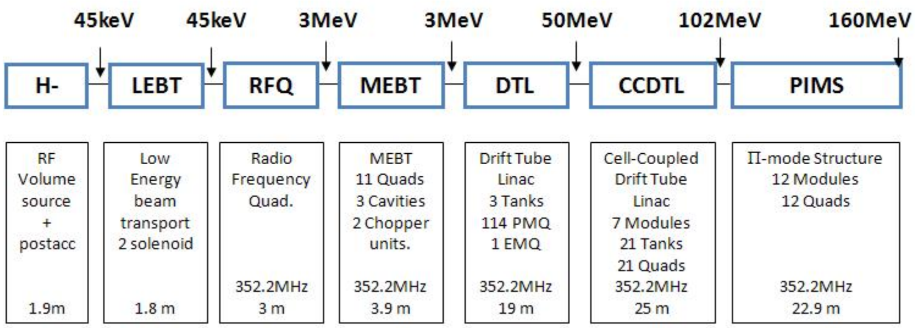

Figure 4.3: The full Linac4 Layout. [47]

The Linac beam parameters are the following:

Ion species:	H^-
Output energy:	160 MeV
Bunch frequency:	352.2 MHz
Max. rep. rate:	2 Hz
Beam pulse Length:	400 μ s
Chopping scheme:	
(transmitted bunches/empty buckets)	222/133
Mean pulse current:	40 mA
Beam power:	5.1 kW
N. particles per pulse:	1.0 $\times 10^{14}$
N. particles per bunch:	1.14 $\cdot 10^9$
Beam transverse emittance:	0.4 pmm mrad (rms)

Table 4.1: The Beam Parameters of Linac4 [48].

The RF structures of the accelerator perform at the frequency of 352.2 MHz reusing some infrastructures from LEP in general, klystrons, circulators, and waveguides.

Linac 4 Source: The beam parameters needed for Linac4 did not match to the existing sources designs. Furthermore designing and constructing a new source needs an extensive time period and it is not guaranteed that will reach the desired values. For that reason CERN decided to adopt an existing design and try to improve it. The requirements of the new accelerator Linac4 and the detailed comparison of the available sources' technologies led to choice of the DESY RF source (Figure: 4.4) as the H- source of the accelerator. It is an RF volume source, which operates without cesium to avoid beam line pollution with the lifetime of 25000 hours [56]. The characteristics of the source are the following:

Table 4.2: Source characteristics of DESY RF source [56].

Extraction Voltage:	35 kV
Beam Current:	40 mA
rms normalised emittance:	0.25 π mm mrad
repetition rate:	2 Hz

Although, Linac4 requires higher output current which will be achieved with special RF generator produced at CERN. The source was modified to achieve output energy before the RFQ at 45 KeV

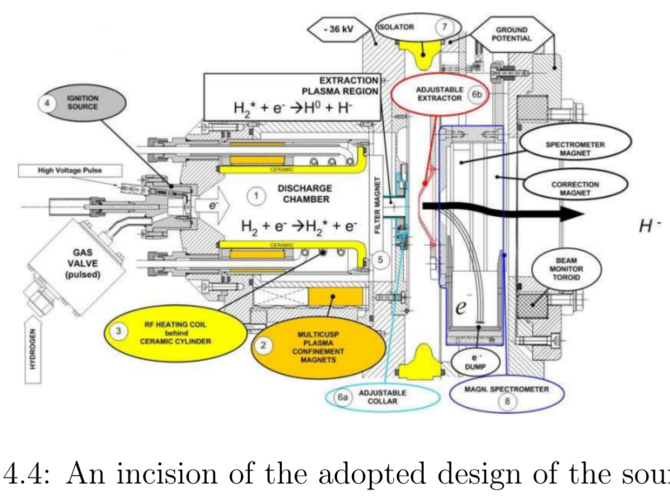

Figure 4.4: An incision of the adopted design of the source [56]

Linac4 LEBT: The basic role of the LEBT (Low-Energy-Beam-Transport) which is connected the source is to provide the necessary beam matching to transfer the beam from the source to RFQ. Furthermore contains diagnostics to monitor the operation of the source. [57] The mechanical design of the Linac4 LEBT is showed below in Figure 4.5. The big emittance and divergence of the beam extracted from the source pose the need of using large-diameter solenoids to achieve the focusing of the beam. Furthermore 2 sets of horizontal and vertical steerers are used for the steering of the beam at the acceptance of the RFQ [56].

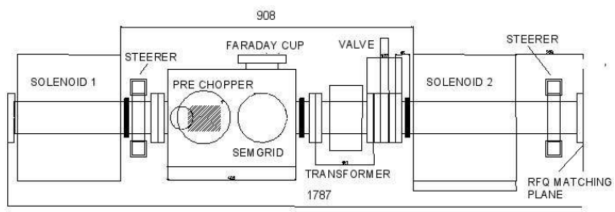

Figure 4.5: The detailed design of the Low Energy Beam Transport Line, with the solenoids, the steerers, the pre-chopper and the diagnostics [56].

Linac4 RFQ: The Beam Dynamics of the RFQ were extensively analyzed with PARMTEQM code. In order to avoid the design of the new RFQ CERN decided to sign a collaboration with French IPHI (Injecteurs de Protons de Haute Intensite) for the construction of the RFQ. CERN modified the RFQ designed by IPHI, resulting in a RFQ 3 meters long with 78 kV intravain voltage and surface field of 34 MV/m (1.84 bigger than the Kilpatrck limit). The RFQ of the Linac 4 takes the beam from the ion source (45 keV) and accelerates it until the energy needed for the injection at the DTL (3 MeV) . It operates at the frequency 352.2 MHz and is designed with higher duty cycle 10% [56].

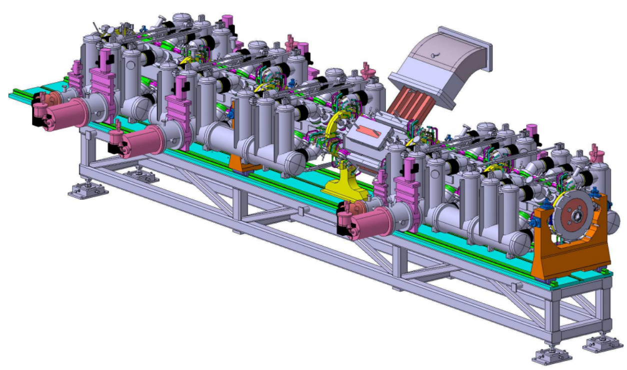

Figure 4.6: The Linac4 assembled RFQ. The RF and vacuum ports at RFQ body are distinguished [56].

The minimum value for the aperture a of RFQ is 0.18 cm and the maximum modulation factor m is 2.38. The whole RFQ cavity is made of three sections of one-meter long. The structure contains 32 round apertures for the tuners and four rectangular placed at the second section to host the RF inputs in order to achieve the RFQ accelerating field. At the first and the last section of the RFQ there are eight circular apertures for the vacuum pumping ports. A representation of the mechanical design of the Linac 4 RFQ is shown in Figure: 4.6 [56].

Linac4 MEBT (Medium Energy Beam Transport): An essential element of the modern accelerators is a chopper line which is often placed after the RFQ where the energy is still low, to achieve the minimum voltage and length of the chopper line. The MEBT of Linac4 consists of 2 chopper plates eleven quads and three cavities. (matching section-chopper-buncher cavity and dump -matching section). The mechanical design is shown at the Figure: 4.7. The chopper line contains a electrostatic beam deflector followed by a dump and its basic role is to stop selected sequences of beam bunches. It is substantial for these bunches to be cleared out at this point with low energy (because of low induced radiation) as they can cause losses at higher energies. This phenomenon is present when we inject beams bunches at the frequency of hundreds of Hz to accelerator parts that have frequency at the range of few MHz. In detail the chopper creates "holes" in the beam which are timed to the rise-time of the distributor of the PSB. In theory the, voltage limit of the deflector of the chopper line and the radiation for the dump of the beam dictate chopping at low energy, although this method poses difficulties to the design of the initial DTL tanks and in addition to the space charge effects at low energies, they lead to the increase of the chopping energy. For that reason the 3 MeV RFQ output energy had been chosen as the right balance. Exempt from that, a chopper must clean the first few tens of µs of the beam that are not stable. Also the chopper structure includes diagnostics and optical elements which are substantial to transfer the beam and match it from the exit of the RFQ to the entrance of the DTL. [56] [57].

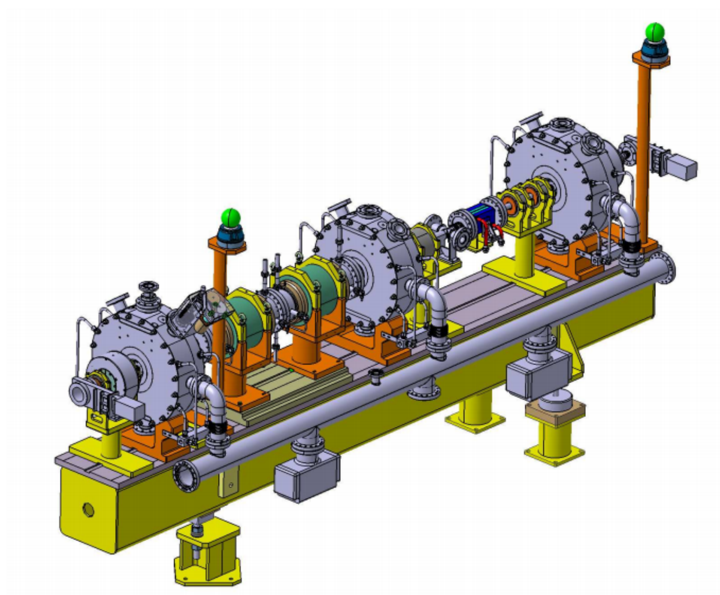

Figure 4.7: A 3D model for the Linac4 MEBT with the matching section (4 quadrupoles plus buncher cavity),the beam chopper (2 quadrupoles with chopper plates inside), the buncher cavity plus quadrupole plus dump (for the chopped beam), and an additional matching section (4 quadrupoles plus buncher cavity) [56].

The most essential constraint on the design of the chopper requires the rise time of the chopper to be smaller than the time between the two bunches. For the frequency of Linac4 (352 MHz) we require a rise-time of 2 ns. The bunches deflected by the chopper end-up to a dump with a shape of a cone. [56]

Table 4.3: Linac 4 MEBT characteristics [56]:

Efective chopper Length:	800 mm
Deflection Angle:	5.7 mrad

Linac 4 Drift Tube:

The DTL of the Linac4 has length of 19m and consists of 3 tanks which output the beam at 50 MeV. The Linac 4 DTL is shown in Figure 4.8. The RF power will be sent into the DTL from the tank klystrons. The first tank has 5 fixed tuners and the next ones 10 fixed tuner to adjust the electric field in the cavity with precise. Tank one uses only one klystron while the second and third tank use 2 klystrons. To keep the tanks on frequency during operation we use one movable tuner per tank [56].

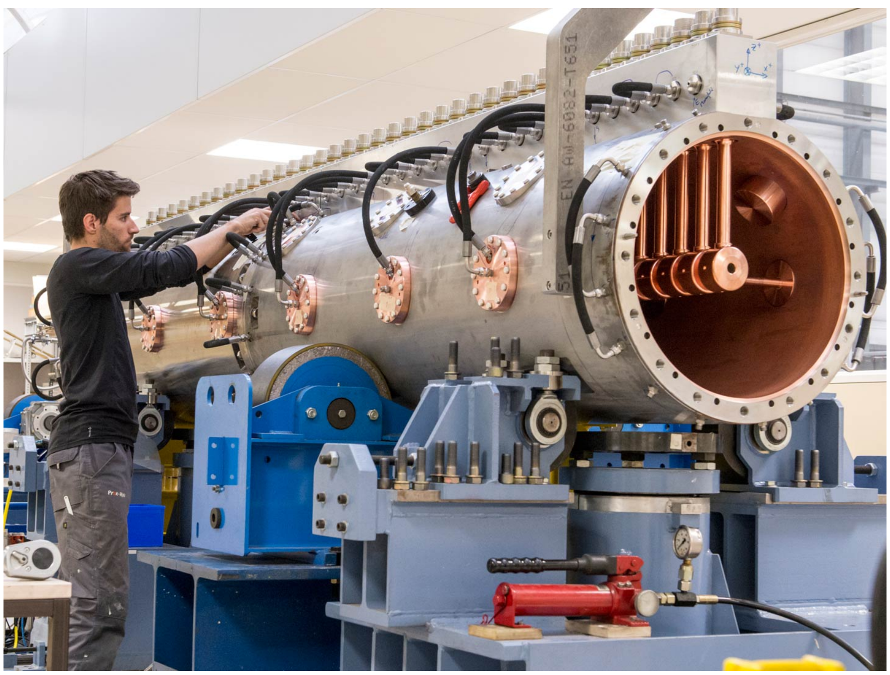

Figure 4.8: Linac4 Drift Tube under assembly [55].

One of the most important elements on a DTL is the kind of magnet it uses. Depending on the requirements different kind of magnets can be implemented. The inability to create a low cost, high duty cycle, high gradient electromagnet

(EMQ) fitting in the tanks of the the new Linac led to the adoption of Permanent Magnet Quadrapoles (PMQ). The PMQs have smaller diameters allowing smaller drift tubes leading to higher shunt impedance and less RF power [56].

The first drift tubes of the structure were lengthened to reduce transit time factor and the synchronous phase of the first DTL can be set to the spectrum $-35^o to -24^o$ to gain more space for the first quadrupoles. Then the synchronous phase is kept up at -24^o until the end of the tanks with a high accelerating gradient to reduce the DTL length [56].

Table 4.4: Linac 4 DTL parameters [57]:

Parameter	Tank 1	Tank 2	Tank 3
Cavity Length (m)	3.90	7.34	7.25
Cell per tank	39	42	30
Average accelerating field (MV/m)	3.1	3.3	3.3
Synchronous phase (deg)	-35 to -24	-24	-24
Focusing scheme	FFDD	FFDD	FFDD
Quadrupole magnet length (mm)	45	80	80

Linac4 Cell Coupled Drift Tube Linac (CCDTL):

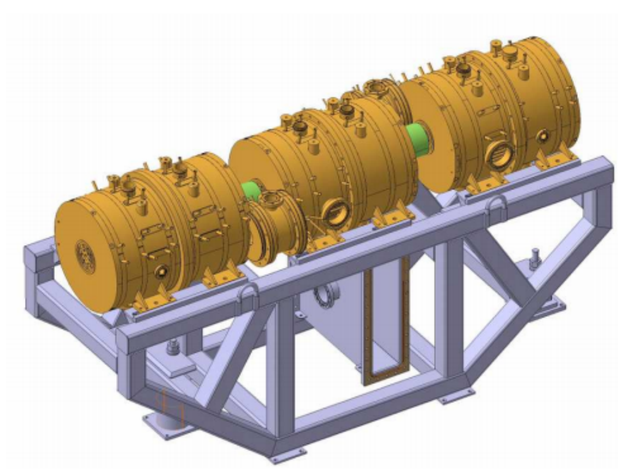

Figure 4.9: A 3D model of one CCDTL module for Linac4 [56].

Above the energy of 40 MeV different Linac structures are preferable due to their advantages (construction, cost, alignment tolerances, maintenance, space for diagnostics) compared to the DTL. Linac 4 uses a CCDTL which operates at the frequency of 352 MHz.This layout was adopted because it permits the accelerating tanks to contain 2 drift tubes which are connected by coupling cells. Between the two tubes the quadrupoles are placed resulting in a structure with focusing period of $7\beta\lambda$. The total length of the structure is 25m and we have 7 modules meaning , 21 tanks (every module is fed by one klystron and contains 3 tanks) and 21 Quads (Electromagnetic Quads adopted). [56]. The mechanical design of only one CCDTL module is shown in Figure: 4.9 **Pi-Mode Structure:**

Figure 4.10: The PIMS prototype designed and built at CERN [54]

.

The PIMS (PI-Mode-Structure) is the last structure of Lina4 with a total length of 21.5 m and consist of 12 modules (every module has seven cells) . The cell length is constant in each module but it changes from module to module as the particle velocity increases. PIMS (see Figure 4.10) accelerates the beam from 100 to 160 MeV. Initially the designers of Linac4 had adopted a SCL as the last stage of acceleration. However even with 20% smaller shunt impedance from the SCL the PIMS was chosen. This was because the PIMPS operates at 352.2 MHz as the other structures instead of the SCL that needs the double frequency leading to complication of the RF system. Moreover PIMS need only 84 cells instead of 400 for the SCL minimizing the construction cost and tuning effort. Between the tanks there are electromagnetic quadrupoles for transverse focusing of the beam. [53] [56]

Chapter 5

Simulation Tools

As it is mentioned above the matrix transformations are applied when we only have linear forces. Although the complexity of the phenomena that take place when a beam of particles propagates through various accelerating elements (such as space charge between the particles) makes necessary the use of simulation programs which provide us various numerical methods for the approximation of the solution of the equations of motion. In the field of particle and accelerator physics , simulations with these codes play a major role in our understanding and application of the beam dynamics laws. When we deal with an accelerator, the simulations interfere at all the stages from design and commissioning until the operation. The particle tracking code used in this thesis is the multi-particle tracking code Travel with its Graphical User Interface PATH Manager and the error study program Delta. This program includes space charge effects, pion decay and the process of mapped electromagnetic fields. During the Technical Student internship at CERN the author was in charge of the maintenance and the development of this code offering vital assistance to the members of HSL section.

5.1. The Travel Code and its GUI

Travel is a multi-particle tracking code which is written in Fortran 90 language and consists of various routines that are connected to each other. It is fully designed and developed at the BE-ABP-HSL section at CERN. Travel and its GUI PATH Manager are a powerful and complete code for simulating beams

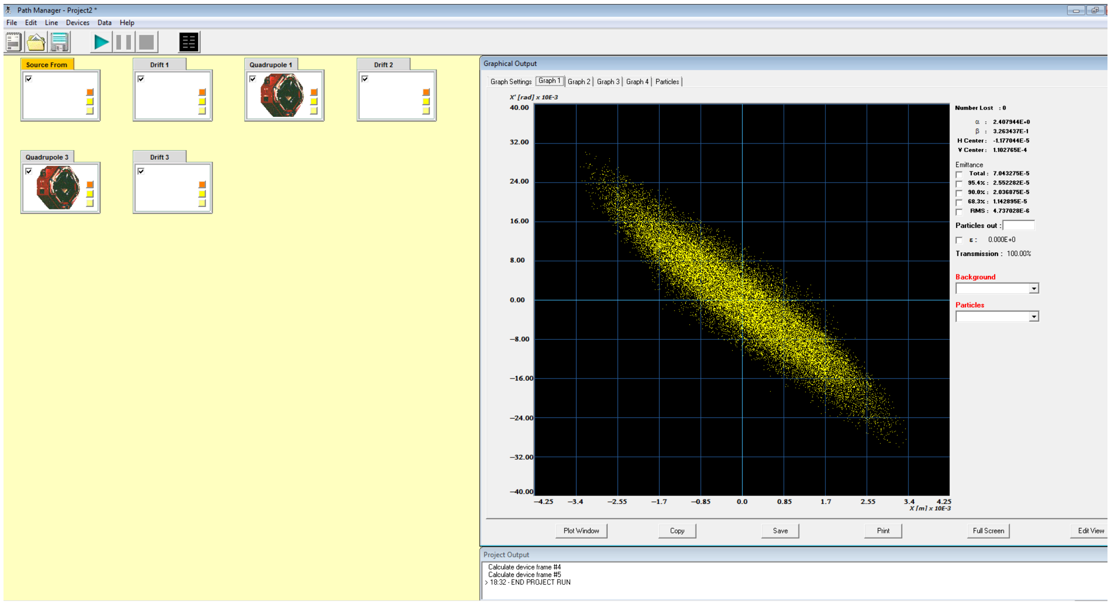

Figure 5.1: The graphical user interface of Travel Code PATH Manager

Figure 5.1 presents the PATH Manager Workspace. The workspace permits the visual representation of accelerating elements as icons which define a beam line. Right click on each element reveals their menu with their properties. The first icon from the left is the input beam. Path Manager offers the possibility to either import a existent project or create a new one. At the top of the main window there is the header menu that controls the program and the right side there are the phase spaces of the beam after each element with all the necessary beam information. At Figure 5.2 the interactive screen of Travel is shown.

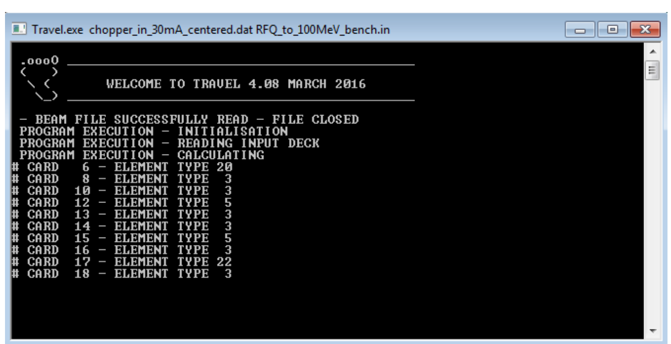

Figure 5.2: The command line Prompt of Travel

The code takes as input the following files:

- **Beam File:**
The file that contains the necessary information about the beam in the simulation. We can create this file in Path Manager which has a special menu (Figure 5.3) for this option, permitting the creation of a file that includes all the characteristics of the beam such as : kind and number of particles, energy, momentum, frequency, distribution, initial displacement etc. The extension of the beam file is .dat in order to be an input to Travel code. Other commonly used extensions for Beam files are .dst and .txt.

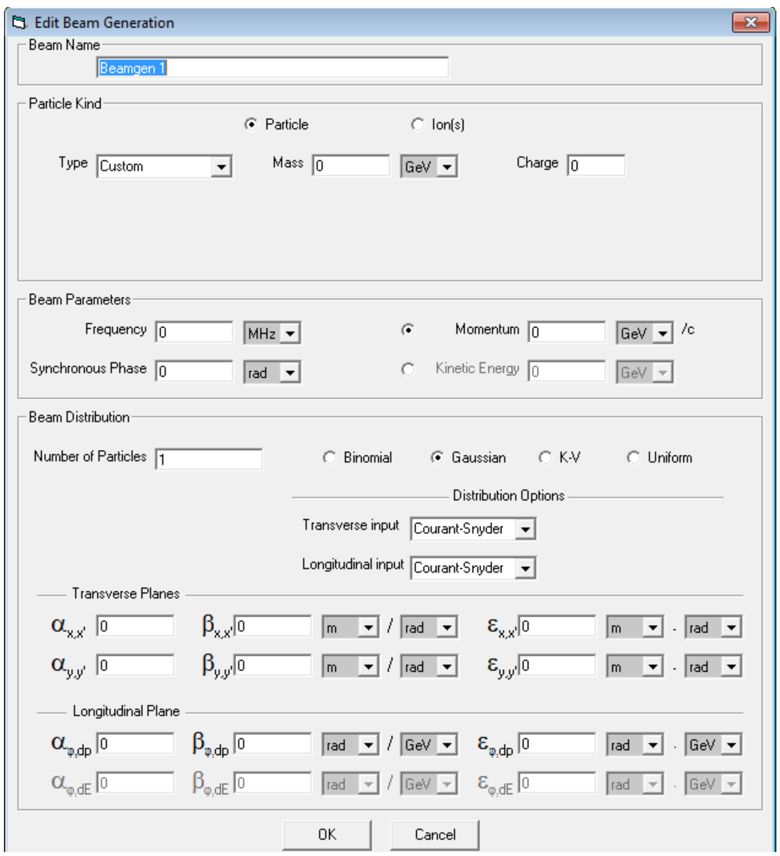

Figure 5.3: The Beam Generation Menu of Path Manager

- **BeamLine file:**
The beam line file contains all the elements that are needed for the transportation and guidance of input beam. Moreover contains vital information about the space charge, the kind of input and output plus other features

of the program. The detailed explanation of the elements and features are described in the Latest version of Travel Manual. [58]

Depending on the elements specified in the Beam Line file the program calls various routines during the execution and simulates the propagation of the beam through the chosen elements. At Figure 5.4 a typical Beam Line File is presented. The numbers at the left part are called "Cards". It is now clear that every feature of the code and accelerator element has its own routine (Card) with the proper equations. The structure of the program offers a vast spectrum of possibilities and choices, permitting the simulation of complex accelerating machines in a simple way. Path Manager interface is created with Visual Basic 6.0 and contains the same features and elements as Travel in a more user-friendly way.

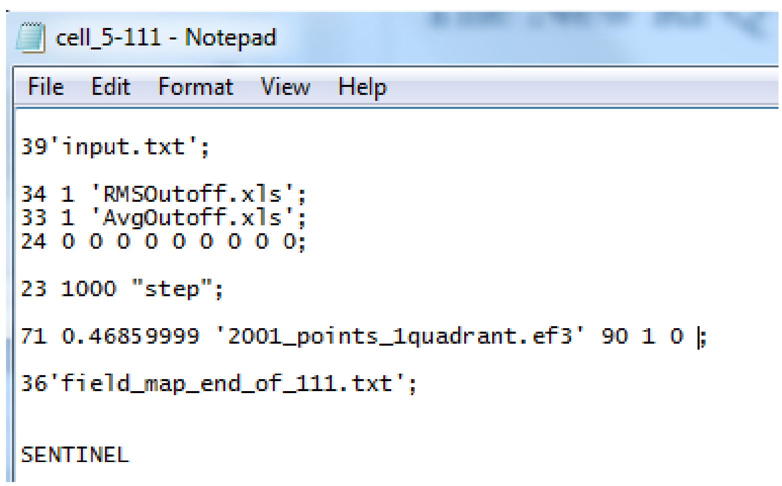

Figure 5.4: A typical Beam Line file

5.2. Performing Simulations

One can choose where the execution of the simulations will take place (Travel or Path Manager) . Path Manager and Travel are connected with each other with the generation of .dll files created during the phase of the compiling. Running a simulation in Travel is the same procedure as in Path Manager but without the visualization of the procedure. A simulation in Travel is executed if all the necessary inputs (Beam file, Beam Line and other input files) are in the same folder. A batch file at the same folder starts Travel.exe and supervises execution. The command line of Travel appears with the information of successful inputs and message that a simulation is in progress. Once we have results depending on what kind of output commands we have in Beam Line file (the output files can be for example, beam files in .dat, .txt or .dst formats or excel files) Travel generates the files at the same folder with the data. Moreover two additional files are created: Deadray.xsl that contains the information for the lost particles and a simulation log ,Travel Out.txt.

5.2.1 FODO Simulation with PathManager

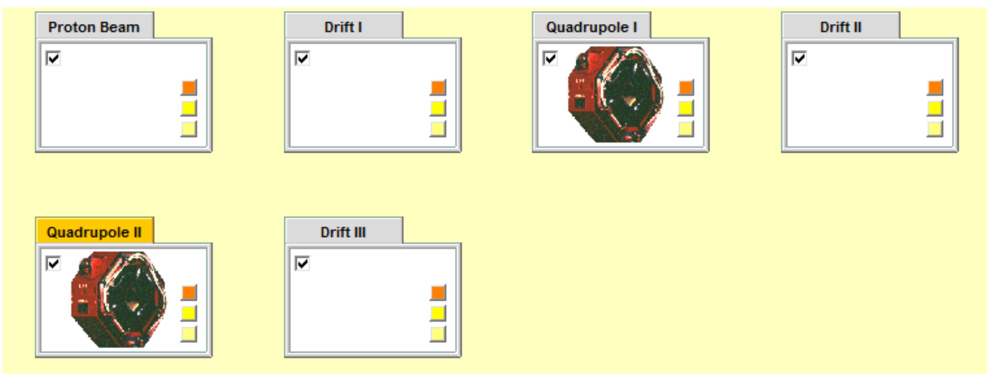

Figure 5.5: BeamLine used for the PathManager FODO project

In order to cast light to the characteristics of the code a simple example of simulating a proton beam through a FODO structure will be given. In Figure 5.5 the beam line of this example is presented. The icons represent the accelerating and focusing elements. For this example, we will use three drifts of 5 cm each and two quadrupoles. "Quadrupole I" has length 5 cm , aperture radius of 1 cm and it is focusing with field strength of +10 kGauss. The second quadrupole has the same characteristics however, it is defocussing with field strength of -10 kGauss. Below at Figures 5.6(a), 5.6(b) the menus of the two elements are presented, and appear with right click on the corresponding icon. For the drift tube the only input value is the length. The quadrupole needs as inputs the length, the pole-tip field and the pole-tip radius aperture. Moreover it has advanced options for the

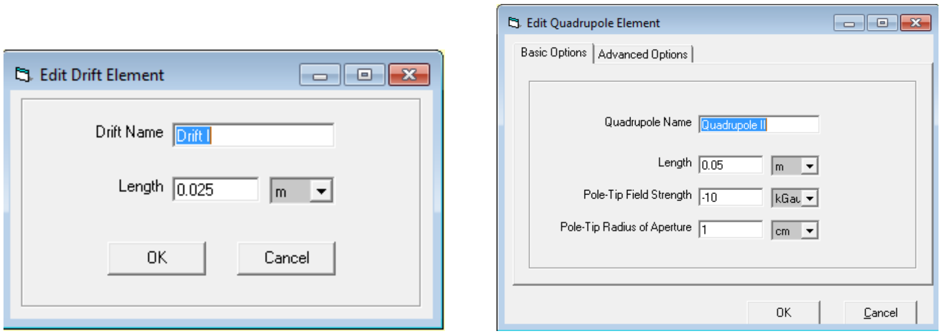

(a) Drift Menu (b) Quadrupole Menu

Figure 5.6: Element Menus at Path Manager

For this example we constructed a 50.000 particle, 352 MHz proton beam of 3 MeV initial energy with Gaussian Distribution. The Courant-Snider parameters of the beam at transverse planes (we do not consider longitudinal plane) are the following:

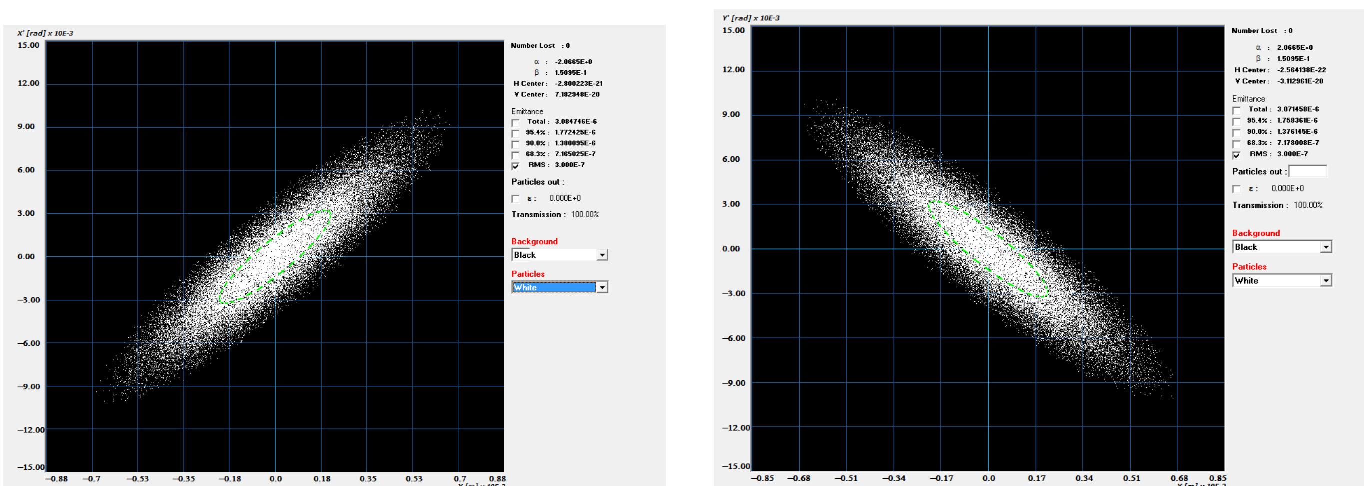

(a) Phase Space of input beam at horizontal plane (b) Phase Space of Input beam at Vertical plane

Figure 5.7: Phase Spaces for the input beam for the FODO example.

$\alpha_{xx'}$	-2.0665 m/rad
$\beta_{xx'}$	0.15095 m/rad
$\epsilon_{xx'}$	0.3 mm·mrad
$\alpha_{yy'}$	2.0665 m/rad
$\beta_{yy'}$	0.15095 m/rad
$\epsilon_{yy'}$	0.3 mm· mrad

The phase spaces of the input beam are presented at Figures 5.7. Path Manager plots the phase spaces of the beam besides the beam line. The beam line file for the simulation at Travel is:

```
fodo - Notepad
File  Edit  Format  View  Help
34 1 'PATHRMS.XLS ' ;
33 1 'PATHAVG.XLS ' ;
23 20;
3 0.025;
5 0.05 10 1 0 0 0 0 ;
23 20;
3 0.05;
23 20;
5 0.025 -10 1 0 0 0 0 ;
23 20;
3 0.025  ;
SENTINEL
```

Figure 5.8: Travel Beam line file for the FODO example

As before mentioned its line represents a command to the code to call certain routines. The routines that control the procedure are the TravelMain and RayRun routine. The first two lines define the kind of outputs. After the execution Travel will create two files as excel files (.xls extension) with the Average and RMS values of the simulation. The card number 23 followed by a number define the number of computational steps in which each element is divided. More computational steps make the simulation more accurate sacrificing simulation time. The codes 3, 5 correspond to drifts and quadrupoles respectively with all their input parameters. Finally the statement SENTINEL informs the program that the beam line file has finished. Below we represent the results of the simulations, x_{rms}, y_{rms} envelope for the FODO lattice where the focusing effects of the structure are marked via the plot window of PATH Manager:

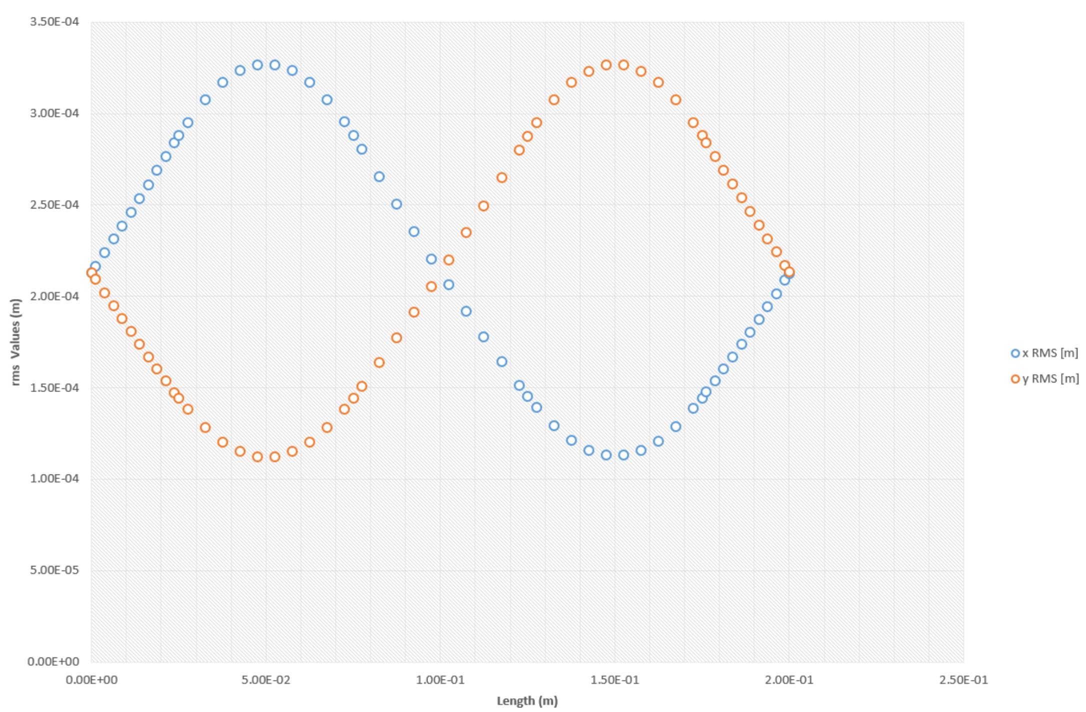

Figure 5.9: The rms size of the beam inside the FODO structure.

5.3. Structure of the code

This thesis is focused on studies of the Electromagnetic field processing routines of the code, with the aim to correct possible mistakes that affect the results and use the code to simulate for the first time the new high frequency RFQ developed at CERN. At this section we are going to present the structure of the code when it process a field map.

Travel gives us the opportunity to simulate the movement of a particle through an EM field (field map). The core of the program splits to two parts, firstly it evaluates the movement of the reference particle and then proceeds to all the particles of the beam. This is in agreement with the basic principle of beam dynamics that we evaluate all the coordinates of the beam particles are relative to the reference particle's coordinates. The key words for this section (see Figure 5.10) are the "mesh points" points with the field values of the discritized input field (black dots) and "computational points" , points that we divide the field for our calculations, depending on the accuracy we want (red dots). Between them , the movement of the particle will be simulated.

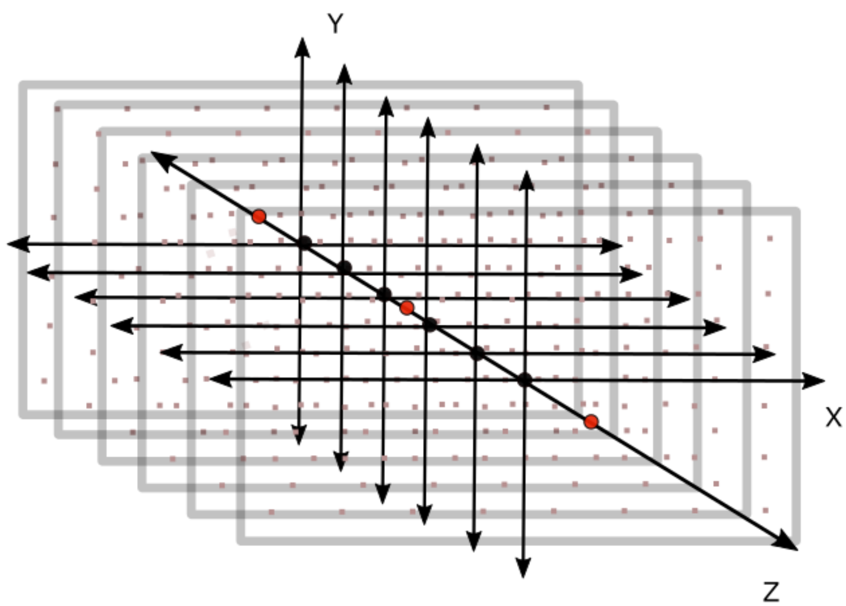

Figure 5.10: 3D schema of the input field map with the mesh points along the three axis and the computational points.

The code processes the field between two computational points and then repeats the same procedure until the end of the field map. Next step is to determine how many and which mesh points are between this segment; this is the role of the indexes along x,y,z axis . Once we find the mesh points we process the movement of the reference particle and the whole beam between the segment which is defined by the two computational points. Every particle is described by two vectors ($\overrightarrow{X} = [xyz]^T$ and $\overrightarrow{V} = [V_x V_y V_z]^T$) for position and velocity respectively. The global velocity is defined:

$$V = \beta c \tag{5.1}$$

where β is the relativistic factor and c the speed of light. The components along the axis are defined:

$$V_z = \frac{V}{\sqrt{1 + x'^2 + y'^2}} \tag{5.2}$$

where x',y' are the divergences of the particle at, x,y plane respectively are defined:

$$V_x = x' V_z \tag{5.3}$$

$$V_y = y' V_z \tag{5.4}$$

At this point we have to determine also the border values of the field at x and y axis, in other words the field borders.

The borders help us to determine if the particle is flagged dead or not during its movement inside the field. Now, after the necessary definitions inside the particle loop, the next step is to start the calculations in our discretized field. We have the x, y, z position for the particle and points with the values of the field (mesh points). We have defined which mesh points are near our particle at the current moment so we will use their information for the interpolation. Thus, we construct a cube [see :Figure 5.11] which contains the particle and the eight closest mesh points at the vertexes. Once the cube is constructed, their field data will be used to calculate the force received by the particle.

5.3.1 Field Interpolation

The most significant part of the code is the interpolation and integration routine. As we mentioned before, we use the information of the cube vertices to calculate the forces along the x,y,z axis. We make an estimation of the force exerted to the particle, depending on the position of the particle inside the cube.

Every field value is participating to the evaluation of the field at the particles' position multiplied by a weighted factor given by the ratios:

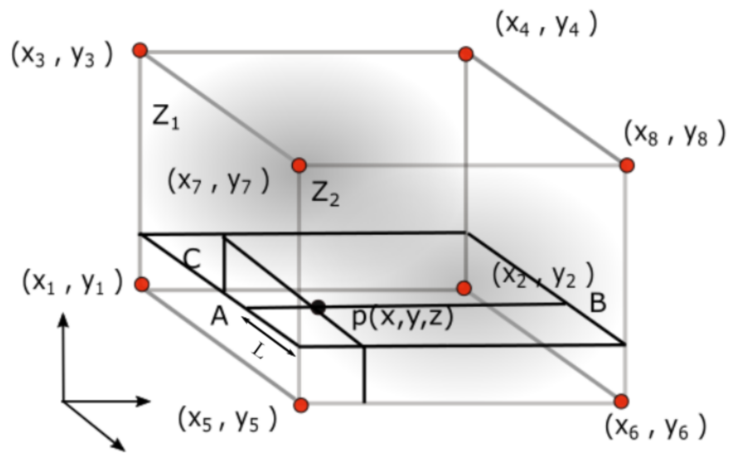

Figure 5.11: The Interpolation Cube.

$$A_{ratio} = \frac{y - y_1}{y_3 - y_1} \tag{5.5}$$

$$B_{ratio} = \frac{y - y_2}{y_4 - y_2} \tag{5.6}$$

$$X_{ratio} = \frac{x - x_1}{x_2 - x_1} \tag{5.7}$$

Then, we use the ratios to estimate the components of the field at point A ($E_i j$ i is component index and j the point index) :,

$$E_{xa} = \frac{1}{2}\left\{(1 - A_{ratio})(E_{x1} + E_{x5}) + A_{ratio}(E_{x3} + E_{x7})\right\} \tag{5.8}$$

$$E_{ya} = \frac{1}{2}\left\{(1 - A_{ratio})(E_{y1} + E_{y5}) + A_{ratio}(E_{y3} + E_{y7})\right\} \tag{5.9}$$

$$E_{za} = \frac{1}{2}\left\{(1 - A_{ratio})(E_{z1} + E_{z5}) + A_{ratio}(E_{z3} + E_{z7})\right\} \tag{5.10}$$

Similarly at point B:

$$E_{xb} = \frac{1}{2}\Big\{(1 - B_{ratio})(E_{x2} + E_{x6}) + B_{ratio}(E_{x4} + E_{x8})\Big\} \tag{5.11}$$

$$E_{yb} = \frac{1}{2}\Big\{(1 - B_{ratio})(E_{y2} + E_{y6}) + B_{ratio}(E_{y4} + E_{y8})\Big\} \tag{5.12}$$

$$E_{zb} = \frac{1}{2}\Big\{(1 - B_{ratio})(E_{z2} + E_{z6}) + B_{ratio}(E_{z3} + E_{z8})\Big\} \tag{5.13}$$

The final estimation for the field components at particles' position is concluded after multiplication with the X_{ratio}:

$$E_x = (1 - X_{ratio}) \times E_{xa} + X_{ratio}E_{xb} \tag{5.14}$$

$$E_y = (1 - X_{ratio}) \times E_{ya} + X_{ratio}E_{yb} \tag{5.15}$$

$$E_z = (1 - X_{ratio}) \times E_{za} + X_{ratio}E_{zb} \tag{5.16}$$

We only chose to describe the evaluation of the electric field components, since the procedure for the magnetic field components is exactly the same.
If the field is a RF field we have to multiply the above-mentioned values with the following factors known from the theory:

$$cos(2 \times \pi \times f \times T) \tag{5.17}$$

$$sin(2 \times \pi \times f \times T) \tag{5.18}$$

where T is the elapsed time. Also for RF fields we have to update the phase at each iteration. At each turn the elapsed time is updated:

$$T_i = T_{i-1} + \frac{\Delta\phi}{2 \times \pi \times f} \tag{5.19}$$

The phase changing of each particle is relative to the phase changing of the reference particle:

$$\Delta\phi_i = \Delta\phi_{i-1} + 2 \times \pi \times f \times (\Delta t - \Delta t_0) \tag{5.20}$$

The integration Length L is defined as shown in Figure 6.11. Starting from that point the time integration step is defined:

$$\Delta T = \frac{L}{V} \tag{5.21}$$

5.3.2 Integration of equations of motion

The last part of the code is a time integration routine. At each the Lorenz force equation is integrated to obtain the new velocity and position of the particle. Starting from the equation of Lorenz force and assuming that the longitudinal velocity is relativistic and much smaller in transverse direction (constant γ along transverse direction) one can derive the equations for forces on three axis:

$$F_x = m\gamma \frac{dV_x}{dt} \tag{5.22}$$

$$F_y = m\gamma \frac{dV_y}{dt} \tag{5.23}$$

$$F_z = m\gamma \frac{dV_z}{dt} + \frac{V_z}{c}^2 \gamma^3 \frac{dV_z}{dt} \tag{5.24}$$

or else,

$$\frac{dV_x}{dt} = \frac{q}{m\gamma}(E_x + V_y B_z - V_z B_y) \tag{5.25}$$

$$\frac{dV_y}{dt} = \frac{q}{m\gamma}(E_y + V_z B_x - V_x B_z) \tag{5.26}$$

$$\frac{dV_z}{dt} = \frac{q}{m\gamma^3}(E_z + V_x B_y - V_y B_x) \tag{5.27}$$

if we differentiate these equations we obtain the acceleration equations:

$$\alpha_x = \frac{1}{c^2\gamma^2}(c^2 F_x + \gamma^2(F_x(V_z^2 + V_y^2) - F_y V_x V_y - F_z V_x V_z)) \tag{5.28}$$

$$\alpha_y = \frac{1}{c^2\gamma^2}(c^2 F_y + \gamma^2(F_y(V_z^2 + V_x^2) - F_z V_y V_z - F_x V_x V_y)) \tag{5.29}$$

$$\alpha_z = \frac{1}{c^2\gamma^2}(c^2 F_z + \gamma^2(F_z(V_y^2 + V_x^2) - F_x V_x V_z - F_y V_y V_z)) \tag{5.30}$$

To solve the differential equation we use the Second order Runge-Kutta- Nyström approximation method. The code uses a routine (DRKNYS-separate .f90 file) which takes as arguments the time integration step, the elapsed time, the position and the velocity, the components of the field and one of the routines DIFFEQEB, DIFFEQE, DIFFEQB depending on the kind of field. These routines contain the Lorenz force equation which will be integrated and they calculate the acceleration. Then the DRKNYS uses them to calculate the new velocity,position and acceleration via second order Runge-Kutta-Nyström method.
The DIFFEQ routine take the time,the velocity and the position and calculates the acceleration at each step.
As the mathematical theory of this method implies if we use the second order method we have to estimate at the positions T, T+$\Delta T/2$, $T + \Delta T$.

First Step: The first call of the DIFFEQ is with arguments T,X,V and F then the routine returns the acceleration depending on them a_1 so:

$$x_1 = x + \frac{\Delta T}{2} V + \frac{\Delta T^2}{8} a_1 \tag{5.31}$$

$$V_1 = V + \frac{\Delta T}{2} \tag{5.32}$$

Second Step:
We call the DIFFEQ routine with $T + \frac{\Delta T}{2}, x_1, v_1$ and we calculate the new approximation of acceleration a_2:

$$V_2 = V + \frac{\Delta T}{2} a_2 \tag{5.33}$$

Third Step:
We call the DIFFEQ with $T + \Delta T/2, x_1, v_2$ to find the a_3:

$$x_3 = x + \Delta T V + \frac{\Delta T}{2} a_3 \tag{5.34}$$

$$v_3 = v + \Delta T a_3 \tag{5.35}$$

Fourth step: The last call is with $T + DT, x_3, v_3$ and the function returns the a_4:

$$x = x + \Delta T V + \frac{\Delta T}{2} a_4 + \frac{\Delta T^2}{6}(a_1 + a_2) \tag{5.36}$$

$$V = V + \frac{\Delta T}{6}(a_1 + a_2 + a_4) \tag{5.37}$$

The last two equations are the approximation for the position and the velocity according to second-order Rungem Kutta-Nyström method.

The basic principle of the code is that we evaluate the quantities of the particles compared to the quantities of the reference particle.Before the particle loop we process the reference particle.The reference particle moves on the center of the field. The procedure of tracking is exactly the same as the one described above about the particles. The only difference of course,is that we do not construct a cube around the particle because its movement is one dimensional but a linear segment for the interpolation.

5.4. Code Optimisation

During the Technical Student internship at CERN the primary task of the author was to provide the simulation tools that will help and support HSL section in their work. It is essential for a code for accelerator physics, which runs complicated and time-consuming simulations to be fast and accurate. Under that prospect the primary goal was to improve the time of the simulations and the accuracy of the results. Secondary, changes implemented into various routines at Travel in order to correct and ameliorate the results. These changes will be presented in this section:

5.4.1 Corrections to the Particles Trajectory

The previous version of the code did not permit the movement of a particle at the edges of the field; a fact that resulted slightly lower transmission from the predicted. Comparison of output beams with other simulation codes indicated the need of changes in the solid algorithm. Changes where implemented in the code in order to permit the movement at the boundaries and improve particle transmission upgrading the Travel's accuracy.

5.4.2 Computational Step Modifications

Too large computational step in the Beam Line file (Card 23) led to the miscalculation of energy on RF fields. This happens because there must be at least one mesh point between two computational points. A routine was added to the code in order to implement this constrain to the simulation. In case someone fills too large computational step , automatically the program limits the number of computational points in accordance with the above mentioned principle. The maximum number of computational points is the half of the number of mesh points in the field. If we set a bigger value at card 23 then the program limits it to this maximum value. Figure 5.12 presents the uncontrolled energy augmentation as a function of increasing computational steps that was observable before the modifications. The blue line indicated the results after the modifications. The output energy must remain constant as function of computational steps.

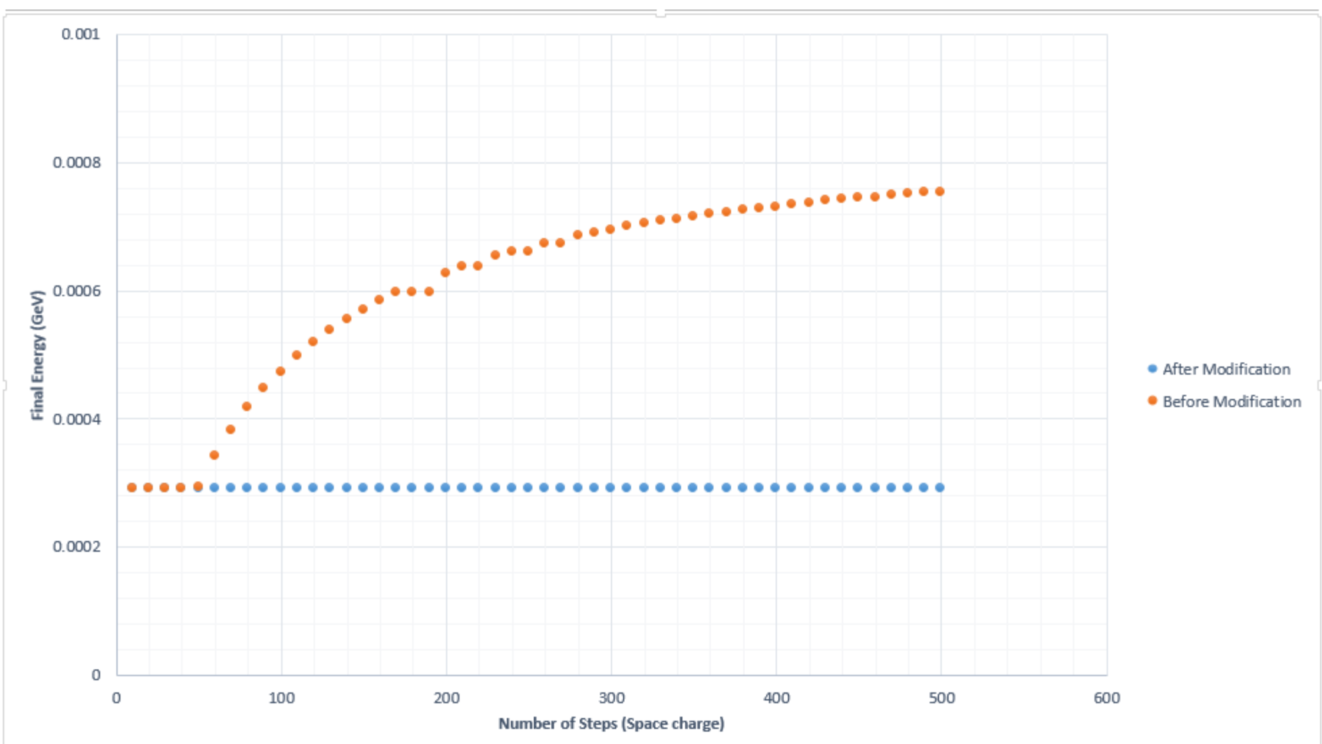

Figure 5.12: Comparison Plot of the average output energy of particles versus the number of computational steps in the code when moving in a 3D RF fieldmap.

5.4.3 Corrections to time evaluation

The previous version of Travel when simulated beams through RF fields was losing the synchronicity between the field and the particles. Changes to the equations of time where implemented in order to achieve the proper synchronicity and the correct energy results. All the values, including phase and time (needed for integration) of a particle are evaluated with the reference particle as reference. There was a need for changing the equations on the code , because they were leading to wrong results. Equation 5.38 gives the time after the application of correction at each calculation; which is the sum of the calculated time to the previous computational step plus the change in time which is given with respect to the phase difference between the current particle and the reference particle $\Delta\phi$:

$$T_i = T_{i-1} + \frac{\Delta\phi}{2 \times \pi \times f} \tag{5.38}$$

The Figure 5.13 shows that an error to time evaluation to the previous version of the code led to the inversion of the beam bunch. The late particles became early and the early ones late. Finally, Figure, 5.14 shows the output energy as a function of field length of a beam of 1000 protons (350 MHz) inside a 50cm RF field. At 5.14(a) the loss of the synchronicity between the particles and the field is clearly visible before the modifications.

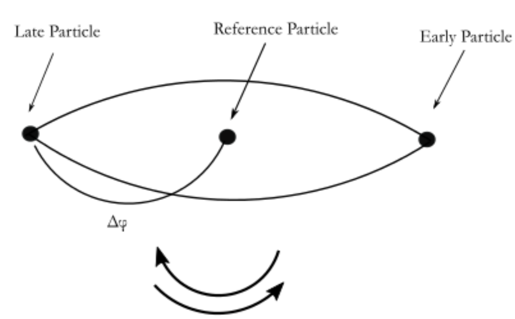

Figure 5.13: Schematic view of the beam bunch with the relation between the particles .

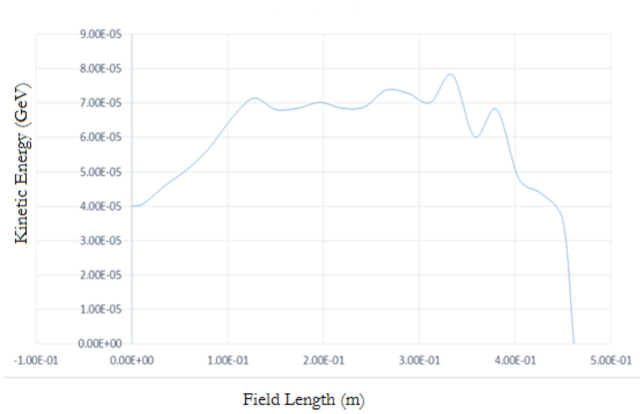

(a) Before Modifications

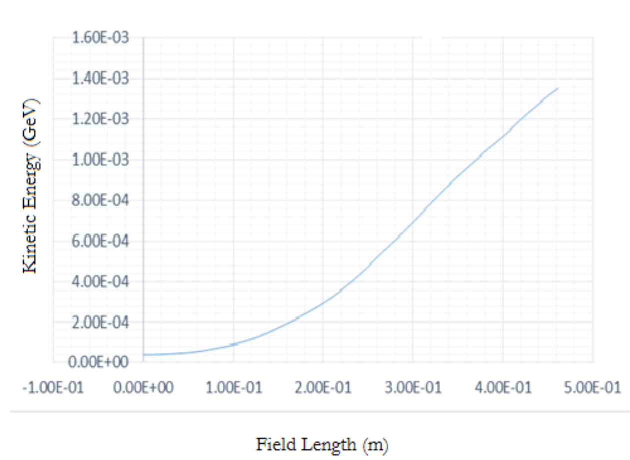

(b) After Modification

Figure 5.14: Output Average Kinetic energy as function of the field length before and after modifications

5.4.4 Corrections to reference particle Trajectory

The previous version of Travel was using different mesh points (see Figure 5.15) for the calculation of movement of the reference particle. Substitution of these mesh points with the correct ones (index corrections) led to more accurate results. Below at 5.15 the schematic view of changes into the code are are shown. The dashed line indicates the wrong trajectory used by the old version of the code and the continuous one the correct trajectory of the reference particle at the center of the beam pipe after the modifications.

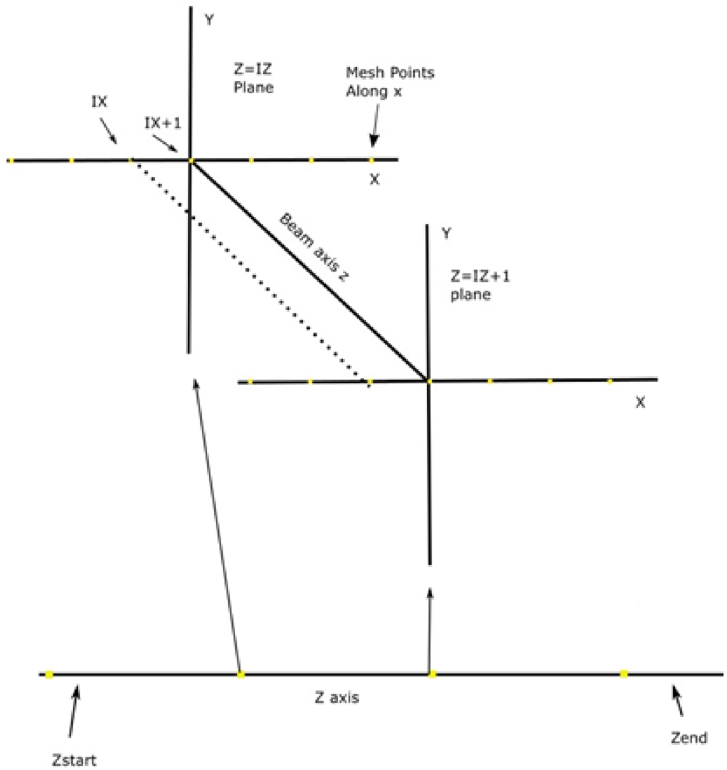

Figure 5.15: A schematic view of changes applied to the reference particle trajectory. The indexes IX ,IY,IZ for the definitions of the closest mesh points to particle are shown. The dotted line corresponds the old mesh points used by the previous version and the continuous one indicates the corrections on the trajectory of the reference particle.

5.4.5 Interpolation Routine

In order to achieve more accurate results it was essential to check the definition of the integration time used by the integration routine.The velocity of particle which moves from one point to another changes and this affects the integration time defined as the integration length divided by the velocity. The code used for the division the velocity of the particle at the initial point of segment on which the particle is moving. This assumption that the velocity stays constant during the move at the segment gives us an approximation of the result. To improve the results a better approximation of the velocity was needed. Firstly a prediction, based on energy gain, for the velocity at the end point of movement was made. After that step the velocities at initial and final position are summed and then divided by two. The interpolated velocity is used at the definition of the integration time to improve the results. The procedure described above is the following:

$$\beta_1 = \frac{V_1}{c} \tag{5.39}$$

$$\gamma_1 = \frac{1}{\sqrt{1-\beta_1^2}} \tag{5.40}$$

$$E_1 = m \times \gamma_1 \tag{5.41}$$

$$\Delta E = qFL \tag{5.42}$$

$$E_2 = E_1 + \Delta E \tag{5.43}$$

$$\gamma_2 = \frac{E_2}{m} \tag{5.44}$$

$$\beta_2 = \sqrt{{\gamma_2}^2 - 1}/\gamma_2 \tag{5.45}$$

$$V_2 = \beta_2 \times c \tag{5.46}$$

$$V = \frac{V_1 + V_2}{2} \tag{5.47}$$

$$\Delta T = \frac{L}{V} \tag{5.48}$$

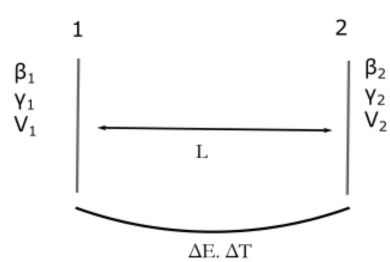

Figure 5.16: This frog was uploaded via the project menu.

5.4.6 Modifications to card 85

The card 85 at Travel changes the α, β of a phase space ellipse, keeping the normalized emmitance constant. The card, however seemed to change also the beam center while it was not supposed to. The equations to card 85 where changed as below in order to avoid the center changing. Matrix equation 5.49 shows the transformation of the phase space ellipse from the initial α_0, β_0 to the new values α_1, β_1:

$$\begin{pmatrix} x \\ x' \end{pmatrix} = \begin{pmatrix} \sqrt{\frac{\beta_1}{\beta_0}} & 0 \\ \frac{\alpha_0-\alpha_1}{\sqrt{\beta_0\beta_1}} & \sqrt{\frac{\beta_0}{\beta_1}} \end{pmatrix} \begin{pmatrix} x-\bar{x} \\ x'-\bar{x}' \end{pmatrix} + \begin{pmatrix} \bar{x} \\ \bar{x}' \end{pmatrix} \tag{5.49}$$

For testing it we used a initially shifted beam from the center and aplied card 85in order to change the ellipse parameters, but keep the center of the ellipse the same.

5.5. Code Development

5.5.1 Emittance Measurement with Pepper Pot

Pepper Pot is a commonly used device for four-dimensional emittance measurement. Pepper Pot is a rectangular device with holes of a certain diameter at x and y axis. At Linac3 there is only one column of holes (Figure: 5.18) that scans the beam during the measurements. Pepperpots cut an incident beam into small pieces (beamlets) which each has a low space charge. Then the measure of the image of this beamlet is performed after a convenient drift space whose length is proportional to the beam energy. The holes of beamlet define precisely the transverse position and the drift space turns the divergence of the particles into a transverse distribution. By scanning the row of holes across the beam and acquiring the image of the beamlets at each stage, using a MCP and a CCD camera, one obtains the particle distribution in phase space. [59] [60] [61]

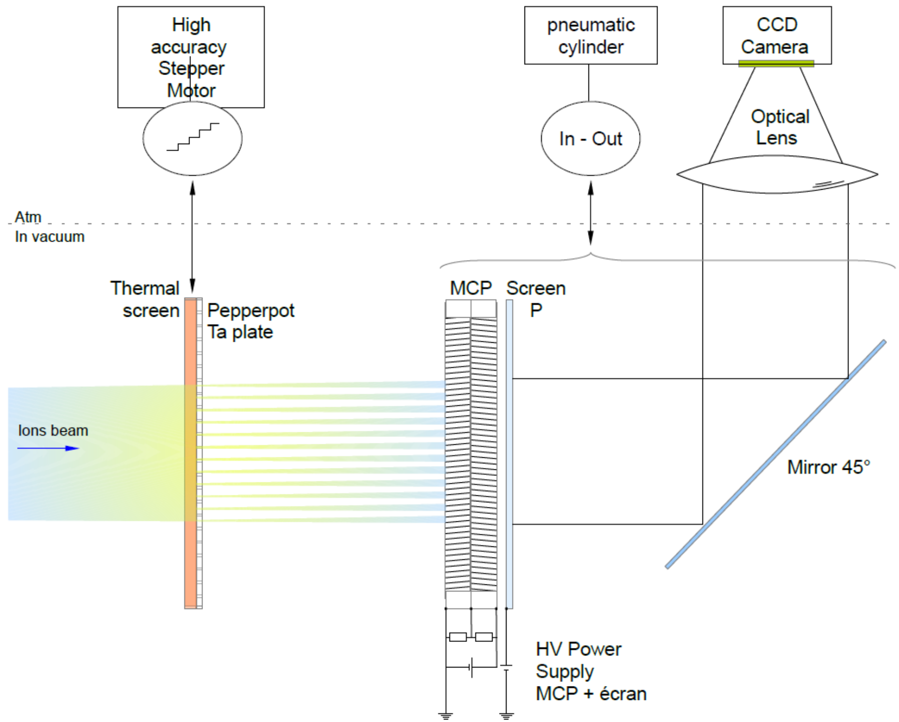

Figure 5.17: The pepper pot Measurent Device total set-up. [62]

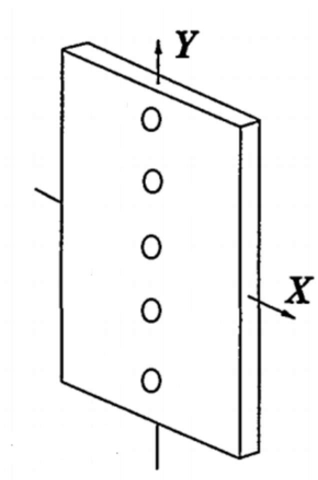

Figure 5.18: The pepper pot mask in Linac3. [59]

5.5.2 The Pepper Pot Routine

The new card for Pepper Pot was applied to Travel and Path Manager (Figure:) to assist the effort of Linac 3 in emittance reconstruction via this technique. The new card has the number 72 and takes the following inputs as parameters:

1. Number of holes along x axis
2. Distance between the center of the holes along x axis in mm
3. Number of holes along y axis
4. Distance between the center of the holes along y axis in mm
5. Radius of holes in mm

All the parameters are shown in the following schema:

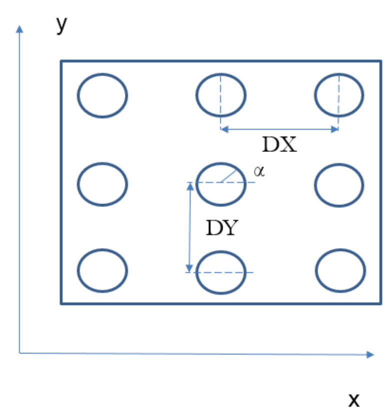

Figure 5.19: Values for card 72.

The pepper pot is automatically adjusted to the center of the beam line. The routine implemented in the code is fast and innovating because for every particle of the beam finds the closest pepper pot hole and checks if the particle passes or not. The new routine was excessively tested also with Matlab using a 30000 particles H^- beam. At Figure: 5.22 the output beam of this example is presented.

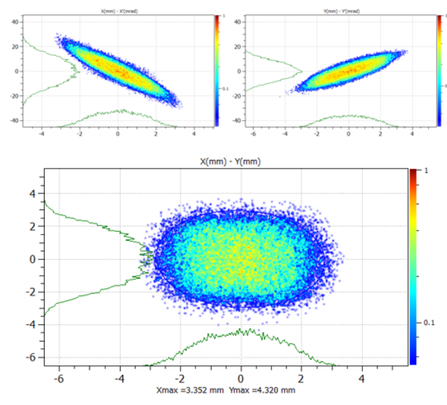

Figure 5.20: The Input beam used for the Pepper Pot Simulations.

Below we present an example of the new card with odd number of holes along x axis and even number of holes along y axis with 0.5 mm distance between them and 0.1 mm radius.

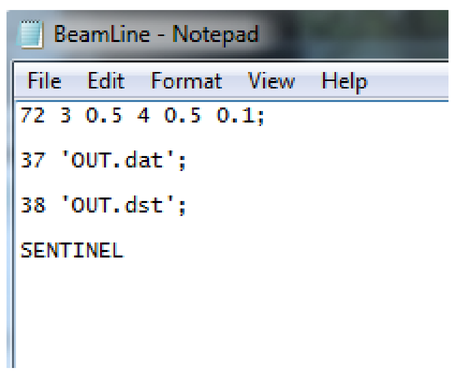

```
72 3 0.5 4 0.5 0.1;
37 'OUT.dat';
38 'OUT.dst';
SENTINEL
```

Figure 5.21: Beam Line file for the new Pepper pot card.

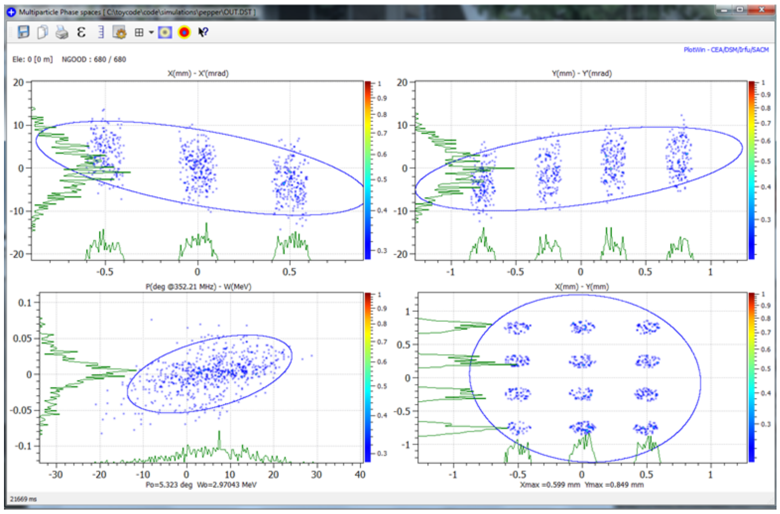

Figure 5.22: Pepper Pot output beam.

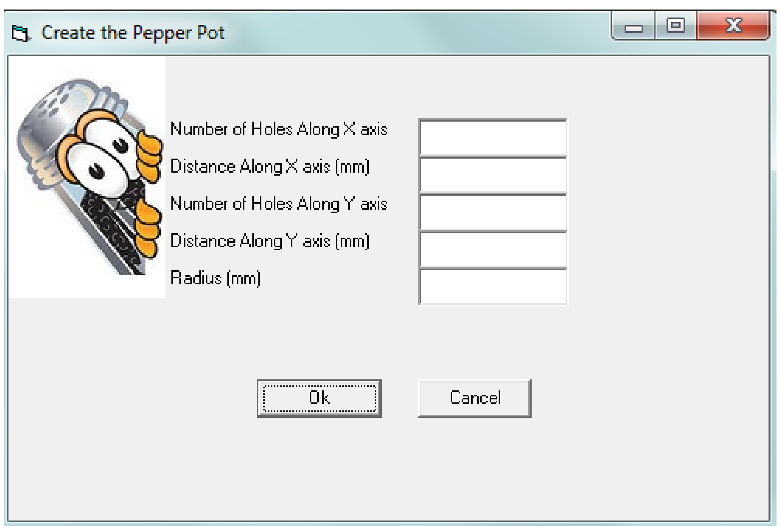

Figure 5.23: Pepper Pot Properties window implemented at Path Manager.

5.5.3 The High Frequency RFQ for Medical Purposes

In the frame of the program for medical applications CERN has designed and constructed a compact 750 MHz RFQ to be used as injector for hadron therapy Linacs. Generally RFQs are the preferred injectors at low energies but they are rarely used for medical and industrial applications. Outside scientific grounds cyclotrons are more preferable because they have been industrialized since a long time and present low cost, and a vast spectrum of knowledge in design, construction and maintenance. Although the reach of higher frequency range, leading to lower dimensions and cost put the RFQs back to the game. This revolutionary RFQ 5.24(a) reaches the energy of 5 MeV only in two meters , is highly modular consisting of four modules of 0.5 m each equipped with 12 tuner ports and one RF input, weighting only 220 kg. Although the hadron therapy requires a low duty cycle, this innovative RFQ is designed with duty cycle of 5% in view of other uses. The beam dynamics and RF design have been optimized to shorthen the total length and to reduce the power consumption. Furthermore it has been designed regarding that the beam will be injected into a higher frequency structure (A great example is the TULIP (Turning Linac in Patient) project at CERN). The transmission is only 30% due to the choice of limiting the longitudinal emittance at the end of the RFQ. Exempt from hadron therapy this extremely compact and low-cost RFQ can be installed at hospitals for the production of isotopes for PET scanning and other emerging techniques (two RFQs in cascade reaching 10 MeV), and for Te production for SPECT tomography (two RFQs followed by a DTL). Production of brachytherapy isotopes, neutrons, and compact ion beam analysis can be accomplished by this new design. To conclude this revolutionary RFQ can be an essential part of a compact light weighed system at hospitals meeting all the requirements, leading to the outcast of cyclotrons. [63]

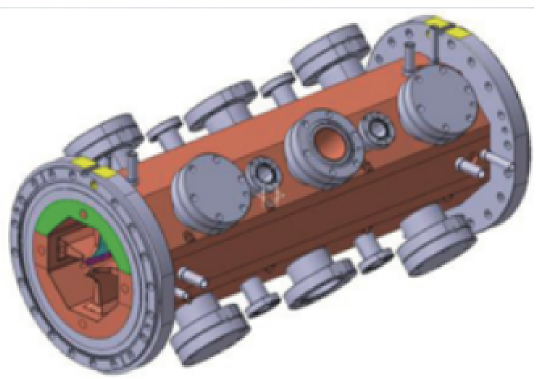

(a) First module of the new HF RFQ [63]

L = 2 m
Freq. = 750 MHz
W_in = 45keV
W_out = 5 MeV
Input /Output peak current = 100 / 30 μA
Transmission= 30%
Peak RF power = 400 kW
Max. duty cycle(max)= 5%

(b) Parameters of the 750 MHz RFQ [63]

5.5.4 The new RFQ Travel Card

In the framework of the beam simulation campaign that followed the design of this RFQ it was essential for the Travel Code to be able to process and simulate RFQs. Thus a new routine was implemented in the Travel source code that can be used to simulate RFQs through their field maps.

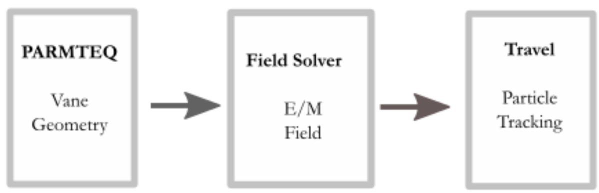

Figure 5.24: The iterative process for the RFQ simulations.

The new routine is able to take and store only the first quadrant of the field as an input and depending on the particle position , using the RFQ field symmetry , can evaluate the interpolated field value of all the four quadrants.
During this procedure the vane geometry of the RFQ was obtained by the simulation program Parmteq and fed into HFSS (Field Solver) in order to obtain the electromagnetic field. Then the file is used as an input to the Travel code. This iterative process (Figure: 5.24) indicates the detailed procedure during the design of the new routine which was tested thoroughly with different beams and field maps in order to investigate properly its properties.
The main goal during the implementation period was to obtain the same accuracy compared to the other field processing routines and simultaneously diminish the simulation time of the whole structure. As a first step the scan of the code and detection of the delays as well as the invention of a way to overcome them was the primary concern .

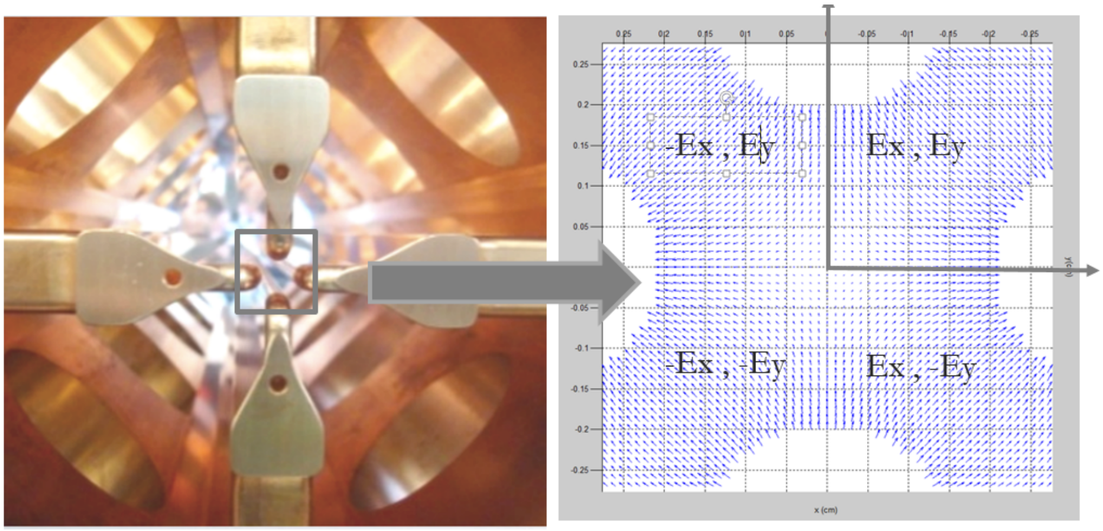

Figure 5.25: The RFQ field (plotted with Matlab) and the field symmetry of the RFQ.

As before mentioned this new routine uses only one quadrant of the fieldmap (Figure: 5.25) and exploits the RFQ field symmetry to evaluate the field in other quadrants. Then the code processes the field and tracks the particles with the same procedure mentioned at 6.3 . This permits to overcome the basic delay of the code which is the input and processing of a large field map file. Furthermore in order to make the field file even more compact and less memory consuming a header was implemented for the coordinates of the mesh points exploiting the fact that the step between the mesh points along the three axes is constant . As shown in Figure: 5.26(a) the old field map had six columns. Three columns for coordinates along x,y,z axis and the last three with field values E_x, E_y, E_z. In 5.26(b) the new more compact field map is presented. The file has only the one fourth of the total values and the three first columns where erased and changed with a three- line header. The header has the following form:

x_{min}	x_{max}	dx
y_{min}	y_{max}	dy
z_{min}	z_{max}	dz

where the the index ($_{min}$) indicates the minimum position of the field point along the axis, the ($_{max}$) the maximum position , and the third column gives the step between the points of the field along the corresponding axis. As the step between field points is assumed constant in all axis from this header we can easily derive the coordinates of the field points.

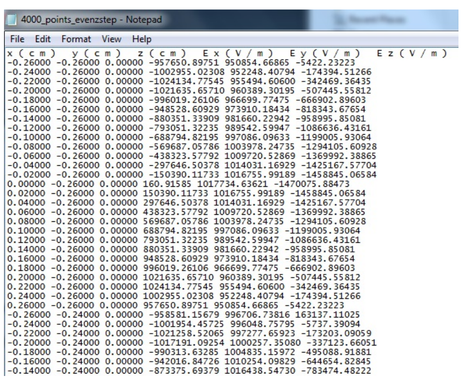

```
4000_points_evenzstep - Notepad
File Edit Format View Help
x ( c m )  y ( c m )  z ( c m )  E x ( V / m )  E y ( V / m )  E z ( V / m )
-0.26000 -0.26000 0.00000 -957650.89751 950854.66865 -5422.23223
-0.24000 -0.26000 0.00000 -1002955.02308 952248.40794 -174394.51266
-0.22000 -0.26000 0.00000 -1024134.77545 955494.60600 -342469.36435
-0.20000 -0.26000 0.00000 -1021635.65710 960389.30195 -507445.55812
-0.18000 -0.26000 0.00000 -996019.26106 966699.77475 -666902.89603
-0.16000 -0.26000 0.00000 -948528.60929 973910.18434 -818343.67654
-0.14000 -0.26000 0.00000 -880351.33909 981660.22942 -958995.85081
-0.12000 -0.26000 0.00000 -793051.32235 989542.59947 -1086636.43161
-0.10000 -0.26000 0.00000 -688794.82195 997086.09633 -1199005.93064
-0.08000 -0.26000 0.00000 -569687.05786 1003978.24735 -1294105.60928
-0.06000 -0.26000 0.00000 -438323.57792 1009720.52869 -1369992.38865
-0.04000 -0.26000 0.00000 -297646.50378 1014031.16929 -1425167.57704
-0.02000 -0.26000 0.00000 -150390.11733 1016755.99189 -1458845.06584
0.00000 -0.26000 0.00000 160.91585 1017734.63621 -1470075.88473
0.02000 -0.26000 0.00000 150390.11733 1016755.99189 -1458845.06584
0.04000 -0.26000 0.00000 297646.50378 1014031.16929 -1425167.57704
0.06000 -0.26000 0.00000 438323.57792 1009720.52869 -1369992.38865
0.08000 -0.26000 0.00000 569687.05786 1003978.24735 -1294105.60928
0.10000 -0.26000 0.00000 688794.82195 997086.09633 -1199005.93064
0.12000 -0.26000 0.00000 793051.32235 989542.59947 -1086636.43161
0.14000 -0.26000 0.00000 880351.33909 981660.22942 -958995.85081
0.16000 -0.26000 0.00000 948528.60929 973910.18434 -818343.67654
0.18000 -0.26000 0.00000 996019.26106 966699.77475 -666902.89603
0.20000 -0.26000 0.00000 1021635.65710 960389.30195 -507445.55812
0.22000 -0.26000 0.00000 1024134.77545 955494.60600 -342469.36435
0.24000 -0.26000 0.00000 1002955.02308 952248.40794 -174394.51266
0.26000 -0.26000 0.00000 957650.89751 950854.66865 -5422.23223
-0.26000 -0.24000 0.00000 -958581.15679 996706.73816 163137.11025
-0.24000 -0.24000 0.00000 -1001954.45725 996048.75795 -5737.39094
-0.22000 -0.24000 0.00000 -1021258.52065 997277.65923 -173203.09059
-0.20000 -0.24000 0.00000 -1017191.09254 1000257.35080 -337123.66051
-0.18000 -0.24000 0.00000 -990313.63285 1004835.15972 -495088.91881
-0.16000 -0.24000 0.00000 -942016.84726 1010254.09829 -644654.82845
-0.14000 -0.24000 0.00000 -873375.69379 1016438.54730 -783474.48222
```

(a) The old field map .

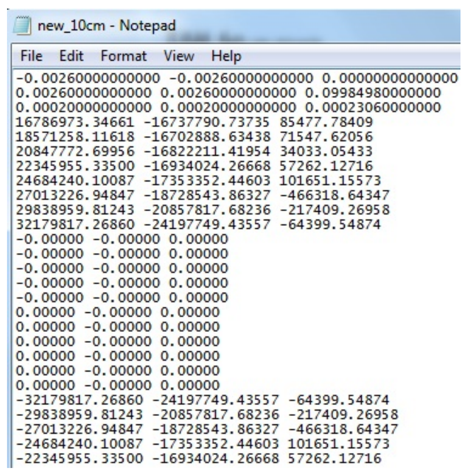

```
new_10cm - Notepad
File Edit Format View Help
-0.00260000000000 -0.00260000000000 0.00000000000000
0.00260000000000 0.00260000000000 0.09984980000000
0.00020000000000 0.00020000000000 0.00023060000000
16786973.34661 -16737790.73735 85477.78409
18571258.11618 -16702888.63438 71547.62056
20847772.69956 -16822211.41954 34033.05433
22345955.33500 -16934024.26668 57262.12716
24684240.10087 -17353352.44603 101651.15573
27013226.94847 -18728543.86327 -466318.64347
29838959.81243 -20857817.68236 -217409.26958
32179817.26860 -24197749.43557 -64399.54874
-0.00000 -0.00000 0.00000
-0.00000 -0.00000 0.00000
-0.00000 -0.00000 0.00000
-0.00000 -0.00000 0.00000
-0.00000 -0.00000 0.00000
0.00000 -0.00000 0.00000
0.00000 -0.00000 0.00000
0.00000 -0.00000 0.00000
0.00000 -0.00000 0.00000
0.00000 -0.00000 0.00000
0.00000 -0.00000 0.00000
-32179817.26860 -24197749.43557 -64399.54874
-29838959.81243 -20857817.68236 -217409.26958
-27013226.94847 -18728543.86327 -466318.64347
-24684240.10087 -17353352.44603 101651.15573
-22345955.33500 -16934024.26668 57262.12716
```

(b) New field map.

These changes led to a **83%** reduction in field map file size making the simulation faster.

5.5.5 Towards a faster code:

One of the most challenging tasks was the investigation of the code for possible bottlenecks and delays that augmented the simulation time and search ways to optimize it. The old version of the code scanned all the field to find the mesh points that are close to the particle. Instead of that a more fast and direct way of detecting the closest points was implemented exploiting the position of the particle. Furthermore in case of the RFQ there is no need to study the magnetic field. Thus the calculations for magnetic field that existed in the Travel routines was not implemented in the new routine leading to less memory allocation. Excessive testing with field maps with different number of mesh points and beams with different number of particles indicated the high dependency of the simulation time on the number of particles, posing the need to adopt different techniques on the code at the future (multicore Processing, multithreading, optimized compiler). The testing of the new code went through a dual procedure. First set of tests were performed with a 50.000 particles proton beam passing through fields with different number of mesh points. Comparison of the old and the new code indicated the same accuracy (Figures: 5.26, **??**) among results and a time gain of approximately **23 %**. Second series of testing where performed with beams with an increasing number of particles being fed in a 5000 mesh points field map. Again, the results were very satisfying concerning the output values leading to a time gain of **21%**. The Series of testing led to the experience that the simulation time increases with higher rate in the increase of particles in a beam, than in the increase of the mesh points along a field. Furthermore our optimisation effort in calculating the field indexes led to the uncoupling,to some degree, of the simulation time from the increasing number of mesh points. Below an accuracy test of a 50.000 proton beam in an 10cm RF field i shown. Matlab was excessively used to compare the results of the new (Card 71) and old Travel Routine (Card 55) for processing field maps. Figure: 5.26 shows the complete agreement in output phase spaces.

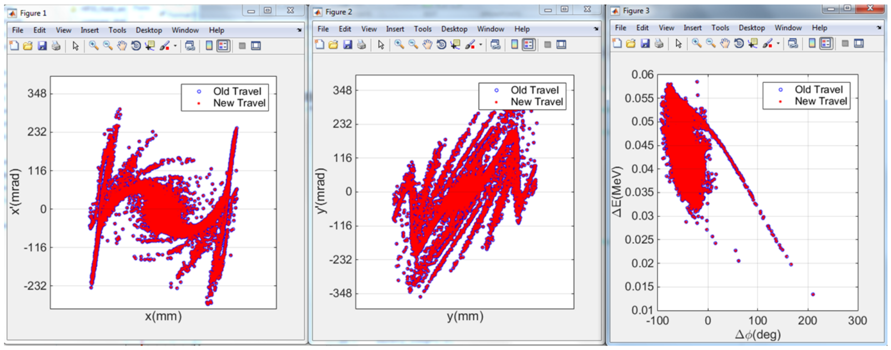

Figure 5.26: Output Phase Spaces of the card 55 and new card 71 validating the accuracy between the two codes.

5.5.6 Sampling Methods

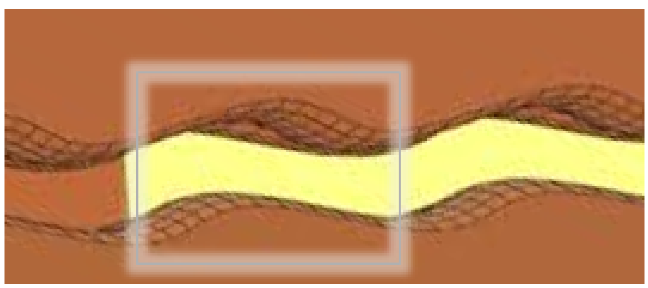

Figure 5.27: Every modulated cell is divided to two accelerating gaps.

Exploring the possibility of processing different kind of field maps with Travel code was also at the center of interest. Until this point all the considered field maps were with constant mesh step along z axis. That means that the shorter modulated cells of the RFQ have fewer and the bigger cells have more sampling field points. What if we try to use a field with changing step along z axis in a way that every cell has a constant number of mesh points? Every modulated cell of the RFQ has been split to two accelerating gap (Figure: 5.27). In the first module of the RFQ we have 111 accelerating cells. That means in the case of constant sampling step along z axis the initial cell corresponds to 8 sampling points and the last step to 45 sampling points. Different format of field maps were generated with Matlab via an interpolation method called Piecewise Cubic

Hermite Interpolating Polynomial (PCHIP). The plots of the interpolated and the initial field components can be seen in Figure: 5.28. Studies and Simulations with the code indicated good agreement in the results when we use above 40 points per cell. A reason for that is the misestimation of the calculations to the last bigger cells compared to the constant step where we have 45 points at the last cells. For these studies we used a different kind of field as shown below. An additional column has been added to the modified field map with the alternating step along z axis (Figure:5.29).

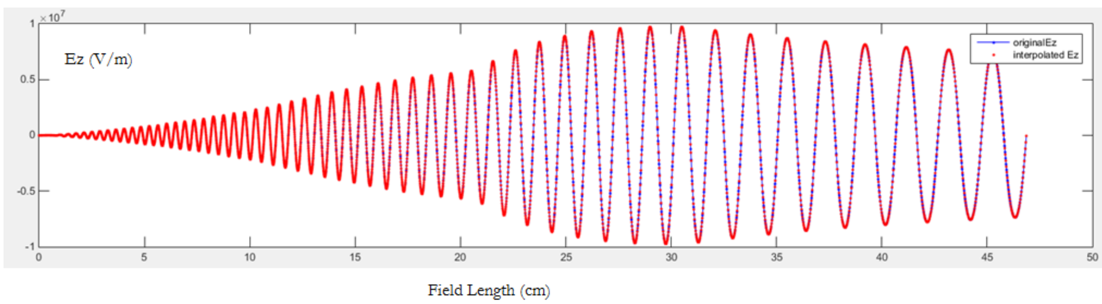

Figure 5.28: E_z As a function of field length for initial and interpolated field for x=y=0.

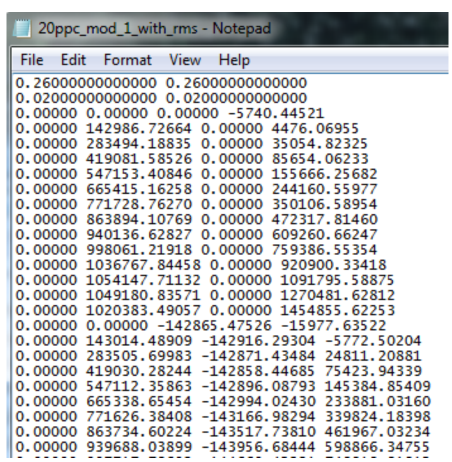

20ppc_mod_1_with_rms - Notepad

File Edit Format View Help

```
0.26000000000000 0.26000000000000
0.02000000000000 0.02000000000000
0.00000 0.00000 0.00000 -5740.44521
0.00000 142986.72664 0.00000 4476.06955
0.00000 283494.18835 0.00000 35054.82325
0.00000 419081.58526 0.00000 85654.06233
0.00000 547153.40846 0.00000 155666.25682
0.00000 665415.16258 0.00000 244160.55977
0.00000 771728.76270 0.00000 350106.58954
0.00000 863894.10769 0.00000 472317.81460
0.00000 940136.62827 0.00000 609260.66247
0.00000 998061.21918 0.00000 759386.55354
0.00000 1036767.84458 0.00000 920900.33418
0.00000 1054147.71132 0.00000 1091795.58875
0.00000 1049180.83571 0.00000 1270481.62812
0.00000 1020383.49057 0.00000 1454855.62253
0.00000 0.00000 -142865.47526 -15977.63522
0.00000 143014.48909 -142916.29304 -5772.50204
0.00000 283505.69983 -142871.43484 24811.20881
0.00000 419030.28244 -142858.44685 75423.94339
0.00000 547112.35863 -142896.08793 145384.85409
0.00000 665338.65454 -142994.02430 233881.03160
0.00000 771626.38408 -143166.98294 339824.18398
0.00000 863734.60224 -143517.73810 461967.03234
0.00000 939688.03899 -143956.68444 598866.34755
```

Figure 5.29: The different format of input field map in case of the changing step along z axis.

5.5.7 New Card Properties

The new card (named card 71) takes as an input the following parameters:

1. Number of card (71)
2. Computational Length
3. input field Name (Usually with the .ef3 format but also .txt is compatible).
4. Initial Phase
5. Electric Scale factor
6. Even or Uneven z flag

The last parameter is the one that permits to the code to know the format of the input field map. Zero corresponds to input field map with constant step along z axis and 1 to input field map with changing step along z axis. An example of a beam line file with the new card 71 is shown below:

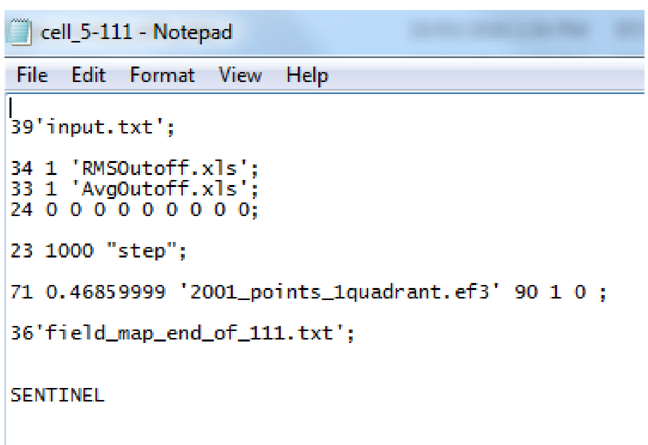
cell_5-111 - Notepad

File Edit Format View Help

```
39'input.txt';

34 1 'RMSOutoff.xls';
33 1 'AvgOutoff.xls';
24 0 0 0 0 0 0 0 0 0;

23 1000 "step";

71 0.46859999 '2001_points_1quadrant.ef3' 90 1 0 ;

36'field_map_end_of_111.txt';


SENTINEL
```

Figure 5.30: Beam Line file for the card 71.

5.6. Results of Modifications

Below the results of the codes are presented. Figure: 5.31 has the phase space of the input beam followed by the Table 5.1 with the beam parameters. Figures:

5.32(a), 5.32(b) have the output phase spaces of the first module of the RFQ from Travel code and PARMTEQ code followed by their parameters (Figures: 5.32(c), 5.32(d)). A comparison of the given plots proves the successful implementation of the modifications. All plots are given using the Plotwin software:

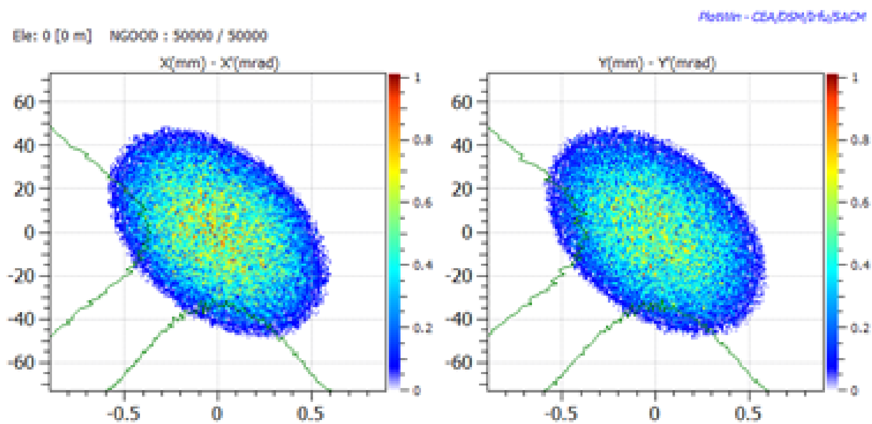

Figure 5.31: Input Beam Phase spaces .

Table 5.1: Input Beam Parameters:

Parameters	X-X'	Y-Y'	$\Delta\phi - \Delta W$
Emittance (rms)	0.0417 $(\pi \cdot mm \cdot mrad)$	0.0417 $(\pi \cdot mm \cdot mrad)$	0.0 $(\pi \cdot deg \cdot MeV)$
Beta	0.0134 $(mm/\pi \cdot mrad)$	0.0134 $(mm/\pi \cdot mrad)$	0.0 $(\pi \cdot deg \cdot MeV)$
Alpha	0.4321	0.4321	0.0

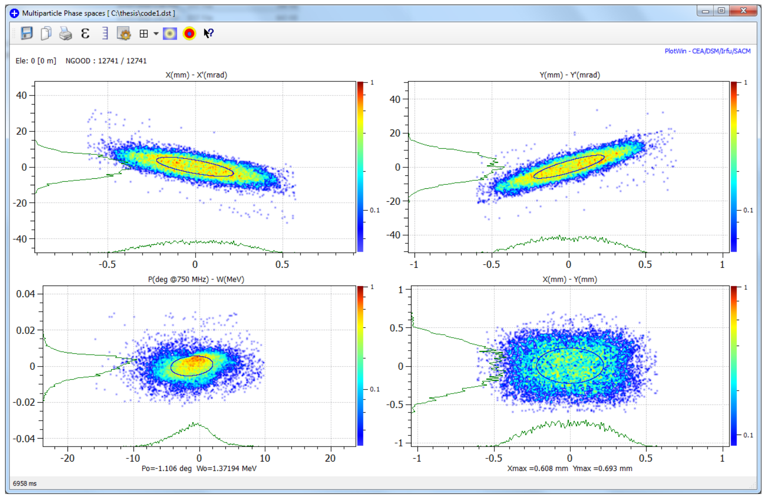

(a) New Travel Version Results

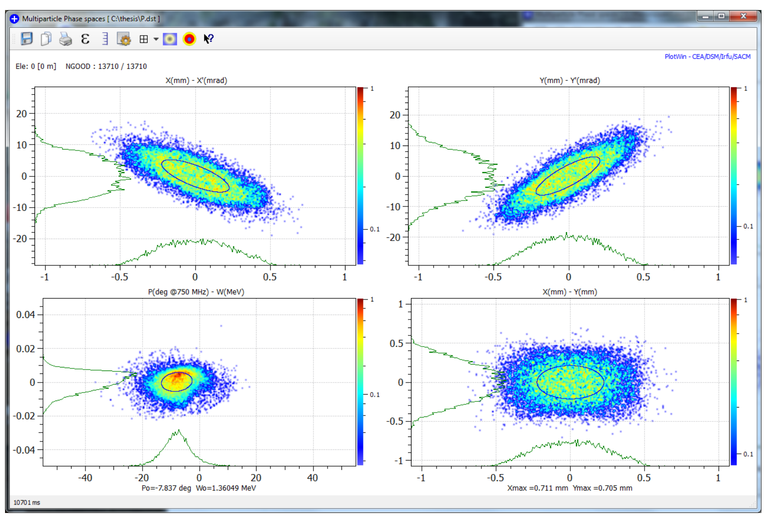

(b) Parmteq Reference Results

X-X'
Emit [rms] = 0.0421 Pi.mm.mrad [Norm.]
Emit [31.33%] = 0.0421 Pi.mm.mrad [Norm.]
Beta = 0.0646 mm/Pi.mrad
Alpha = 1.1007
Y-Y'
Emit [rms] = 0.0415 Pi.mm.mrad [Norm.]
Emit [31.41%] = 0.0415 Pi.mm.mrad [Norm.]
Beta = 0.0589 mm/Pi.mrad
Alpha = -1.4221
Phase-Energy
Emit [rms] = 0.0302 Pi.deg.MeV [Norm.]
Emit [42.34%] = 0.0302 Pi.deg.MeV [Norm.]
Beta = 970.0089 deg/Pi.MeV
Alpha = -0.1355
X-Y
Emit [rms] = 0.0479 mm² [Norm.]
Emit [34.06%] = 0.0479 mm² [Norm.]
Beta = 1.0544
Alpha = 0.0069

Beta = 0.053793062 Gamma = 1.001449994
Mo = 938.27203000 MeV

4D (X-X'-Y-Y')
E [rms] = 0.0017487486 (Pi.mm.mrad) ² [Norm.]

(c) Parameters of the Travel Output beam

X-X'
Emit [rms] = 0.0446 Pi.mm.mrad [Norm.]
Emit [33.24%] = 0.0446 Pi.mm.mrad [Norm.]
Beta = 0.0586 mm/Pi.mrad
Alpha = 1.0018
Y-Y'
Emit [rms] = 0.0450 Pi.mm.mrad [Norm.]
Emit [33.65%] = 0.0450 Pi.mm.mrad [Norm.]
Beta = 0.0634 mm/Pi.mrad
Alpha = -1.6002
Phase-Energy
Emit [rms] = 0.0174 Pi.deg.MeV [Norm.]
Emit [46.40%] = 0.0174 Pi.deg.MeV [Norm.]
Beta = 591.4815 deg/Pi.MeV
Alpha = -0.1728
X-Y
Emit [rms] = 0.0505 mm² [Norm.]
Emit [33.07%] = 0.0505 mm² [Norm.]
Beta = 0.9568
Alpha = -0.0030

Beta = 0.054018458 Gamma = 1.001462198
Mo = 938.27203000 MeV

4D (X-X'-Y-Y')
E [rms] = 0.0020063665 (Pi.mm.mrad) ² [Norm.]

(d) Parameters of the PARMTEQ reference beam

Figure 5.32: Comparison of the results between the PARMTEQ and New Travel Release

All the modifications applied to old and new routines led to the correction and amelioration of the results, and release of the new Travel (4.0.8) and Path Manager (2.8.5) Versions in March 2016. The installation package was created and distributed to all the members of HSL section to support their work on Linacs. This new Release includes also Delta Error Study Program, Beam Iteration v1.0 (program for Parameter Scan and forward method) Beam Converters and their Manuals and various examples. Furthermore includes a FORTRAN timer the open source ptime.exe which permits the calculation of the time of the simulations.

5.7. Linac4 100 MeV comissioning

Travel and PATH Manager played a major role in all the commissioning stages of Linac4. Here at this chapter some simulations during the 100 MeV comissioning will be presented regarding the start up of the DTL tanks. During the start-up of the machine the DTL tanks operational phase must be set. The tanks are turned on one-by-one and at each step the phase is scanned in order to investigate in which phase value the transmission is maximum and check if the beam can be passed intil the measurement bench. At each step,if there is need, the values of the electromagnetic quadrupoles are modified to fine-tune the transmission until the measurement bench. For the scan of the phase in the window $-180^{\circ} - +180^{\circ}$ the Beam Iteration v.1.0 program was used. Simulations indicated that the beam cannot reach the measurement bench (0 % transmission for any phase value) in the cases that only the MEBT is on and all the tanks until the measurement bench are off. The same effect appeared when the MEBT and the tank I of the DTL are on. Modifying the values of the electromagnetic quadrupoles did not ameliorate the results. Below the case that MEBT, DTL Tanks I,II are on is presented . These phase scans plots with transmission and energy respectively are shown in Figures 5.34, 5.35:

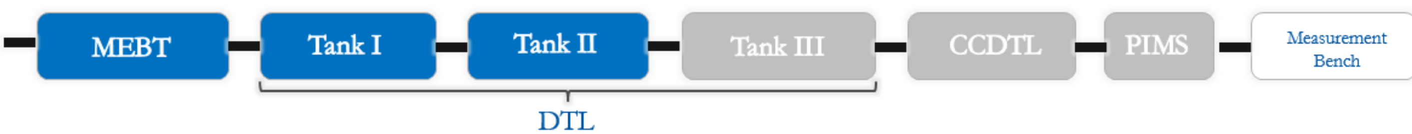

Figure 5.33: Beam line for with MEBT Tank I and II on.

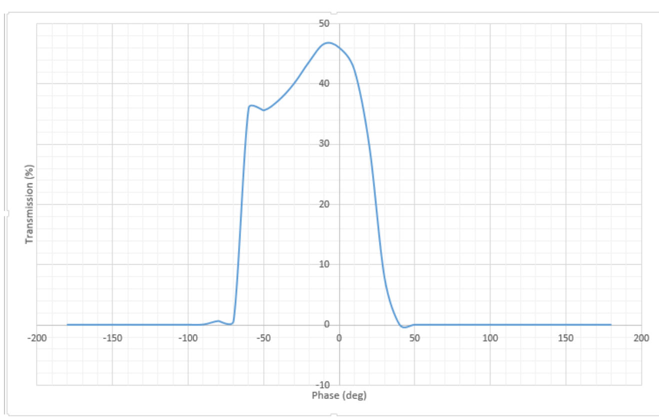

Figure 5.34: Transmission versus the phase for the case that the DTL Tanks I,II are on .

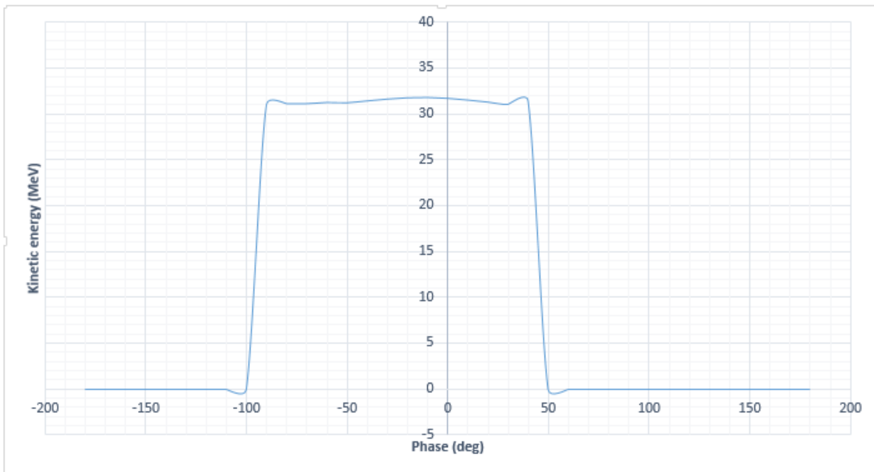

Figure 5.35: Average Kinetic energy (MeV) versus the phase for the case that the DTL Tanks I,II are on .

The optimized transmission (after the modification of the quadrupoles) and the energy versus the accelerator length plots are:

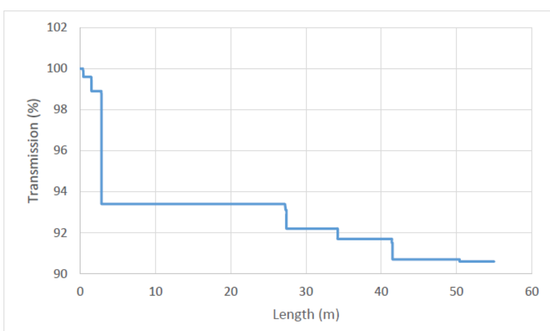

(a) Optimized Transmission versus the beam line length

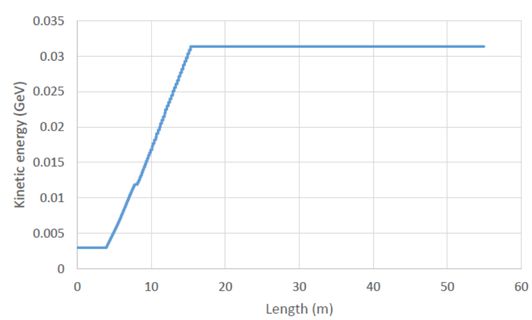

(b) Average kinetic energy versus the beam line length

Figure 5.36: Transmission and Energy versus the length for DTL tanks I,II on

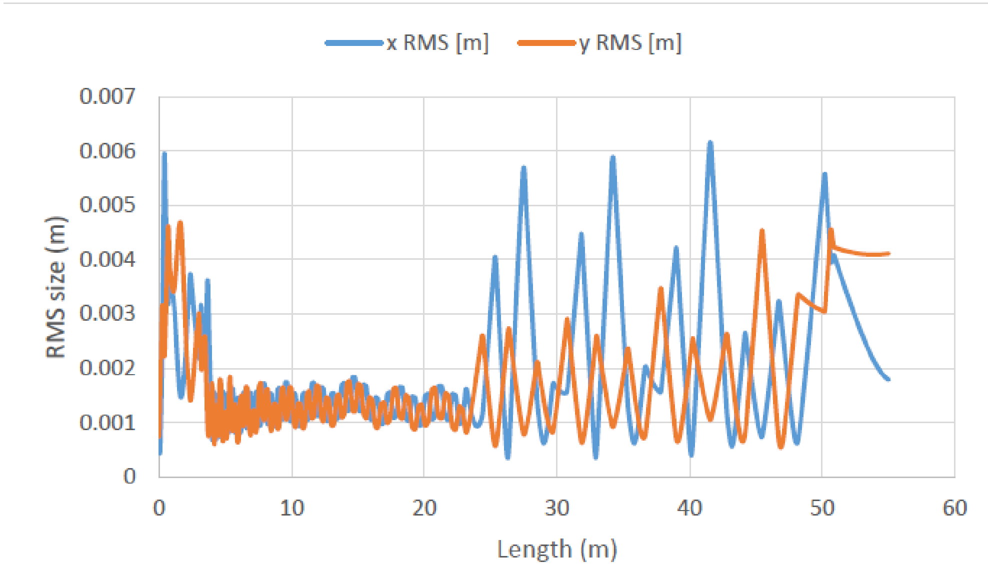

Figure 5.37: Optimized RMS envelope for DTL Tanks I, II on .

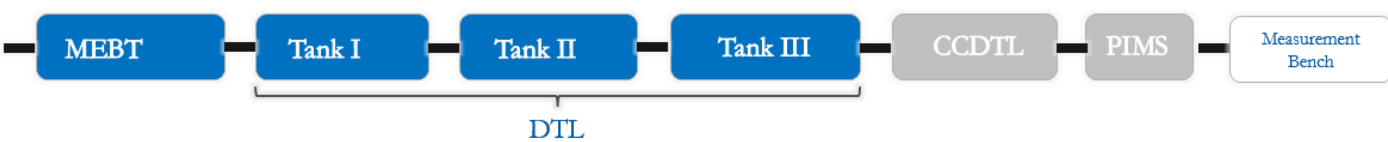

Figure 5.38: Beam line with Tanks I, II ,III of the DTL on.

At Figures: 5.38, 5.39(a), 5.39(b),5.40(a),5.40(b) the same procedure is presented for all the DTL tanks on. At all the cases the transmission and energy is measured at the test bench and the plots presented are after the fine tuning of the electromagnetic quadrupoles. For the second case when we have all the tanks of the DTL and after the fine-tuning of the quads we manage to have a transmission of 93% and average output energy of 50 MeV. Below at the tables the optimum values for the electromagnetic quadrupoles that exist between the elements in the beam line are shown.

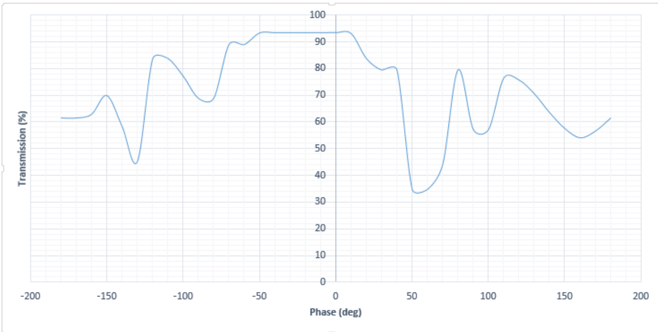

(a) Transmission versus the phase for the case that the DTL Tanks I,II,III are on

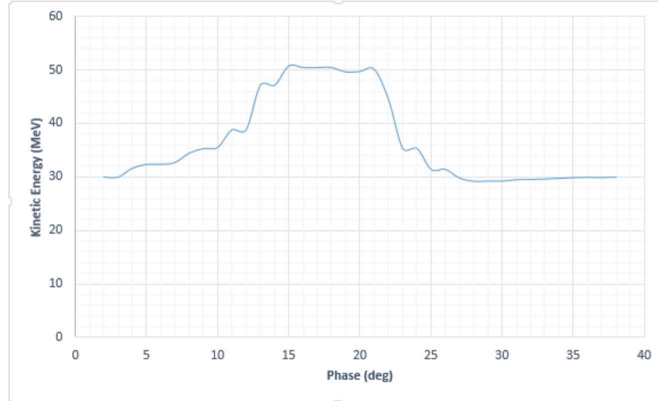

(b) Average Kinetic energy (MeV) versus the phase for the case that the DTL Tanks I,II,III are on

Figure 5.39: Transmission and Average Kinetic energy versus the phase for all the tanks of the DTL on

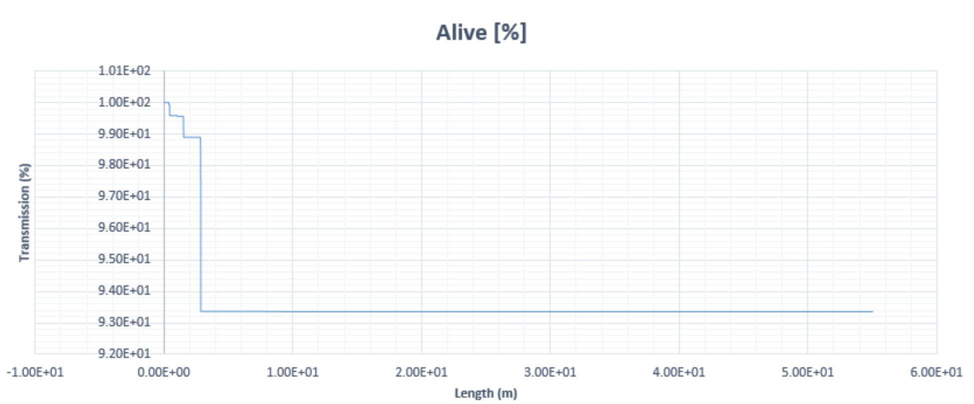

(a) Optimized transmission versus the beam line length for all DTL tanks on.

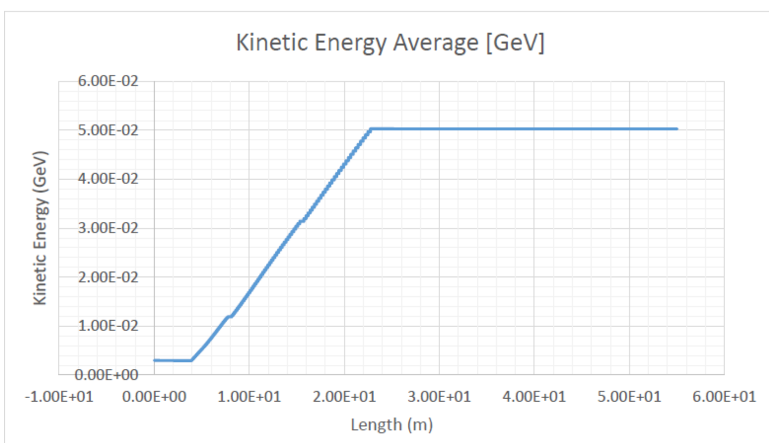

(b) Average Kinetic energy versus the beam line length for all DTL tanks on

Figure 5.40: Transmission and Energy versus the length for DTL tanks I,II,III on.

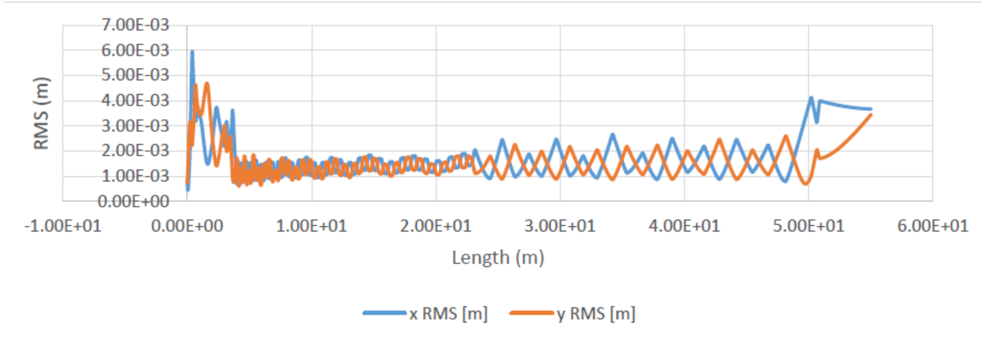

Figure 5.41: RMS envelope for all DTL tanks on.

Below at the tables 5.2, 5.3 the optimum values for the electromagnetic quadrupoles that exist between the elements in the beam line are shown. The first column of the tables has the location of the electromagnetic quadrupoles, the second the code name of each quad and the last two columns contain the fine-tuned quad strength and current.

Table 5.2: Tanks I,II on:

Location	Name	Quad Strength (T/m)	Quad Current (A)
DTL1	L4D.MQF.0210	-20.937	82.93
DTL-CCDTL	L4C.MQF.0110	-18.806	73.99
CCDTL1	L4C.MQD.0210	13.120	51.58
CCDTL2	L4C.MQF.0310	-12.306	48.89
CCDTL3	L4C.MQD.0410	11.670	46.19
CCDTL4	L4C.MQF.0510	-11.424	45.25
CCDTL5	L4C.MQD.0610	10.800	42.74
CCDTL6	L4C.MQF.0710	-13.52	53.71
CCDTL-PIMS	L4P.MQD.0110	6.54	25.61
PIMS1	L4P.MQF.0210	-9.03	35.66
Test Bench 1	L4P.MQD.0310	9.3	36.82
Test Bench 2	L4P.MQF.0410	-3.28	13.05

Table 5.3: Tanks I,II,III on:

Location	Name	Quad Strength (T/m)	Quad Current (A)
DTL1	L4D.MQF.0210	-20.937	82.93
DTL-CCDTL	L4C.MQF.0110	-18.806	73.99
CCDTL1	L4C.MQD.0210	13.120	51.58
CCDTL2	L4C.MQF.0310	-12.306	48.89
CCDTL3	L4C.MQD.0410	11.670	46.19
CCDTL4	L4C.MQF.0510	-11.424	45.25
CCDTL5	L4C.MQD.0610	10.800	42.74
CCDTL6	L4C.MQF.0710	-10.593	42.09
CCDTL-PIMS	L4P.MQD.0110	10.803	42.31
PIMS1	L4P.MQF.0210	-22.000	86.87
Test Bench 1	L4P.MQD.0310	22.000	87.10
Test Bench 2	L4P.MQF.0410	-12.000	47.73

Chapter 6

Emittance Reconstruction Application at Linac3

6.1. Introduction

Aim of this chapter is to present the design and operation of a fully automatized application for the emittance reconstruction of the beam at Linac3 LEBT. The first sections emphasize on the emittance reconstruction method used: the quadrupole variation method, the place of the reconstruction ,the specificity of the machine and the physical and mechanical design constraints that had to be taken into consideration for the implementation of this project at Linac3. Section 6.3 enters at the realm of the beam instrumentation field, with the presentation of the SEM grid as a beam measuring device and the procedure that is followed for the data processing. Sections 6.4 have more technical character describing in detail the CERN data transfer infrastructure and the application design framework. The last sections are dedicated to the presentation of the new application named `ERIS`, with technical details and measurement results.

6.2. Quadrupole Variation Method

The retrieval and knowledge of the phase space along the beam line is vital for the particle accelerating structures during their design and operation. Several techniques exist to measure and reconstruct the emittance of the beam at a certain point of the structure. The method used for this application is the quadrupole variation method where the emittance can be reconstructed by measuring the beam profile while varying upstream quadrupole magnets.

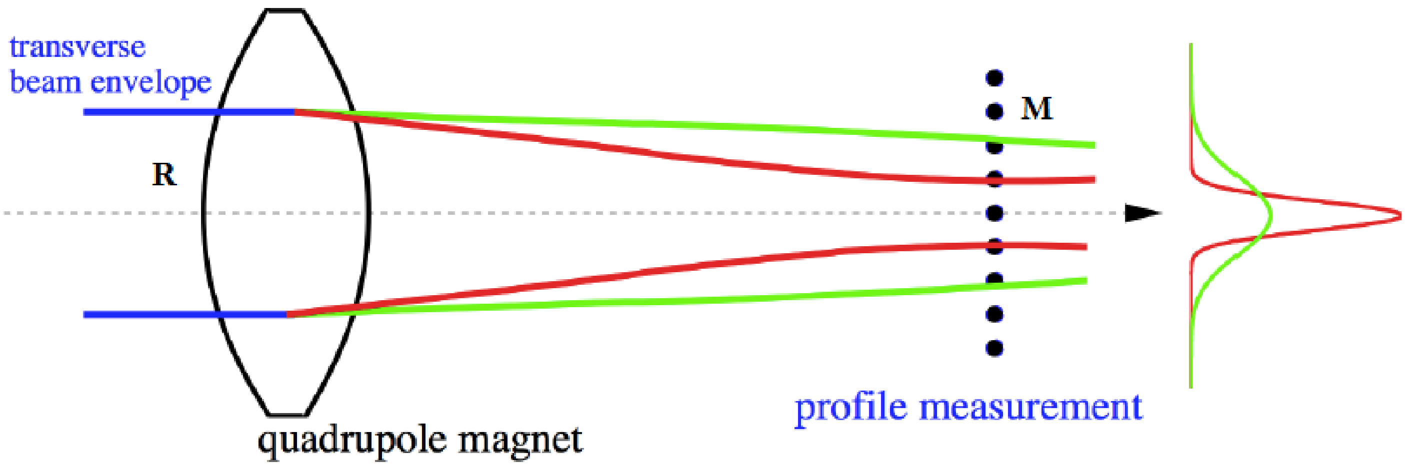

Figure 6.1: The Quadrupole Variation Method [57].

As shown in Figure: 6.1 the Twiss parameters $(\sigma_{11}, \sigma_{12}, \sigma_{22})$ of the beam at point R can be calculated using 3 or more measurements at the SEM-grid at point M with different settings of the up-stream quadrupole magnet. The are numerous variations of this technique using more quadrupoles or more more SEM grids for the reconstruction (multi-screen techniques). For the case of Linac3 a triplet of quadrupoles will be used together with drifts and a SEMgrid for the profile measurements. The real beam size of is not easy to get evaluated due to the noise in measurements and the tails of the beam distribution. On the other hand the rms beam size is less sensitive to errors, and therefore it is used for the emittance reconstruction. It is important to note before we proceed that this method is applicable only if the space charge effects are considered **negligible**.

The beam matrices of the beam at the reconstruction and measurement point are connected with equation (3.30): [64], [65], [66], [67], [68], [69], [70], [71],

$$\sigma_M = \mathfrak{R} \sigma_R \mathfrak{R}^T$$

At this case the $\mathfrak{R}$ is the transfer matrix between the point of reconstruction and the point of measurement. The first element of the beam matrix is the square of the measurement beam width. More analytically:

$$x_{rms}^2 = \sigma_{11}^M = \mathfrak{R}_{11}^2 \sigma_{11}^R + 2\mathfrak{R}_{11}\mathfrak{R}_{12}\sigma_{12}^R + \mathfrak{R}_{12}^2 \sigma_{22}^R \tag{6.1}$$

where the exponents ${}^{M},{}^{R}$ correspond to the beam matrix elements at the measurement and reconstructing point respectively. it is clear that three different beam width measurements are needed to solve the system of equations and fully define the beam matrix at the reconstruction point. For a set of n measurements ($n > 3$), we define the vectors:

$$\Sigma^M = \begin{pmatrix} \sigma_{11}^{1M} \\ \sigma_{11}^{2M} \\ \vdots \\ \sigma_{11}^{nM} \end{pmatrix}, \qquad \Sigma^R = \begin{pmatrix} \sigma_{11}^{Q} \\ \sigma_{12}^{Q} \\ \sigma_{22}^{Q} \end{pmatrix} \tag{6.2}$$

and:

$$A = \begin{pmatrix} \mathfrak{R}_{11}^2(1) & 2\mathfrak{R}_{11}(1) & \mathfrak{R}_{12}^2(1) \\ \vdots & \vdots & \vdots \\ \mathfrak{R}_{11}^2(n) & 2\mathfrak{R}_{11}(n) & \mathfrak{R}_{12}^2(n) \end{pmatrix} \tag{6.3}$$

then the equation 6.1 for n measurements can be expressed:

$$\Sigma^M = A\Sigma^Q \tag{6.4}$$

This overdetermined system can be solved with least squares fitting method:

$$\mathcal{X}^2 = \sum_{i=1}^{N} \left[\sigma_{11}^{iM} - 2R_{11}^2(i)\sigma_{11}^R - 2R_{11}(i)R_{12}(i)\sigma_{12}^R - R_{12}^2(i)\sigma_{22}^R \right]^2 \tag{6.5}$$

The aim to minimize $\mathcal{X}^2$ is met when the derivatives with respect to the coefficients that have to be evaluated are zero:

$$\frac{\partial \mathcal{X}^2}{\partial \sigma_{11}^R} = 0, \quad \frac{\partial \mathcal{X}^2}{\partial \sigma_{12}^R} = 0, \quad \frac{\partial \mathcal{X}^2}{\partial \sigma_{22}^R} = 0 \tag{6.6}$$

Using the linear least squares fitting method, the beam matrix at the reconstruction point can be derived from the following equation:

$$\Sigma^R = (A^T A)^{-1} A^T \Sigma^M \tag{6.7}$$

Once the vector Σ^Q is defined we have all the elements of the σ matrix. The parameters of the ellipse and the emittance can easily be deducted from the equations (3.28), (3.29):

$$\epsilon = det(\sigma)$$

$$\beta = \frac{\sigma_{11}^R}{\epsilon}, \qquad \alpha = -\frac{\sigma_{12}^R}{\epsilon}, \qquad \gamma = \frac{\sigma_{22}^R}{\epsilon}$$

Each measurement of beam width gives a set of parallel lines in the phase space tangent to the beam ellipsoid with equations:

$$x_{rms}^i = \mathfrak{R}_{11}x + \mathfrak{R}_{12}x' \qquad (6.8)$$

$$-x_{rms}^i = \mathfrak{R}_{11}x + \mathfrak{R}_{12}x'$$

where the exponent ^{i} corresponds to the i^{th} measurement. The results of the calculations and measurements are shown in the left of Figure: 6.2; a retrieved ellipsoid (equation of ellipse is the equation: (3.27)) in phase space enclosed by tangent lines (Equations: 6.8) corresponding to the set of measurements:

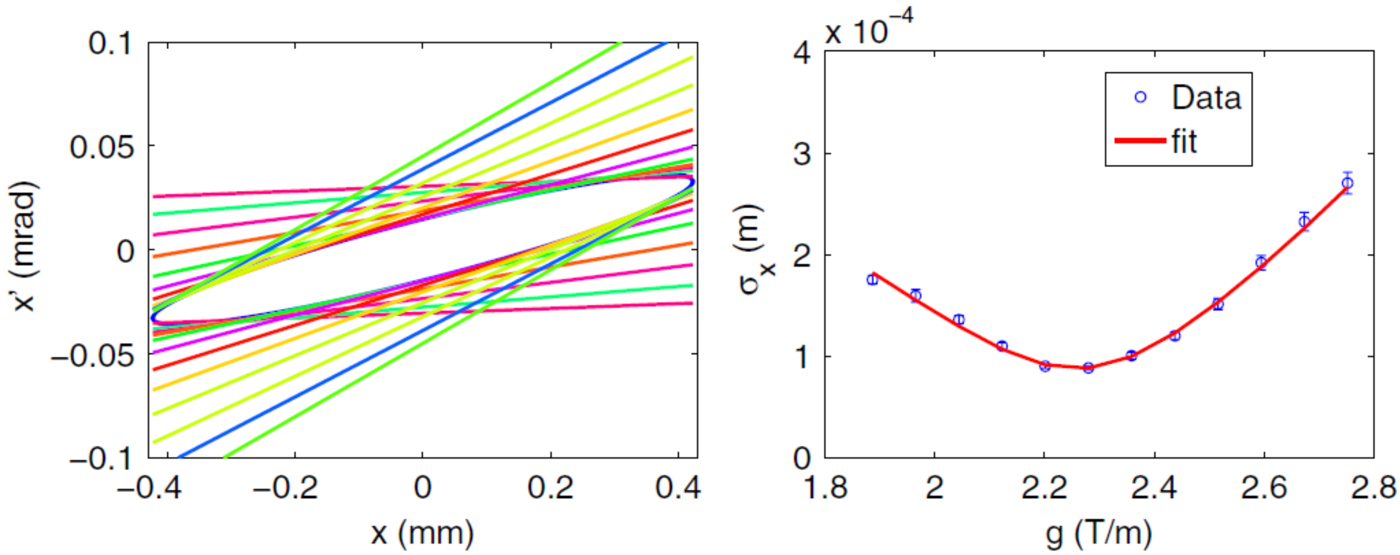

Figure 6.2: The Quadrupole Variation Method plots [65].

On the right plot of Figure: 6.2 a comparison of the simulated $\mathcal{X}^2$ fit and the measured points provides useful information about the quality of the reconstruction acting as a figure of merit for the quality of the reconstruction at the given measurement points.

Bellow at Figure: 6.7 the Measurement and reconstruction point at Linac3 are shown:

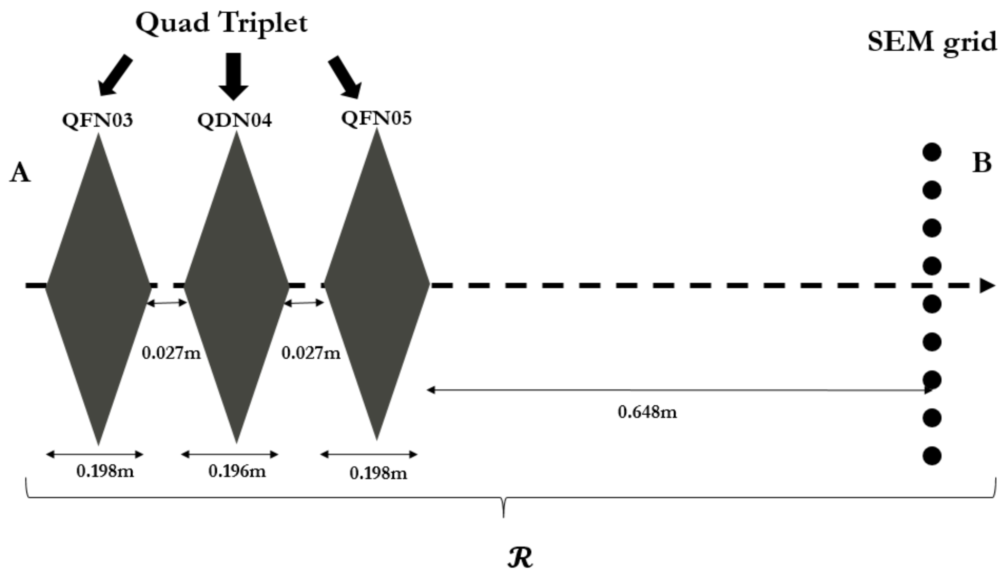

Figure 6.3: The reconstruction place at Linac3 with the corresponding lengths of quadrupoles and drifts.

The recostruction takes place at the Low-Energy-Beam-Transport (LEBT) of Linac3 (marked point at the Lina3 design blueprints) - Figure: 6.4 .

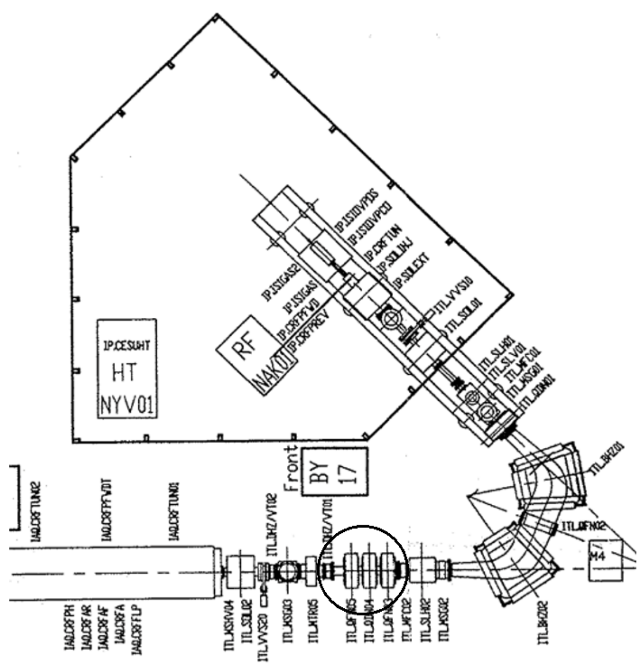

Figure 6.4: Linac3 technical design with the exact place of the emittance reconstruction inside the whole structure.

6.3. SEM grid and Data Processing

6.3.1 Secondary Electron Emission Grid

A SEM grid as its name proves exploits the phenomenon of the secondary electron emission (Emission of electrons from a surface due to impact with a beam). It is constructed as a rectangular frame with parallel and crossed wires inside . When a particle passes electrons are created from the wires ,a current that it can be measured indicating the density of the particles hitting the wire. With the SEM grids we measure the beam profile but we have to screen every wire individually, thus we need a number of out data channels propotional to the wires. The following figure shows a SEM grid with crossed horizontal and vertical cables for horizontal and vertical beam profile respectively. The distance between the stripes affects the resolution of the measurement [57].

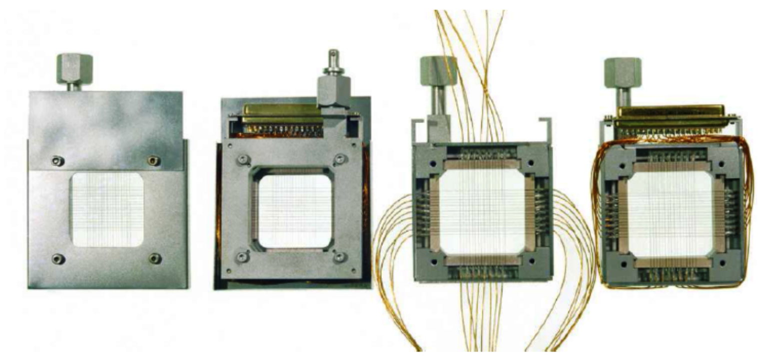

Figure 6.5: A SEM grid [57].

6.3.2 Statistical Profile Processing

The deduction of beam width (x_{rms}) from the measured profiles is done by simple statistical calculations on the obtained distributions. An obtained distribution of the signal strength along the wire is like in Figure 6.6:

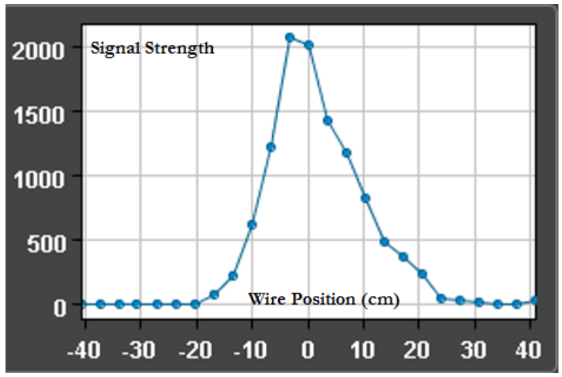

Figure 6.6: A SEM grid.

The mean value and the dispersion are given from the classic statistic equations:

$$\mu = \frac{\sum_{i=1}^{N} x_i s_i}{\sum_{i=1}^{N} s_i} \tag{6.9}$$

$$x_{rms} = \sqrt{\sigma_{11}} = \frac{\sum_{i=1}^{N} s_i (x_i - \mu)^2}{\sum_{i=1}^{N} s_i} \tag{6.10}$$

6.4. Inspector Framework

6.4.1 CERN infrastructure

In order to control the large number of complex devices and machines CERN has a three layer architecture that controls and monitors the data transfer from the low-level circuit logic until the level of the CERN Control Center (CCC) [64], [72], [73], [74]:

1. **Device Layer:** Its the first and basic layer where all the devices are located.The devices communicate with the upper next layer in hierarchy using the FESA framework (Front End Software Architecture). A physical device is assigned to a rack and connected with a computer using the FESA framework.

2. **Middle Layer:** The front end computer transfers the device data to the Middle Layer for processing. Furthermore it processes all the operator com-

mands and stores the settings sent to the devices. It is the layer that effectively connects the physical devices with the operators. It communicates with the front-end computer using JAPC (Java- API-Application Programming Interface for Parameter Control). The middle layer transforms the data given from the high-level control of the devices to low-level settings for the devices.

3. **Application Layer:** At this layer all high-level applications used by the operators are contained. With these applications the operator can control a device, make measurements, and depict vital device information and setting ,exchanging data with the Middle Layer.

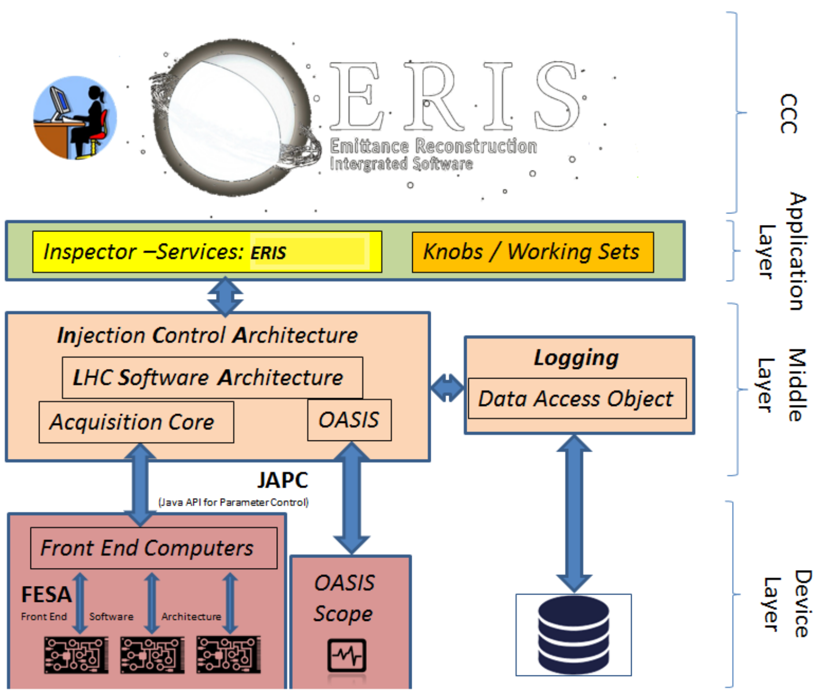

Figure 6.7: CERN data transfer layer Architecture.

6.4.2 Inspector

Inspector is a graphical framework that permits the design of User Interfaces for the control of a device inside CERN grid. It permits a easy, flexible and fast design of a GUI without any prior-programming or design knowledge. Inspector facilitates the control of a device and the depiction of the vital operational machine information. The framework is characterized by the term data-driven. That means that the user selects the value that wants to visualize or change and drags-and-drops it to the panel in accordance with the data type. It offers a vast spectrum of possibilities permitting to perform complex control of the accelerator chain devices in a simple way. Inspector has a client-server architecture and uses a proxy to communicate and pass data to the available corresponding servers. The flexibility and the adaptability of this framework offers the possibility to create new servers depending on the needs and transfer the data to other ones in case of server failure. There are three kinds of servers: *data* for direct data, *synthetic* for real time evaluation of data and *logging* & *alarm* servers. The rapid prototyping of this framework, permits the handling of applications and algorithms developed at different environments and programming languages (such as Matlab ,C, Python) with no effort. Furthermore it contains a Warning system which can alert the operator on the cell phone or mail on the situation of the devices and a Equation Editor that allows to process data from different sources in real time. Last but not least the powerful data processing tool *Blueprint* embeds high-level scripting and Python support in a visual way. [64], [72], [73], [74]:

6.4.3 Inspector Services

Inspector permits to the operator to monitor a device and perform calculations and measurements. Although, to implement more complicated procedures and execute complex algorithms the development of the Inspector-Services extension was of crucial role. A service is a code, which implements and executes an algorithm. The underlying implementation of the Inspector Services framework is done in Java, thus a service can be designed using any Java development IDE (such us Eclipse or NetBeans). Services along with the Services Toolkit that permits to implement complex and demanding mathematical expressions in an easy and fast way create a powerful tool for data processing. In addition Services Toolkit aids to the data sharing and communication between different Services, monitors the execution flow as well as the input and the output on the Inspector panels. After the design process the Service is stored to Service Code Repository and installed on dedicated servers (Service Servers) from where it can be deployed and executed. Inspector panels and designed user interfaces allow access to the Service Code Repositories and the dedicated server from any computer. The base philosophy of the Inspector and Inspector Services is the centralized installation, instantiation and execution of the services and the decentralized client control, establishing a client-server interaction. There are two kinds of Service servers: ***Services Repository Servers*** which contain the source codes of the services and Services ***Execution Servers***. Each one of them has its own proxy that forwards the request from the Inspector Workstation to the corresponding Server as shown in Figure: 6.8

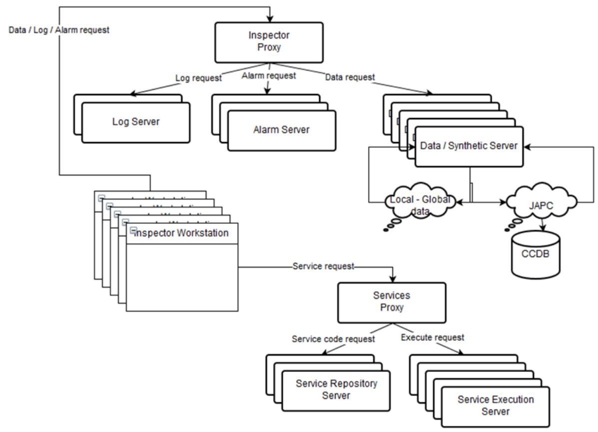

Figure 6.8: Inspector and Inspector Services Servers Flowchart. [72]

Inspector permits the design of various front-end applications with great visuals and customization as the one at (Figure: 6.9) for the monitoring of Linac4 RF system. The user drags and drops the data that he wants to visualize and takes valuable information. The panels are aesthetically attractive, highly interactive containing clickable and blinking areas that trigger an action upon different kinds of clicks.

Figure 6.9: An Inspector application for the RF control of Linac4. [74]

At the right the Synthetic Devices List (global variables for drag-and-drop) and the Services panel is shown permitting access to Services Servers and Data

Server via the creation of Data or service requests (see Figure: 6.8). At the top of the screen there is the menu Toolbar with all Inspector settings. [72], [73], [74]:

6.5. ERIS [64]

Figure 6.10: The ERIS Logo.

ERIS: (*Emittance Reconstruction Integrated Software*) is an application (collection of Services) that automatize the emittance reconstruction at Linac3 as described in the 6.1 section. The application sets the values of the scanned quadrupoles takes the measurement profiles on the SEM grid and reconstructs the emittance before the quad triplet. The detailed algorithm flowchart is shown below at Figure: 6.11:

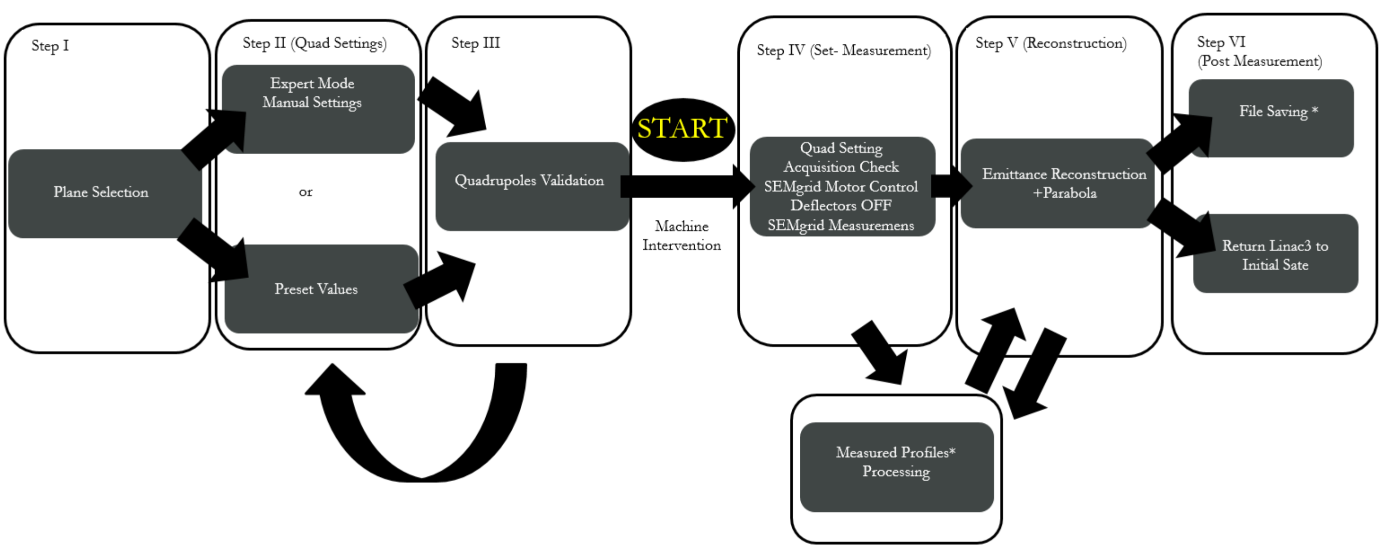

Figure 6.11: ERIS algorithm flowchart.

The graphical user interface (GUI) of the application as launched from the Linac 3 control room is shown in Figure: 6.12.

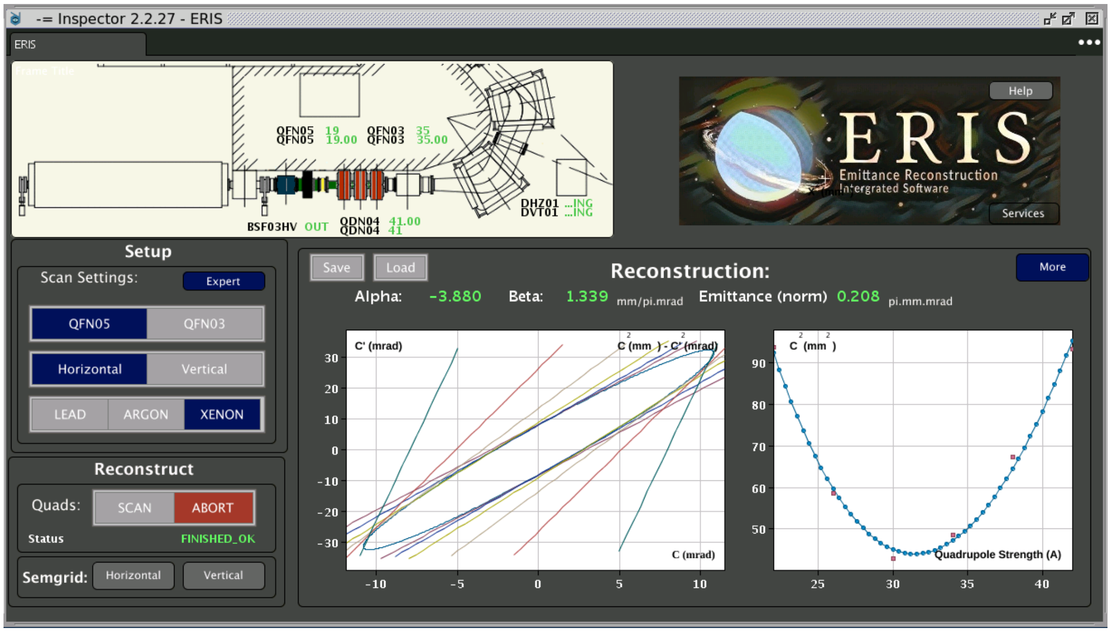

Figure 6.12: The central panel of the application.

At the top left side there is a blueprint design of the Linac3 LEBT showing the quadrupole triplet, the drifts, the deflectors and the SEMgrid. By double-clicking on each of the elements vital information regarding the acquisition values of quadrupoles, the deflectors' state and the SEMgrid motor position are showed. In general , for normal data acquisition the deflectors must be OFF to avoid emittance growth of the beam, the SEMgrid motor in place "IN" and the input values from the quadrupoles must agree with the acquired values. The GUI is completed by the control buttons of the application on the left side and the plotting section on the right. The plotting section shows the reconstruction results and the α, β and normalized emittance ϵ only for the current plane. Horizontal and vertical reconstruction results appear together by clicking on the button "More" (see Figure 6.16). The operator, in order to monitor the correct instantiation and function of the project services has to press the "Services" button inside the ERIS logo area; a log panel appears with details for the correct instantiation of application services. The Services states are: `Running`,`Finished OK`, `Halted`, `Stopped`, Error. The operator can monitor whether everything is ok with the services and the machine or if an error appeared, in that case exception handling routines are called to prevent and avoid possible unwanted situations.

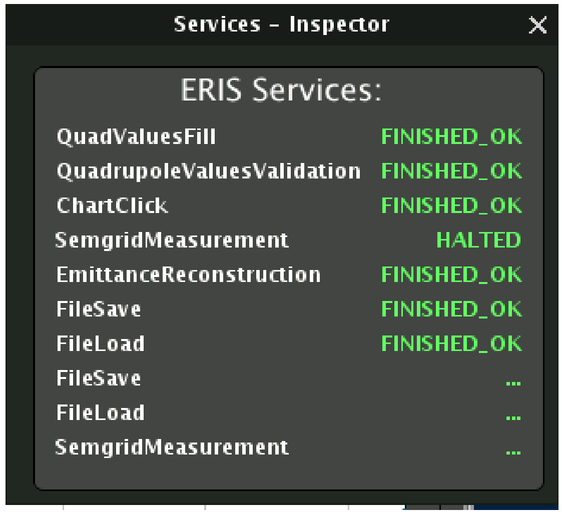

Figure 6.13: Monitoring ERIS services.

A measurement starts with the choice of one kind of particles (Lead 29^+ (Pb 29^+), Argon (Ar) and Xenon (Xe). The first step of the algorithm is to choose a plane for the reconstruction (horizontal or vertical). At this point the front-end operator has two options: either to choose the preset settings for the three quadrupoles or click on the "Expert mode" button and enter them manually by hand or via a stored file (see Figure 6.14). The preset values (QFN05, QFN03 buttons) are four sets of quadrupole strength values that scan the first or the third quadrupole of the triplet for horizontal and for vertical plane. These settings were chosen after detailed analysis of previous LEBT transverse emittance reconstruction measurements at Linac3. Once the values of the quadrupole current are chosen, the operator has access to the validation chart inside the expert mode window. The validation chart matches and shifts the sets of parallel tangent lines to the axis origin. The angle distribution of the lines is a figure of merit for the quality of the reconstructed emittance and a cross-check for the operator that the chosen values are reliable for the reconstruction. Moreover the expert mode contains the part of the pulse that is captured by the SEMgrid. By default the program uses the first 200μs of the pulse (50 first gates- gates are 4μs separated) for calculations but the operator can modify it from the expert mode, leading to recalculations with the desired gates. The application stores the SEMgrid data for every gate for every wire for the total of six measurements. Then the signals are averaged on the gates to extract the profiles on Figure: 6.15. The operator has the possibility to process the obtained profiles with the exclusion of certain wires with the definition of a certain area by clicking the middle mouse button and dragging on the measured profiles. At each processing step the results on the plotting windows are refreshed.

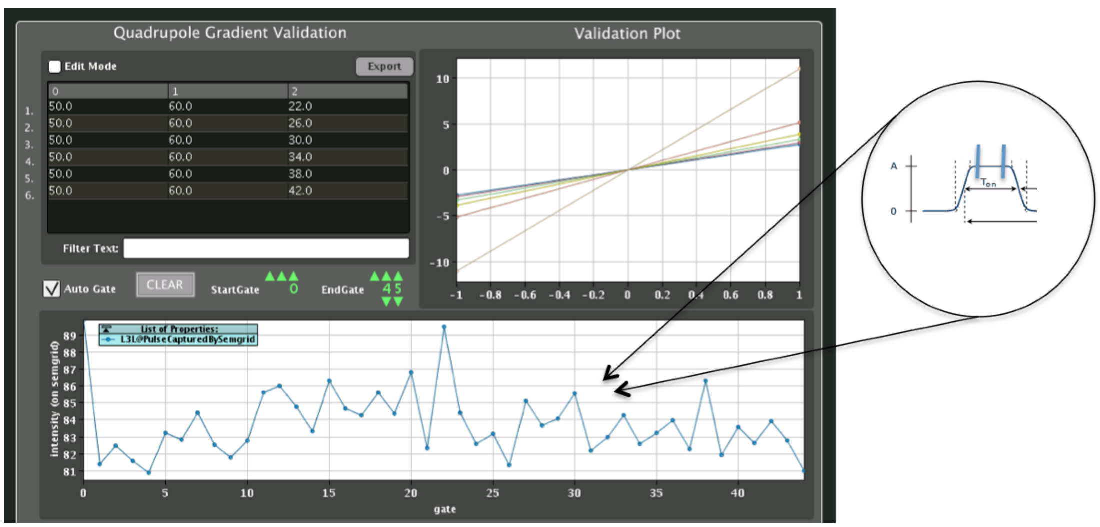

Figure 6.14: The "Expert Mode" panel, with the preset values, Validation Lines, and part of pulse captured by the SEMgrid.

With the click on the "SCAN" button the chosen values are set to the quadrupoles, the SEMgrid motor moves the SEM grid inside the beam pipe, the deflectors are turned off and measurements are starting to appear inside the measurement profiles windows of the corresponding plane (see Figures: 6.15 for horizontal plane). A window of 2 sec was given between two SEM grid measurements in order to avoid possible errors.
Finally, the reconstructed emittance ellipse within the tangent parallel lines and the comparison of the x_{rms} points with the $\mathcal{X}^2$ fit are shown in the main menu of the application along with the α, β, γ and emittance values. After a measurement the machine is returned to its initial state (SEMgrid out, Deflectors' state: ON and quadrupoles on their initial values). Finally, by clicking on "Save" button the

operator can save two files (for horizontal and vertical plane) with the SEMgrid Measurements, the Processed Measurements, the gates used for sampling and the used quadrupole values in a desired Path.

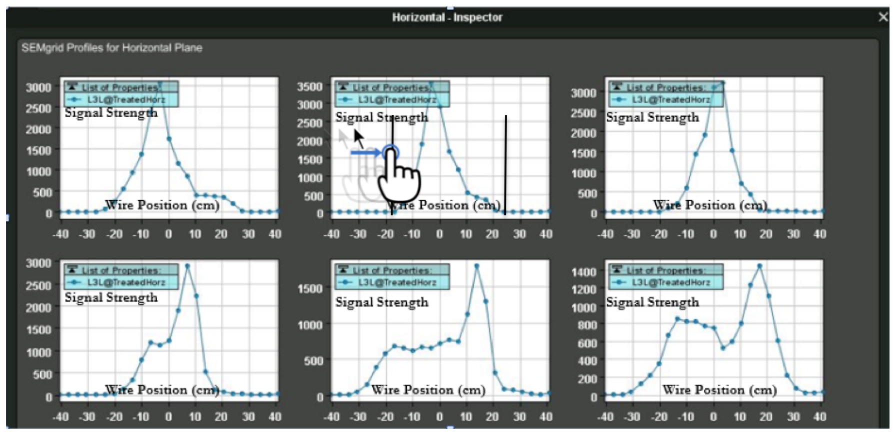

Figure 6.15: Horizontal SEMgrid Measurements. The operator can drag the mouse and process the acquired data in order to exclude unwanted values.

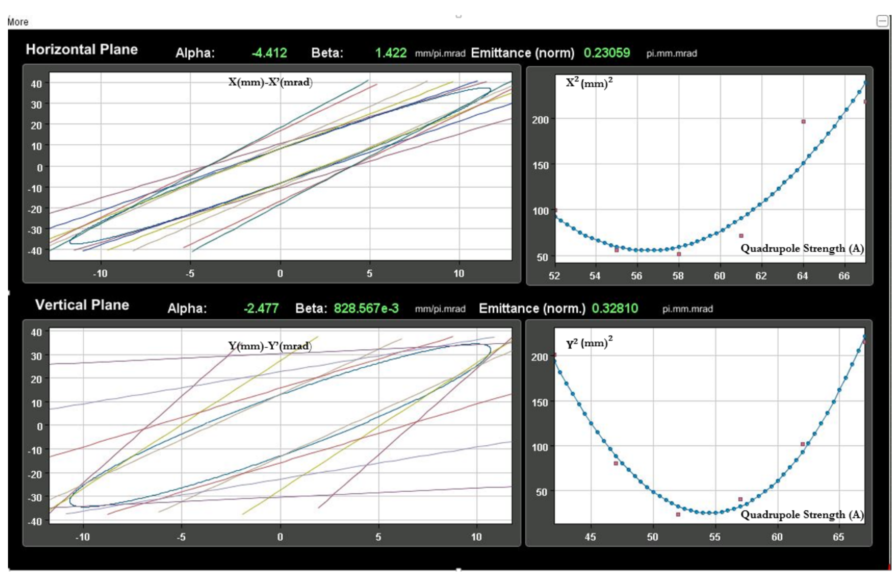

Figure 6.16: The panel with the results of the process for the two planes.

ERIS is a powerful, aesthetic and fast diagnostic tool for transverse emittance measurements and reconstruction on Linac3; operating at the crucial point of

Linac's LEBT, where the characterization of the beam after the source is of essential need. The undisputed assets of this application are the measurements and reconstruction in unprecedented time, the flexibility and the possibility to make instantly calculations that would need hours of post processing or beam time. The user-friendly interface that permits the operation even from non-experts places ERIS amongst the highly innovative applications on beam instrumentation field. Furthermore it presents high adaptability and can be easily transferred with a minor amount of changes to other accelerators and applications, whereas the extracted data can be fed to other analytical tools. [64]

References

[1] CERN - LHC The Guide
http://cds.cern.ch/record/1165534/files/CERN-Brochure-2009-003-Eng.pdf

[2] https://en.wikipedia.org/wiki/CERN

[3] CERN - The Accelerator Complex
http://home.cern/about/accelerators

[4] CERN- The Large Hadron Collider http://home.cern/topics/large-hadron-collider

[5] CERN Accelerator Chain
http://te-dep-epc-oms.web.cern.ch/te-dep-epc-oms/operation-en/operation.stm

[6] The Cockroft-Walton Accelerator
https://www.pinterest.com/pin/399694535660296706/

[7] Electrostatic Accelerators
https://cds.cern.ch/record/1005042/files/p95.pdf

[8] Induction Linacs
https://cds.cern.ch/record/399423/files/p79.pdf

[9] Presentations on Linacs, Jean-Baptiste Lallement, Veliko Dimov - Joint Universities Accelerators School (JUAS)- 2015 January, 26
http://indico.cern.ch/event/356897/timetable

[10] RF Linear Accelerators, Thomas P. Wangler - Wiley-VCH Publications Second Complete Revised and Enlarged Edition

[11] Status of the RF System, S. Choroba, DESY

[12] Resonant Cavities and Waveguides, MIT:
http://web.mit.edu/22.09/ClassHandouts/Charged%20Particle%20Accel/CHAP12.PDF

[13] CAS-The CERN accelerator school, Andy Wolski–Theory of Electromagnetic Fields
http://cas.web.cern.ch/cas/Denmark-2010/Lectures/Wolski-2.pdf

[14] Fields in Waveguides – a Guide for Pedestrians Peter Tenenbaum DRAFT June 13, 2003
http://www.desy.de/njwalker/uspas/coursemat/notes/unit2notes.pdf

[15] Cavities-Presentation,Qiong Wu,Sergey Belomestnykh,Wencan Xu April 19/21, 2011
http://www.c-ad.bnl.gov/ardd/docs/rf4me_$v2$.pdf

[16] Cavity Types, F. Gerigk (CERN/BE/RF),CAS, RF for Accelerators, Ebeltoft, Denmark,11 June 2010
https://cas.web.cern.ch/cas/Denmark-2010/Lectures/Gerigk.pdf

[17] Accelerator Physics -S.Y. Lee, Second Edition

[18] RF Theory and Design - Notes Jeremiah Holzbauer Ph.D. USPAS - Grand Rapids
http://uspas.fnal.gov/materials/12MSU/RF_Design_Lecture_Notes.pdf

[19] RF-Basics, F. Gerigk (CERN/BE/RF), CAS, High Power Hadron Machines, 27 May 2011
https://cas.web.cern.ch/cas/Bilbao-2011/Lectures/Gerigk1.pdf

[20] RF Cavity Design Erik Jensen CERN BE/RF CERN Accelerator School Accelerator Physics (Intermediate level) Chios 2011
https://cas.web.cern.ch/cas/Greece-2011/Lectures/Jensen.pdf

[21] RF Cavities Y. Papaphilippou, N. Catalan Lasheras-USPAS, Cornell University, Ithaca, NY 20th June – 1st July 2005

[22] Presentation: Chapter 4 Accelerator Structures I Single-Cavity
http://uspas.fnal.gov/materials/11ODU/Proton_4.pdf

[23] Presentation: RF Engineering Introduction, Fritz Caspers- Uppsala University, December 2011

[24] Particle Accelerator Physics- Helmut Wiedemann, Fourth Edition, Springer publications.

[25] RF Linear Accelerators for medical and industrial applications, Samy Hanna-Artech House

[26] The physics of particle accelerators, An Introduction-Klauss Wille, OXFORD Publications.

[27] Linear accelerators Maurizio Vretenar CERN, Geneva, Switzerland

[28] DRIFT TUBE LINAC DESIGN AND PROTOTYPING FOR THE CERN LINAC4 S. Ramberger, N. Alharbi, P. Bourquin, Y. Cuvet, F. Gerigk, A.M. Lombardi, E. Sargsyan, M. Vretenar, CERN, Geneva, Switzerland, A. Pisent, INFN/LNL, Legnaro, Italy

[29] DYNAMICS AND ACCELERATION IN LINEAR STRUCTURES J. Le Duff Laboratoire de l'Accélérateur Linéaire

[30] Oystein Midttun, Ion and proton Linacs- University of Agder and European Spallation Source (ESS)-University of Oslo

[31] THE INTERDIGITAL H-TYPE (IH) STRUCTURE, AN ACCELERATING STRUCTURE FOR LOW ENERGY BEAMS M. BRES, A. CHABERT, F. FORET, D. T. TRANt and G. VOISIN Institut de Physique Nuc!eaire, Universite de Lyon 69- Villeurbanne, France

[32] H-TYPE LINAC STRUCTURES U. Ratzinger* GSI Darmstadt, Darmstadt, Germany

[33] Radio Frequency Quadrupole Alessandra Lombardi, CERN accelerator School Presentation

[34] The Radio Frequency Quadrupole (RFQ) A.M. Lombardi CERN, Geneva, Switzerland

[35] RADIO-FREQUENCY QUADRUPOLE LINACS A. Schempp Johann Wolfgang Goethe University, Frankfurt am Main, Germany

[36] EXPERIMENTAL CHARACTERIZATION OF THE NEW PS BOOSTER INJECTOR AT CERN-Eleonora Belli, Master Thesis in Artificial Intelligence and Robotics- Sapienza Universita Di Roma 2014-2015

[37] Strong Focusing https://en.wikipedia.org/wiki/Strong_focusing

[38] Lattice Design in Particle Accelerators Bernhard Holzer, DESY

[39] Superconducting Accelerators https://en.wikipedia.org/wiki/Superconducting_radio_frequency

[40] Superconducting Cavities Jacek Sekutowicz DESY

[41] The science and technology of superconducting cavities for accelerators Hasan Padamsee Cornell University, Ithaca, NY 14853, USA

[42] Superconducting cavities for accelerators Dieter Proch Deutsches Elektronen–Synchrotron DESY, Notkestrasse 85, 22603 Hamburg, Germany

[43] Panofsky-Wenzel Theorem Classical Mechanics and Electromagnetism for Accelerators USPAS 2013 Gabriel Marcus June 23, 2013

[44] Linac2 http://home.cern/about/accelerators/linear-accelerator-2

[45] Linac1 http://home.cern/about/accelerators/linear-accelerator-2

[46] Linac2 project-ps50.web.cern.ch/project-ps50/Document_draft/PS50_Linac2-v2(KH).pdf

[47] Linac3 https://project-ps50.web.cern.ch/project-PS50/Document_draft/Linac3v2.pdf

[48] Linac4 http://linac4-project.web.cern.ch/linac4-project/description.html

[49] https://www.youtube.com/watch?v=FmUkbLvmShA

[50] http://engineering.sjsu.edu/

[51] https://twiki.cern.ch/twiki/bin/view/SPL/BeamDynamics

[52] https://twiki.cern.ch/twiki/bin/view/SPL/Linac4Web

[53] DESIGN OF THE PI-MODE STRUCTURE (PIMS) FOR LINAC4 F. Gerigk, R. Wegner, CERN, Geneva, Switzerland http://cds.cern.ch/record/1217611/files/fr5rep051.pdf

[54] Cern Bulletin Issue 11-12/2011 - Monday 14 March 2011 https://cds.cern.ch/journal/CERNBulletin/2011/11/News%20*Articles*/1335108

[55] Linac4 Drift Tube Linac under assembly by Katarina Anthony https://cds.cern.ch/journal/CERNBulletin/2011/11/News%20Articles/1335108

[56] Linac4 Technical Design Report: L. Arnaudon, P. Baudrenghien, M. Baylac (LPSC) , G. Bellodi, Y. Body, J. Borburgh, P. Bourquin, J. Broere, O. Brunner, L. Bruno, C. Carli, F. Caspers, S. Cousineau (ORNL), Y. Cuvet, C. De Almeida Martins, T. Dobers, T. Fowler, R. Garoby, F. Gerigk, B. Goddard, K. Hanke, M. Hori, M. Jones, K. Kahle, W. Kalbreier, T. Kroyer, D. Küchler, A.M. Lombardi, L.A. Lopez-Hernandez, M. Magistris, E. Mahner, M. Martini, S. Maury, T.K. Meinschad, E. Page, M. Paoluzzi, M. Pasini, U. Raich, C. Rossi, J.-P. Royer, E. Sargsyan, J. Serrano, R. Scrivens, M. Silari, M. Timmins, W. Venturini Delsolaro, M. Vretenar, R. Wegner, W. Weterings, T. Zickler. http://project-spl.web.cern.ch/project-spl/documentation/l4tdr.pdf

[57] CERN LINAC4 Beam Dynamics Studies and Commissioning up to 12 MeV- Veliko Atanasov Dimov. PhD Thesis, Bogazici University Istanbul 2015

[58] TRAVEL v4.07 , User Manual April 2007 Arnaud PERRIN – PS/PP/BD, Jean-François AMAND – PS/PP/BD, Torsten Mütze – AB/ABP/HSL, Jean-Baptiste LALLEMENT – AB/ABP/HSL, Sara Lanzone - AB/ABP/HSL

[59] Emittance Formula for Slits and Pepper-pot Measurements Min Zhang Fermi National Accelerator Laboratory October 1996

[60] PEPPER-POT BASED EMITTANCE MEASUREMENTS OF THE AWA PHOTOINJECTOR J. G. Power, M. E. Conde, W. Gai, F. Gao, R. Konecny W. Liu, and Z. Yusof ANL, Argonne, IL 60439, U.S.A. Ph. Piot and M. Rihaoui NIU, DeKalb, IL 60115, U.S.A.

[61] A LOW ENERGY ION BEAM PEPPER POT EMITTANCE DEVICE M. Ripert, A.Buechel, A. Peters, J.Schreiner, T.Winkelmann, HIT, Heidelberg, Germany

[62] Pantechnic Pepper Pot Software User Manual

[63] A COMPACT HIGH-FREQUENCY RFQ FOR MEDICAL APPLICATIONS M. Vretenar, A. Dallocchio, V. A. Dimov, M. Garlasché, A. Grudiev, A. M. Lombardi, S. Mathot, E. Montesinos, M. Timmins, CERN, Geneva, Switzerland

[64] ERIS : Automatized Transverse Emittance Reconstruction application for Linac3. Emmanouil Trachanas, Georgios Voulgarakis, Veliko Atanasov Dimov, Giulia Bellodi, Alessandra Lombardi and Evangelos Gazis

[65] Chromatic effects in quadrupole scan emittance measurements A. Mostacci, M. Bellaveglia, E. Chiadroni, A. Cianchi, M. Ferrario,D. Filippetto, G. Gatti, and C. Ronsivalle-PHYSICAL REVIEW SPECIAL TOPICS - ACCELERATORS AND BEAMS 15, 082802 (2012)

[66] Automated Transverse Beam emittance measurement using a slow wire scanner at the S-Dalinac- P. Dijkstal, M. Arnold, C. Burandt, F. Hug, N. Pietralla-Institut fur Kernphysik, TU Darmstadt, 64289 Darmstadt, Germany.

[67] Automated Emittance Measurement in the SLC- M.C. Ross, N. Phinney, G. Quickfall, H.Shqaee, J.c Sheppard. Standford Linear Accelerator Center , Standford USA.

[68] Automatic Emittance Measurement At the ATF* X.J Wang, R. Malone, K. Batchelor and I. Ben-Zvi, Brookhaven National Laboratory , Upton, New York 11973

[69] M. Minty and F. Zimmermann "Measurement and control of charged particle beams", Springer (2003)

[70] J. Buon "Beam Phase Space and Emittance" CERN 94-01, Vol. I

[71] H. Braun, Emittance Diagnostics I,II, CERN School on Beam Diagnostics, Dourdan, France 2008

[72] Autopilot Regulation for the Linac4 H^- Source G. Voulgarakis, J. Lettry, S. Mattei, B. Lefort and V.J. Correia Costa.

[73] J. Lettry et al., Rev. Sci. Instrum. 87, 02B139 (2016)

[74] Presenting Inspector `https://wikis.cern.ch/display/INSP/Inspector+Home`